Effects of age and mechanical loading on articular cartilage metabolism and corresponding consequences for tissue health

By

Shannon K. Walsh

A dissertation submitted in partial fulfillment of

the requirements for the degree of

Doctor of Philosophy

(Comparative Biomedical Sciences)

at the

UNIVERSITY OF WISCONSIN - MADISON

2020

Date of final oral examination: April 27, 2020

The dissertation is approved by the following members of the Final Oral Committee:

Corinne R. Henak, Assistant Professor, Mechanical Engineering

Lih-Sheng Turng, Professor, Mechanical Engineering

Ray Vanderby, Professor, Biomedical Engineering

Peter Muir, Professor, Surgical Sciences

Barak Blum, Assistant Professor, Cell and Regenerative Biology

ACKNOWLEDGMENTS

It is a genuine honor to be joining the ranks of UW-Madison scientists. I am grateful for the outstanding education I've received here and am glad to be able to give back in the form of this dissertation. I am especially proud to hail from the Comparative Biomedical Sciences program and would like to thank the CBMS administration, especially Susan Thideman and Dr. Marulasiddappa Suresh, for caring so deeply about students' well-being and providing us with such a great program. It has been my pleasure to serve on the CBMS Academic Committee and to play a small role in shaping the future of the program.

I am extremely fortunate to have conducted my thesis work under the mentorship of Corinne Henak. Graduate school is unavoidably difficult, but the relationship a student has with their advisor plays a massive role in setting the tone for the student's entire experience. In that respect, I could not have been luckier. Corinne took me on as her first student—a risky move on her part considering my complete lack of engineering experience. This vote of confidence and Corinne's unwavering respect for her students as independent researchers continually motivated me to take on challenges and to trust my own skills throughout graduate school. It has been such a privilege to watch this lab group grow from its inception and am excited to see how this research evolves in the coming years. I take great pride in my affiliation with the Henak Lab and will genuinely miss our weekly meetings.

I would like to thank my thesis committee members Ray Vanderby, Peter Muir, Tom Turng, and Barak Blum, for their guidance over the last five years. I have enjoyed every one of our meetings and value the insightful discussions we've had. My research has benefited immensely from their unique perspectives and expertise and am grateful for their service on my committee.

Additionally, I would like to thank my collaborators Corey Neu, Ellyse Schneider, Laura Amundson, Melissa Skala, and Lisa Arendt for their valuable contributions, as well as Tom Crenshaw for his mentorship and insights over the years.

I have been fortunate to make many friends since moving to Madison, and their support has been sincerely appreciated. I'd like to thank my rugby teammates for keeping me sane, my CaSPers for constantly inspiring me, and my fellow Henak Lab members for enduring my sense of humor. Most of all, I need to thank Guebum Han. His encouragement and companionship enabled me to push through the toughest times and I am forever grateful for his friendship.

Without a doubt, I would not be where I am without the love and support of my stellar family. My sister Cait has been my comic relief and has *always* been down to laugh through life with me—the key to my academic longevity. She has kept me grounded and has given me helpful perspective when I most needed it. My brother-in-law Luc has voluntarily read every abstract and manuscript I've ever written, which I find truly boggling and incredibly heartwarming. And my most brilliant contemporaries, Kieran, Casey, and Milo, have continually pushed the bounds of my knowledge with profound lines of scientific questioning reaching far beyond the scope of biomedical sciences, whilst somehow also building up my ego. According to them, I literally discovered the sky. There is seriously nothing more thrilling than getting to be Aunt Shan.

Lastly, thank you Mom. Your steadfast support has been crucial to any success I've achieved. You have instilled in me the tenacity to take on big challenges and the grit to see them through. My life has been blessed with many great role models of strength and generosity, and you will always be chief among them.

Chapter A: Maturation & Metabolism of Articular Cartilage: A User's Guide to Aging Joints

Shannon K. Walsh

A1. Setting the Stage

A1.1. What's in a joint?

When you think of skeletal joints, you probably think of synovial joints. These are the connections between long bones, such as the tibia and the femur in the leg, that allow range of motion. Knees, hips, shoulders, elbows, wrists, and ankles are all examples of synovial joints (Figure A-1A). Although their geometries differ and allow variable types of motion, synovial joints all share the same major anatomical components (Figure A-1B). Of course, there are the long bone endings, the surfaces of which are each lined with a layer of articular cartilage. Unlike the cartilage found in the ears and nose, articular cartilage is specifically designed to provide cushion for bones by withstanding and distributing mechanical loads across the joint surface, ultimately protecting the underlying bone from pain and wear. Tendons, which connect muscle to bone, and ligaments, which connect bone to bone, provide joint stabilization and restrict motion to certain planes. Lastly, a soft fatty tissue called synovium (a.k.a. synovial membrane) produces synovial fluid, the viscous lubricant which fills the remaining space within the joint and provides nearly frictionless joint motion.

A1.2. Cartilage is tough, but aging is tougher

Articular cartilage, also referred to as joint cartilage or cartilage from this point forward, is composed of a cage-like mesh of collagen fibers. These fibers provide a scaffold for large, branched molecules called proteoglycans to lay within. In addition to providing extra structural support, proteoglycans play the very important role of keeping cartilage hydrated. Since proteoglycans are negatively charged, they keep positively charged water molecules bound within the tissue. Collagen, proteoglycans, and water give cartilage the ability to endure heavy and consistent compression. Embedded within this dense framework are cells called chondrocytes. These cells are responsible for maintaining cartilage health by breaking down old tissue and creating new tissue as necessary.

Like any body part, joint cartilage undergoes structural and biological changes throughout the aging process. From birth to adolescence, the cartilage thins, becoming more compact. As this occurs, the molecular components within the tissue take a more sophisticated form for enhanced resiliency to repetitive loading (Figure A-1C). This structural advantage comes at a price, however, as the residing cell population becomes sparser and the remaining cells lose some of their important stem cell-like properties, which will be discussed later on in the chapter. *Unlike* most tissues, by the time the body reaches skeletal maturity and ceases growing, cartilage loses the ability to repair itself if injured.

Beyond adolescence, cartilage continues experiencing aging effects. The nature and severity of these changes vary from person to person, but often include additional tissue thinning, cartilage damage, and decreased proteoglycan concentration. Losing proteoglycan content is consequential for tissue health and integrity, as this causes cartilage to become dehydrated and therefore less capable of distributing mechanical loads to prevent its own fracture or that of the underlying bone. Proteoglycan-deficient cartilage can be thought of much like a waterbed that has been drained and is therefore less capable of providing sufficient cushion or properly distributing loads across the material. Additionally, the cell population continues to decrease throughout aging, and the very sparse remaining cells often lose the ability to perform key functions for tissue maintenance.

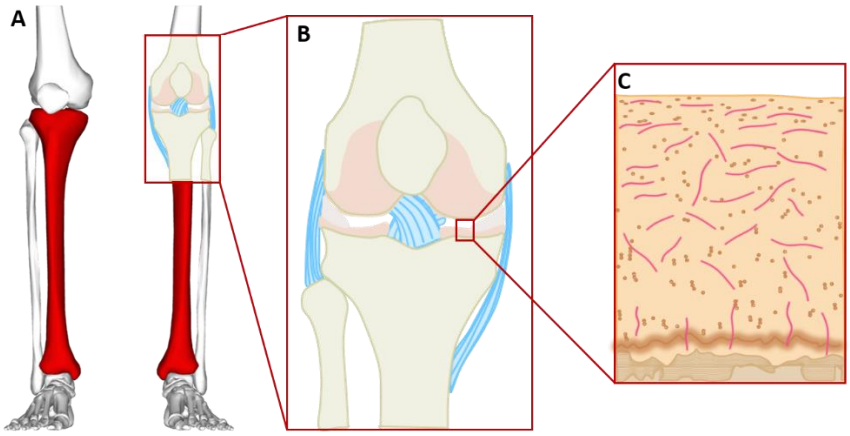

Figure A-1. Schematic of multi-scale anatomy. **(A)** Human skeleton depicting tibia (shin bones) in red and the location of the femorotibial (knee) joint, one example of a synovial joint[1]. **(B)** Expanded schematic of a knee joint depicting bones (tan), articular cartilage (pink), and ligaments (blue). **(C)** Expanded schematic of fully developed articular cartilage cross section, depicting the tissue from the joint surface (top) to the underlying bone (bottom). Orientations of collagen fibers are represented by pink lines; chondrocytes are represented as brown dots.

Given the effects of aging described above, it is unsurprising that so many people eventually experience cartilage breakdown over time. As cartilage wears down, the underlying bone is exposed to friction, grinding, and impact that it is not designed to withstand. This is a condition known as osteoarthritis (OA), and it is a very common and painful disease that can become debilitating to those affected. Although OA differs from rheumatoid arthritis, an autoimmune condition in which antibodies attack the body's own cartilage causing inflammation and eventual tissue breakdown, these diseases share many of the same symptoms, including joint swelling, pain, and reduced range of motion. The global burden of OA is expected to rise in the coming decades as average life expectancy continues to increase. Simply put, we are outliving our joints. With artificial joint replacements currently only able to last approximately a decade, alternative therapies for joint preservation are necessary to maintain quality of life in the aged population. Thus, cartilage regeneration (the re-growth of tissue that has degraded) is a *very* active field of study, as researchers are constantly in search of novel ways to treat or prevent OA!

A1.3. Injuries: they don't help

Although OA can develop as a result of consistent joint wear over a lifetime, as is often the case, injuries can certainly initiate and expedite this degenerative (tissue breakdown) process. Athletic injuries, auto accidents, and other traumas which directly injure joint cartilage can initiate an unfortunate cascade of events. First, the impacted cells die, and, if untreated, a combination of subsequent mechanical stress and joint inflammation progressively break down the cartilage until severe OA has developed. Alternatively, injury to another joint-stabilizing tissue such as a ligament can result in secondhand cartilage damage over time. This occurs when the joint geometry is compromised such that the joint is now loaded in a different conformation than it was pre-injury, and previously non-weight-bearing cartilage is now being exposed to heavy loading that it is ill-equipped to handle. Anterior cruciate ligament (ACL) or meniscus tears within the knee often lead to long-term cartilage damage in this manner, as the knee becomes destabilized and more vulnerable regions of cartilage are subjected to concentrated mechanical stresses during ambulation (walking).

Orthopedic (skeletal system) injuries such as ligament tears often warrant surgery, and this procedure can also lead to cartilage damage post-operation in several ways. First, the surgical procedure itself can inflict direct damage upon the cartilage attached to or near the tissue being

repaired. Following surgery, the joint experiences significant inflammation throughout the first stage of recovery and rehabilitation, a condition which can also take a toll on the health of surrounding tissues including cartilage. Additionally, although such surgeries are intended to restore joint biomechanics to their original state, matching pre-injury mechanics perfectly is nearly impossible given current surgical limitations, resulting in subtle abnormalities to the joint's geometry and eventual secondary damage in many cases (Figure A-2). Finally, orthopedic injuries and subsequent surgeries often require patients to completely immobilize the affected joint for some period of time to prevent further injury and to allow time for tissue healing. While this practice prevents injured joints from excessive loading, a total lack of motion is not healthy for articular cartilage either. This tissue is designed to experience frequent compression and requires some degree of loading for tissue health. Cartilage cells fail to act properly with respect to maintaining tissue buildup and breakdown in the total absence of mechanical loading signals. In fact, whether cartilage cells are loaded too much or too little, the consequence is ultimately the same; the rate of cartilage breakdown exceeds the rate of cartilage buildup, and the tissue degenerates. In this regard, one can imagine chondrocytes as factory workers, where both an excessive workload (excessive mechanical burden) or a complete lack of instruction (insufficient mechanical loading) result in underperformance and minimal factory output. As previously mentioned, aging can *also* cause cartilage cells to stop functioning properly in this same manner. With all these biological and mechanical challenges leading to cartilage breakdown, it is no wonder that OA is so common.

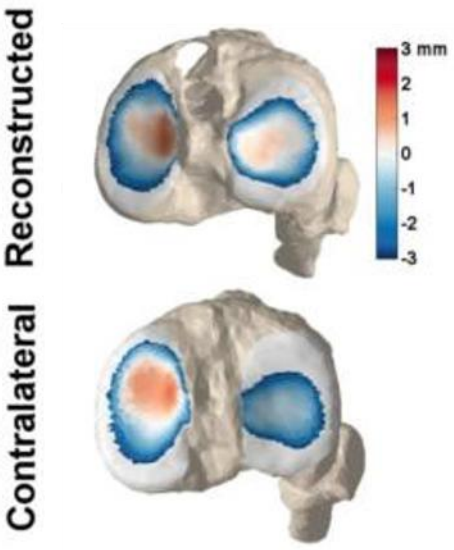

Figure A-2. Representative map of tibia cartilage contact in reconstructed (operated) knee compared to the contralateral (unoperated knee) in a patient who has undergone ACL reconstruction surgery, as determined by magnetic resonance imaging (MRI)[2]. Red hue indicates contact between the joint surfaces and blue indicates space.

A2. My Research

A2.1. Mechanics + Biology = Mechanobiology

Articular cartilage is notoriously challenging to study. Relative to other tissues, including juvenile cartilage, adult cartilage is essentially a biological desert; chondrocytes are sparsely distributed throughout a very dense network of structural molecules and demonstrate much lower rates of biological activity than most other cell types (Figure A-3). Given these limitations, many methods of measuring cell activity within cartilage tissue aren't powerful or sensitive enough to detect subtle changes in chondrocyte behavior within live tissue samples and are therefore inadequate for many cartilage research applications.

For this reason, lots of cartilage research happens on chondrocytes that have been chemically isolated from the network of collagen fibers and proteoglycans they reside within. These studies can give us great insights into specific chondrocyte functions on a fundamental level. For instance, researchers can simulate tissue injury by artificially damaging isolated cells, typically via hazardous chemicals, and can then observe chondrocytes' response to injury. This experimental "injury" model can also be used to test potential treatments, allowing researchers to determine which ones have the most potent therapeutic effect on the cells, thereby indicating which treatments are worth investigating further. However, isolated cell studies are insufficient to fully understand natural mechanisms of cartilage function within the body. Articular cartilage is unique in that it is avascular (lacking blood vessels) and aneural (lacking nerves); hence the "biological desert" reference. Without receiving chemical signals from blood or nerves like most cells do, chondrocytes rely heavily on mechanical signals from tissue compression to know what is going on in their environment and how to respond, much like a person's working senses often sharpen when one has been compromised. Therefore, taking these cells out of their native three-dimensional environment and observing them in the absence of the mechanical cues they receive in the body gives an incomplete look at how they operate on a holistic level.

The overarching goal of my work was to develop ways to observe and understand cartilage biology in the context of the mechanical loading experienced by this tissue; a research field known as mechanobiology. To be clear, this is already an established and well-occupied field with many scientists producing high-caliber research that analyzes numerous aspects of cartilage biology and various types of mechanical loading. I specifically aimed to analyze the short-term cartilage

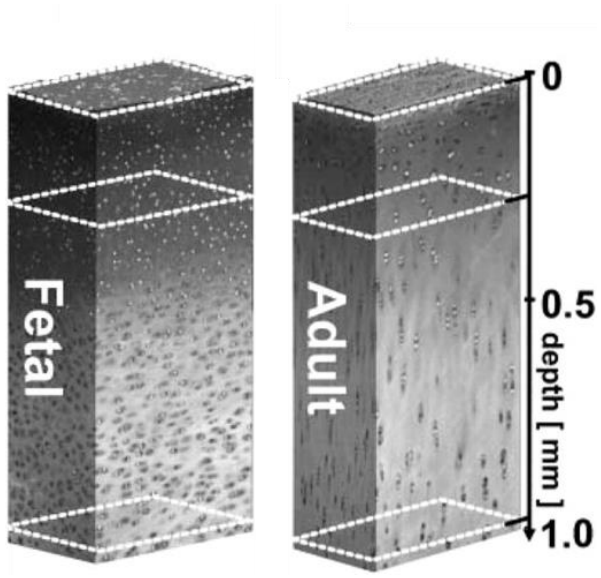

Figure A-3. Three-dimensional representation of adult cartilage compared to fetal cartilage, depicting the volume and distribution of cells throughout the tissue from the joint surface (depth = 0 mm) toward the underlying bone surface (> 1 mm)[3].

response to injury-inducing mechanical compression with respect to chondrocyte metabolism, progenitor status, and anabolic gene expression—biological factors suspected to be critically involved in cartilage injury and degeneration—which will be discussed further in the following sections.

A2.2. Metabolic imaging: cancer research comes in clutch

Motive: When most people think of metabolism, they probably think of whole-body metabolism: food intake, exercise, body composition. Broadly, metabolism is the combination of processes by which biological energy is created, stored, and used. These processes can be observed on a cellular level as well. Mammalian cells derive energy from a couple of biochemical processes: glycolysis, the quick chemical breakdown of glucose which yields a relatively small amount of energy, and oxidative phosphorylation (oxphos), a slower chemical process in which electrons are transferred between molecules to create a lot of energy. A growing body of recent literature has indicated that metabolic dysfunction, typically demonstrated by a reduction in one or both of these processes, is a common feature of cartilage breakdown and osteoarthritis progression.

Challenge: Previous cartilage metabolism studies have been limited to either observing a snapshot of metabolic activity at a specific point in time, monitoring generic metabolic activity that is not specific to these individual metabolic processes, or studying cells that have been isolated from the tissue as previously discussed.

Research goals:

(1) Develop a method to observe specific chondrocyte metabolism over time in native, three-dimensional cartilage samples

(2) Use this method to determine the immediate effects of mechanical loading on cartilage metabolism

Approach: We borrowed a technique previously used in cancer research and adapted it for use in cartilage. This technique, known as optical redox imaging, can detect relative levels of glycolysis and oxidative phosphorylation activity by measuring the accumulation of chemical byproducts given off by each of these processes, respectively (Figure A-4). Conveniently, these byproducts are fluorescent, meaning the sample doesn't need to be stained with any artificial elements and can therefore be imaged repeatedly over time.

Key outcomes:

- It can be done! Optical redox imaging is capable of detecting metabolic changes in cartilage samples over time without needing to isolate cells from their tissue matrix.
- Slow, mild compression of cartilage, such as what the tissue experiences during walking, appears to induce a proportionately mild and temporary response in glycolysis activity but not oxphos activity.
- Fast, damaging compression of cartilage, simulating an injury, appears to induce a more drastic and long-term response in both metabolic processes.
- Taken together, these results corroborate previous suggestions that oxphos is a particularly important component of the cartilage breakdown process *and* validate our experimental model as an effective tool for studying cartilage metabolism in a way previous studies have not been able to.

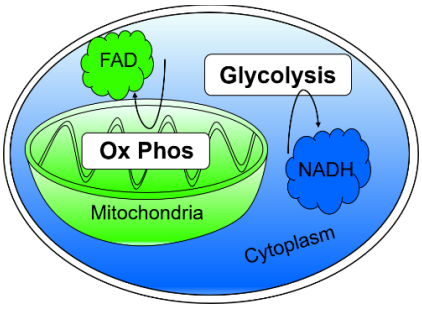

Figure A-4. Schematic of a cell, depicting intracellular locations of the two main metabolic processes (oxidative phosphorylation and glycolysis) and their respective autofluorescent byproducts, FAD and NADH. Since these byproducts fluoresce on their own, relative amounts of green and blue fluorescence can be imaged and interpreted as relative activity of each of these metabolic processes.

A2.3. Cartilage aging: the (scientific) solution is in the (clinical) problem

Motive: In addition to cell metabolism, recent studies have implicated progenitor cell activity as another potentially important component of cartilage regeneration. Progenitor cells can be thought of as stem cells that are specific to a certain tissue. They are not truly stem cells, for they cannot give rise to multiple types of tissue, but they share certain features with stem cells such as the ability to multiply, migrate, and differentiate into the "terminal" cells which produce and/or maintain a specific biological tissue. Essentially, progenitors are the interns of the cell population; they know what they'd like to become, but haven't yet reached their final stage of development, and are working very hard in the meantime. Researchers have shown that cartilage in juveniles contains a greater proportion of certain progenitor cells than adult cartilage does, suggesting the lack of progenitor cells may be involved in adult cartilage degradation.

Gene expression serves as a good indicator of cells' intentions, which makes gene expression analysis an attractive approach for evaluating cellular activity. Every mammalian cell (excluding sperm or eggs) has a complete copy of our DNA in its nucleus. Our DNA serves as a blueprint for all the proteins in our entire body. However, not every cell needs to be making every protein all the time. Heart cells need to make cardiac tissue, liver cells need to make hepatic tissue, etc. Therefore, each cell only expresses (or "turns on") the genes necessary for the tissue it belongs to, and only when the corresponding protein needs to be produced. We wanted to determine the effects of aging on cartilage cells' gene expression to know if adult cells were attempting to make more or less of certain cartilage-specific proteins than juvenile cells.

Challenge: Cartilage degradation is notoriously difficult to study because it is inherently difficult to make observations about a process that's *not* occurring—in this case, regeneration.

Approach: To circumvent this challenge, we joined the abundant community of researchers who compare adult cartilage to pre-adolescent cartilage, the only type of cartilage that naturally regenerates, to understand where things are going wrong mechanistically in mature cartilage.

Research goals:

(1) Determine the effects of aging on chondrocyte metabolism, progenitor status, and expression of anabolic genes (those geared toward building the tissue up, vs. catabolic genes which result in tissue breakdown and turnover)

(2) Determine the consequences of aging on cartilage *response* to mechanical loading and tissue culture with respect to the biological factors listed above. Rapid mechanical loading is generally expected to incite a damage-oriented response from cells, and tissue culture (simulating the body environment by incubating samples in warm nutrient-rich fluid) has been shown to inspire some cells to become more progenitor-like.

Key results:

- Old cartilage appears to be trying to revert to a more juvenile biological state! We anticipated shifts in cartilage metabolism, progenitor cells, and gene expression throughout aging, but we expected it to happen in a consistent, linear pattern. That is, we expected changes to occur throughout aging in *one direction.* We did not expect to see aged cartilage attempting to mimic the growth-oriented biological activity demonstrated in young samples by reverting to pre-adolescent levels of metabolic activity, gene expression, and progenitor cell activity.
- Mechanical loading and tissue culture caused quite a few fluctuations in progenitor cells and gene expression patterns in juvenile samples, less so in adolescent samples, and hardly any in adult samples. In other words, despite the promising attempt to reverse inherent aging changes demonstrated in aged samples, old cartilage seems to be "set in its ways" when it comes to *actually* responding to environmental disturbances. It's as if the cells in aged samples have acknowledged their shortcomings but lack the tools to make actual improvements. This may help explain the unsuccessful development of effective therapies for aged cartilage. As they say, "you can lead an old chondrocyte to water, but you can't make it drink."

A2.4. Why does this matter?

Much like adding a pebble to the top of a mountain, these studies (like all studies) add a small bit of knowledge to the existing body of wisdom built up by previous researchers in the field. All this work serves to push the boundary of our collective understanding, occasionally culminating in scientific or medical breakthroughs which surge the field forward thanks to all who contributed. My work, outlined above, has both short- and long-term implications for cartilage research:

Short-term: We know that adult cartilage is unable to repair itself and therefore cannot prevent the accumulation of damage. However, this research provides evidence that aged cartilage is *trying* to

combat aging effects. While this intention clearly does not translate into capability, these findings can help to guide our research moving forward by steering us toward specific aspects of tissue regeneration which demonstrate some promise in aged cartilage.

Long-term: Optical redox imaging (ORI) holds great promise for cartilage research and medicine. Given that this method can accommodate longitudinal (time series), informative metabolic monitoring during and after environmental changes such as mechanical loading or exposure to treatments, ORI opens many doors for cartilage researchers. We have demonstrated a couple of possible applications of this technique (imaging pre- and post-mechanical loading, across aging spectrum), but there are countless more that this method could be applied to. Simply put, ORI can be used to aid our understanding of tissue physiology as well as to test novel potential therapeutics from a metabolic perspective. Additionally, and perhaps most excitingly, because ORI is a relatively non-invasive and non-destructive technique there is some potential for eventually adapting this technique for clinical use in diagnosing cartilage damage in the body long before any macroscopic injury is present, letting us get ahead of osteoarthritis with early treatment.

Beyond the act of doing the research itself, *communicating* this work to the public is also very important! Ideally, the scientific and non-scientific community should be engaged in an ongoing, two-way dialogue in which the public is able to express their needs (particularly where research can help), scientists can express what type of community support they need to conduct the necessary work, and the fruits of this collaborative effort are communicated and celebrated by all. On that note I would like to sincerely thank the Wisconsin Initiative for Science Literacy at UW-Madison for sponsoring and supporting the creation of this chapter. I sincerely commend the sentiment behind the program's mission and encourage all researchers to embrace science communication as a fundamental component of our responsibilities as scientists.

1. 2013. File:Tibia - frontal view2.png - Wikimedia Commons. [cited 2020 Apr 1] Available from: https://commons.wikimedia.org/wiki/File:Tibia_-_frontal_view2.png.
2. Kaiser J, Vignos MF, Liu F, et al. 2016. American Society of Biomechanics Clinical Biomechanics Award 2015: MRI assessments of cartilage mechanics, morphology and composition following reconstruction of the anterior cruciate ligament. Clin. Biomech. 34:38–44.
3. Jadin KD, Wong BL, Bae WC, et al. 2005. Depth-varying density and organization of chondrocytes in immature and mature bovine articular cartilage assessed by 3d imaging and analysis. J. Histochem. Cytochem. 53(9):1109–19.

ABSTRACT

Articular cartilage poses a major clinical challenge. Beyond skeletal adolescence, cartilage loses regenerative functionality, rendering this tissue vulnerable to accumulation of damage over time. Thus, age and mechanical overloading are predisposing factors for development of osteoarthritis (OA), a globally burdensome condition. Metabolic dysregulation has also been identified as a key feature of cartilage degeneration. Therapeutic OA treatments are lacking, due in large part to an incomplete understanding of the complex interplay between these predisposing factors. This knowledge gap can be addressed by studying the interactive effects of tissue age, mechanical loading, and metabolic activity in cartilage. The aims of this thesis were: (1) determine the consequences of maturation on chondrocyte identity and activity, (2) develop a method of observing the real-time effects of loading on cartilage metabolism and analyze loading rate- and age-dependent sensitivity to compression with respect to metabolism, gene expression, and progenitor functionality, and (3) identify the downstream implications of metabolic activity for tissue health. Maturation and loading effects were analyzed with respect to progenitor cells and gene expression, identifying age-dependent expression of chondroprogenitor markers and anabolic genes and revealing maturation-dependent sensitivity to mechanical loading and tissue culture. A metabolic imaging technique, optical metabolic imaging (OMI), was adapted for use in articular cartilage, and was employed to analyze the effects of physiological and superphysiological compression on metabolism. This work demonstrated transient metabolic flux following compression, with differential pathway-specific and time-dependent effects following physiological and superphysiological loading. Metabolic consequences of maturation were studied by mapping metabolic activity as a function of age in samples spanning pre- and post-adolescence. Maturation-dependent metabolic activity was observed in both the glycolytic and oxphos

fluorescence channels, showing a pattern of nonlinearity in optical redox ratio across age groups. The consequences of metabolism were probed via chemical inhibition; glycolytic inhibition suppressed expression of both anabolic and catabolic genes pertinent to tissue maintenance while oxphos inhibition did not. Finally, an association between tissue metabolism and degree of degeneration was revealed in mature cartilage. This interdisciplinary approach to understanding cartilage mechanobiology provides novel insights into cartilage function and has meaningful implications for future research.

TABLE OF CONTENTS

LIST OF FIGURES

LIST OF TABLES

LIST OF ABBREVIATIONS

ACI – autologous chondrocyte implantation

ACLT – anterior cruciate ligament transection

DMM – destabilization of the medial meniscus

DMOAD – disease modifying osteoarthritis drug

ECM – extracellular matrix

GAG – glycosaminoglycan

MACI – matrix-associated autologous chondrocyte implantation

MFx – microfracture

MSCs – mesenchymal stem cells

MRI – magnetic resonance imaging

NSAID – nonsteroidal anti-inflammatory drug

OA – osteoarthritis

OMI – optical metabolic imaging

Oxphos – oxidative phosphorylation

PCM – pericellular matrix

PCR – polymerase chain reaction

PKA – partial knee arthroplasty

PRG4 – proteoglycan 4 (lubricin)

PRP – platelet-rich plasma

PTOA – post-traumatic osteoarthritis

RNA – ribonucleic acid

ROS – reactive oxygen species

SASP – senescence-associated secretory phenotype

SMOAD – symptom modifying osteoarthritis drug

TKA – total knee arthroplasty

TRPV – transient receptor potential vanilloid

Chapter 1: Introduction

1.1. Motivation

1.1.1. Articular Cartilage

Articular cartilage is a specific type of cartilage which lines the bone endings within synovial joints. The extracellular matrix (ECM) of this tissue is comprised of an interwoven collagen mesh network filled with large, branched proteoglycan molecules, and embedded within the ECM are cartilage cells known as chondrocytes[1]. This tissue is kept hydrated by the negatively charged glycosaminoglycan (GAG) component of proteoglycans, which bond ionically to water molecules[2]. The abundance of water present within cartilage is critical for the tissue's ability to dissipate energy during loading[3,4].

The morphology of cartilage serves to protect the embedded chondrocytes from damage induced by tissue deformation. Unlike other types of cartilage, such as the more homogenous elastic cartilage found in the ear or nose, articular cartilage is hyaline cartilage and is therefore comprised of three zonal layers (superficial, middle, and deep), each with distinct collagen fibril orientation[1,5]. Several studies have highlighted the importance of the superficial zone in particular for load distribution and protection of underlying cells[1,6,7]. Furthermore, while articular cartilage contains primarily type II collagen fibrils, chondrocytes are each surrounded by a pericellular matrix (PCM) comprised of alternative collagen types[8]. The PCM provides stress shielding for cells during loading and mediates cell mechanobiology—the transduction of mechanical deformations into biological cell signals[1,9,10].

Chondrocytes are heterogeneously distributed throughout cartilage, aligning with the depth-dependent orientation of the surrounding collagen fibrils[5]. As the sole cell type present in cartilage, chondrocytes are responsible for maintaining the ECM via anabolic and catabolic activity[11–13].

Some chondrocytes are capable of additional, often region-specific functions, such as the surface zone cells which produce proteoglycan 4 (PRG4), also known as lubricin, a substance that binds to the articular surface and contributes additional lubrication beyond that provided by synovial fluid to minimize cartilage-on-cartilage friction[14–19]. Since adult cartilage is avascular and aneural, chondrocytes rely heavily on mechanical cues during joint motion to initiate cell signaling with the appropriate downstream effects such as anabolic or catabolic activity[20].

1.1.2. Osteoarthritis

Osteoarthritis (OA) is a debilitating condition characterized by the breakdown of the synovial joint. Although cartilage degeneration is perhaps the hallmark feature of OA, the various tissue components of the joint function together as an organ, and therefore this condition often eventually involves inflammation and degradation of several joint tissues[21,22]. Global estimates rank OA as a leading cause of disability, consistently topping the list of most prevalent musculoskeletal conditions[23–27]. In recent decades, the U.S. has experienced a surge of OA incidence[28]. Although increased average lifespan and rates of obesity alone are insufficient to account for the increase in nationwide OA prevalence, these factors are expected to contribute to the ever-increasing burden of this condition in the coming years[28].

Clinical OA presentation is highly variable, due in part to variations in diagnosis methods[29,30]. Standard radiographs are typically employed as the starting point for diagnostic imaging of orthopedic issues, whether the patient is presenting with generalized pain or an acute injury, to first assess bone structure and rule out fracture. Radiographic images can be used to assess macroscopic loss of joint space due to cartilage degradation, limiting this method to detection of severe OA beyond the early stages, at which point the opportunities for intervention have narrowed considerably[31,32]. Comparatively, advanced magnetic resonance imaging (MRI) is better suited for

soft tissue imaging both from a structural and biochemical standpoint and is therefore capable of detecting earlier stages of cartilage deterioration, such as proteoglycan loss, prior to major structural tissue loss[33,34]. MRI is commonly indicated following radiographs when soft tissue damage is suspected, either to the cartilage or the surrounding tissues. Alternatively, although unable to provide tissue composition information, arthroscopic imaging is able to display mild surface fibrillation or other subtle irregularities; characteristics that also precede the more severe damage and may not be detectable by radiographs and MRI[35,36]. Arthroscopic detection of mild cartilage damage is often the byproduct of a procedure intended to diagnose or repair damage to another tissue such as a ligament or meniscus. Ultimately, employment of any orthopedic diagnostic method is only prompted by patient-reported symptoms such as pain or loss of mobility. While cartilage damage can certainly result from an acute injury that would warrant immediate diagnostic imaging, a subtype of OA known as post-traumatic osteoarthritis (PTOA), OA can also progress slowly and consistently from cumulative microdamage over a lifetime[37]. Thus, the severity of joint degradation at the time of presentation often relies on perception of pain or discomfort, subjective metrics with high interpatient variability[38].

Regardless of the nature of cartilage damage or the timing of its detection, current treatment options are limited to symptom modifying OA drugs (SMOADs) rather than those capable of mitigating the disease (disease modifying OA drugs, DMOADs). Nonsurgical treatments include pharmacological agents intended primarily to alleviate pain, and in some cases to restore mobility through reduction of inflammation. Common treatments include acetaminophen, corticosteroids, nonsteroidal anti-inflammatory drugs (NSAIDs), and narcotics[23]. However, the duration and efficacy of these treatments is limited, evidenced by the fact that Paracetamol, a brand of acetaminophen, is considered a first-rate SMOAD by many standards despite evidence of its

minimal alleviation[23,39]. Furthermore, some pharmacological treatments pose the risk of nontrivial side effects, such as cardiovascular complications caused by frequent use of NSAIDs[40]. For severe cases of mobility loss and cartilage degeneration, more aggressive intervention may be indicated. Autologous biologics approaches such as platelet-rich plasma (PRP) and autologous cell implantation (ACI), variations of which have involved both chondrocytes and mesenchymal stem cells (MSCs), have been used to treat a range of osteoarthritic conditions, both as standalone intraarticular injections and in conjunction with surgical procedures, to initiate a regenerative response[41–43]. PRP is an especially attractive treatment option due to the relatively low risk and cost associated with treating a patient with autologous blood product. Similarly, microfracture (MFx) has been employed to debride diseased cartilage from the joint and to supply the region with blood from the underlying bone, which is also intended to incite regeneration through access to growth factors and stem cells[44–47]. However, the efficacy of these treatments has been reported to be mixed at best, with high interpatient variability likely stemming, in part, from the inherent variation in the quality of biological products being delivered. Additionally, further studies are needed to determine which procedures or regenerative products are optimal for varying OA phenotypes[23,48]. Despite the variety of treatment options available, none are broadly effective at preventing the progression of cartilage degradation once initiated, or restoring degraded tissue[23,49]. This therapeutic deficiency is due largely to an incomplete understanding of cartilage breakdown initiation on a mechanistic level; the failure of common diagnostic techniques to detect pre-symptomatic OA contributes to this knowledge gap.

The pathological progression of OA is known to be driven by both biological and mechanical factors. Thus, OA has been studied extensively with respect to tissue aging and mechanical insult. However, despite the established body of knowledge, developing a more comprehensive

understanding of the complex mechanobiological underpinnings of OA is essential to overcoming the multifaceted challenges associated with cartilage regeneration.

1.2. Background

1.2.1. Maturation & Aging

Articular cartilage undergoes several changes with respect to tissue morphology throughout skeletal maturation. From birth to adolescence, collagen fibrils within this tissue experience gradual elongation and reorganization, with post-adolescent cartilage featuring three distinct zones: a thin superficial zone with densely packed fibers oriented parallel to the articular surface, a middle zone with randomly oriented fibrils, and a deep zone with fibrils aligning transverse to the adjacent subchondral surface[50–53]. Chondrocyte morphology and distribution follow suit throughout maturation, decreasing in concentration and reorganizing to mimic collagen orientation throughout the three zones[5]. Lastly, proteoglycan content shifts from being relatively uniform in immaturity to demonstrating a depth-wise gradient in adult tissue such that concentration is lowest at the joint surface and greatest at the subchondral surface[51]. Accompanying these changes is an overall decrease in tissue thickness throughout maturation which continues beyond adolescence, and continues indefinitely for some to the point of full-thickness focal lesions in weight-bearing regions[54]. This anisotropic composition has been proposed to defend both cell survivability and structural integrity under physiological loading[1,55,56]; a paradigm supported by studies illuminating the particular importance of the superficial zone[6,57].

Perhaps most consequentially, cartilage loses all capacity for repair or regeneration once skeletal maturity is reached[23,58]. In this context, tissue repair refers to the biosynthetic replacement of lost tissue with nascent tissue, though not necessarily matching the native tissue in mechanical or biological properties, and regeneration refers to true healing through replacement with tissue

matching the original properties of the degraded tissue. While juvenile cartilage is able to regenerate to some degree, structurally compromised cartilage in adults, whether resulting from a singular incident of trauma or accumulation of wear, inevitably develops into progressively degradative tissue as mature cartilage does not demonstrate the capacity for self-healing[58,59]. This phenomenon has been recapitulated experimentally by surgically inducing cartilage damage and tracking longitudinal tissue health. Such studies, which primarily occur in small murine or lapine animal models but occasionally employ larger ovine and equine models, typically involve either direct trauma to the articular surface, or disruption of joint stability via anterior cruciate ligament transection (ACLT) or destabilization of the meniscus (DMM)[59–66]. Exposure to monosodium iodoacetate, a potent metabolic inhibitor, has also been used to induce cartilage damage in rat joints via cellular breakdown and corresponding loss of extracellular tissue maintenance[67,68]. Though rates of subsequent degradation vary across models, these studies corroborate the imminent deterioration of cartilage health following induction of damage due to the inability of this tissue to regenerate. Additionally, age-dependent tissue neogenesis has been demonstrated in ovine and bovine tissue *in vitro* through various experimental models[58,69–71]. Excised samples subjected to a scalpel cut demonstrate differential tissue repair throughout a subsequent eight-week incubation period, wherein wound sites in immature, pre-adolescent samples are filled in with presumably nascent tissue whereas mature samples show no appreciable tissue repair[58]. Similarly, cartilage explants incubated over several weeks demonstrate differential outgrowth activity, where only pre-adolescent samples show evidence of outward cell migration and modification of sample morphology consistent with new tissue formation[58,69].

There are several cellular changes associated with cartilage maturation which may play a role in the corresponding differential repair capacity of this tissue. As cartilage progresses through

adolescence, the overall cellularity of the tissue decreases, and remaining cells take on less uniform distribution and morphology, largely aligning with the zonal organization of surrounding collagen fibrils[5]. Beyond total cell counts, the functional properties of resident cells shift throughout maturation as well. As previously mentioned, many cells can be observed migrating outward from immature cartilage explants in culture, whereas this activity appears to be greatly depressed if not halted altogether in mature tissue[69]. Similarly, isolated chondrocytes from immature cartilage (henceforth referred to as immature chondrocytes) have a shorter doubling time than the post-adolescent counterpart, indicating greater proliferative potential than those isolated from mature cartilage (henceforth referred to as mature chondrocytes)[72]. On average, immature chondrocytes demonstrate heightened relative expression of genes associated with growth and expansion compared to chondrocytes from post-adolescent tissue, whereas mature chondrocytes favor expression of structural integrity genes[69]. Given the differential properties of these total cell populations on average, it is perhaps unsurprising that immature tissue has been shown to possess larger populations of some cartilage-specific progenitor cells (chondroprogenitors) than mature tissue, or that mature chondrocytes demonstrate common senescence features—such as reduction of growth, proliferation, and metabolic activity, and secretion of senescence-associated secretory phenotype (SASP) factors—to a greater extent than immature chondrocytes on average[58,59,73,74]. Finally, all of these maturation-associated changes come at a price beyond inherent loss of regenerative capability, as mature chondrocytes have proven to be inferior to immature chondrocytes with regard to biomedical utility[69,71,72]. The insufficient performance of mature chondrocytes incorporated in cartilage defect repair materials has likely played a role in the limited the success of ACI treatments across multiple procedure generations[47,75].

Though clinically challenging from a treatment perspective, the age-dependent response of cartilage provides a valuable scientific tool for studying cartilage function. Immature cartilage serves as a model of regenerative cartilage that can be leveraged to identify the mechanisms by which adult cartilage fails to repair. Determining the causes and implications of maturity-dependent cartilage properties with respect to tissue function would greatly reduce the existing knowledge gap and enable successful development of regenerative therapies for cartilage.

1.2.2. Mechanical Loading

Cartilage is avascular, aneural, and experiences limited nutrient diffusion due to the density of the ECM[1,76,77]. Therefore, mechanical loading is critical for chondrocyte signaling, both for solute transport and for direct mechanobiological signal transduction[77–80]. As such, cartilage requires a moderate amount of tissue loading for optimal chondrocyte maintenance of the tissue matrix[20]. Inappropriate mechanical loading, whether excessive or insufficient, disrupts the homeostatic balance between chondrocyte anabolism and catabolism. Given the hypoproliferative nature of cartilage, imbalance results in excessive catabolic breakdown of tissue and insufficient anabolic tissue synthesis regardless of cause and can initiate and propagate a cascade of tissue degradation, eventually resulting in OA.

Numerous mechanical models of *in vitro* cartilage injury have been established, typically compromising tissue integrity or function through compressive loading considered superphysiological, either in terms of loading rate or magnitude or both. Earlier studies employed a drop tower system in order to induce loads capable of causing tissue damage[81–84]. Tabletop testing machines are now often used instead to deliver customized displacement- or load-controlled loading regimes with greater flexibility[85–87]. However, drop-tower systems are still sometimes employed as it is challenging to deliver sufficiently fast loads to induce cartilage injury

using motor-driven systems[88–90]. Altogether, these studies have provided critical insights into the mechanical thresholds of cartilage on macro and micro scales, which can help inform *in vivo* mechanical loading studies[91]. Establishing specific magnitude and frequency criteria for true impact loading as opposed to high-rate physiological loading has been of particular importance for aiding interpretation of studies seeking to characterize the early events of PTOA. For instance, based on cartilage fissuring thresholds and cell death rates, impact loading has been suggested to be that which exceeds a strain rate of 500 s^{-1} with corresponding strain of approximately 20-30% and no greater than 500 mm^2 impact area[81,91]. However, a contrasting study which sought to establish these same criteria in cartilage removed from bone rather than full osteochondral cores found much lower thresholds for induction of comparable damage, citing 6.7 s^{-1} strain rate as a benchmark for cartilage impact[92]. Indeed, it is essential for sample type and loading setup to be taken into account when determining specific thresholds for induction of tissue damage.

A variety of approaches have been developed to induce mechanically-driven PTOA in live animal models. As previously discussed, indirect approaches such as ACLT and DMM are purported to critically alter the biomechanical stability of the joint, leading to improper cartilage loading and subsequent tissue degradation[59–66]. Additionally, several methods of delivering injurious compression directly to the articular surface have been developed, including open-joint exposure to rapid compression using various impactor devices[83,93–95]. Noninvasive trauma has also been applied through external mechanical manipulation of the limb, typically in small animal models[60,63,95,96]. This abundant body of literature has revealed key features of OA progression such as cartilage surface discontinuity or fissuring, loss of proteoglycan content, tide mark advancement or doubling, or cell clustering or necrosis, providing important temporal information regarding the sequence of degradative events and thereby enhancing clinical capacity for accurate OA diagnosis

and prognosis[97,98]. Furthermore, these studies serve to corroborate the findings of *in vitro* models, validating the physiological relevance of such models for further use in disease prevention and treatment research.

Although PTOA and non-traumatic OA likely display clinical discrepancies in disease progression, PTOA studies are crucial to understanding the early events of cartilage regeneration failure on a fundamental level. Opportunities for studying spontaneous OA are largely constrained to select animal models known to predictably develop OA, such as Dunkin-Hartley guinea pigs. Furthermore, PTOA studies provide a valuable model for testing potentially protective therapies for degeneration prevention that can be clinically administered at the time of joint injury; treatments which may also prove effective in halting or slowing the progression of non-traumatic OA as well.

While cartilage research methodologies have made great strides from both a mechanical and a biological perspective, the current challenge lies in synthesizing advanced techniques across disciplines to determine the cascade of short- and long-term of mechanobiological effects of superphysiological loading on tissue health. Still, several gaps in knowledge remain with respect to the mechanobiological underpinnings of articular cartilage homeostasis and pathology, warranting further development of mechanical loading systems and biological tools which can be integrated with one another.

1.2.3. Metabolism

Eukaryotic cells derive energy through two main anaerobic metabolic processes: glycolysis, a relatively quick cytosolic process, and oxidative phosphorylation (oxphos), a slower but more energetically lucrative mitochondrial process[13,99]. Metabolic flux, a shift in relative reliance on glycolysis and oxphos, has long been a field of active research, particularly in cancer cells, which

demonstrate a shift in metabolic preference for aerobic glycolysis as they acquire a cancerous phenotype[100–102]. In cartilage, glycolysis has been associated with cell proliferation, while oxphos has been linked to biogenesis; this holds particularly true for growth plate cartilage[13]. Unlike articular cartilage, growth plate cartilage is highly metabolically active, functioning to calcify existing tissue on the ossification end and to produce new cartilage tissue on the reserve end[103]. Studying the energy homeostasis mechanisms of growth-oriented tissues such as tumors and growth plate cartilage can yield meaningful insights into the regenerative shortcomings of primarily post-mitotic tissues such as articular cartilage.

Recently, metabolic dysregulation has been implicated as a key feature of cartilage degradation and the progression of OA[104–106]. While native cartilage has low metabolic activity and low oxygen concentration, mitochondrial function has been shown to play an important role in cartilage damage in response to mechanical loading[79,107,108]. Reactive oxygen species (ROS), known to induce cell death when present in excess, are released by mitochondria in a strain-dependent manner[79,108]. Consistent overloading of cartilage leads to accumulation of ROS and eventual mitochondrial dysfunction, pointing to a likely role for metabolic dysregulation in the onset and progression of osteoarthritis[109]. Specifically, excessive exposure to ROS leads to decreased mitochondrial membrane polarization, proton leakage, and overall reduction of ATP generation. Given that OA is often associated with mechanically mediated accumulation of damage, this dose-dependent ROS-driven mitochondrial dysfunction observed following repetitive loading may point to a key component of OA pathogenesis. Interestingly, OA cartilage has demonstrated a shift in phenotype from healthy cartilage that instead appears more similar to the endochondral ossification of growth plate cartilage, including metabolic activity such as expression of type X collagen and other differentiation-related genes as well as apoptotic cell

death[12,13,110–113].

Optical metabolic imaging (OMI) leverages the autofluorescence an electron donor produced by glycolysis, and an electron acceptor and produced by oxphos[114]. Optical redox ratio, a calculated ratio of the fluorescence-based accumulation of these two byproducts, provides a measure of the relative amounts of oxphos to glycolysis activity, and thereby a metric by which metabolic preference shifts can be detected. Previous use of this imaging technique has been limited to non-cartilage tissues; primarily those adopting cancerous functionality[101,114–117]. Though OMI has not been applied to cartilage, several other methods have been used to evaluate various aspects of chondrocyte metabolism. Synthesis of extracellular matrix proteins, enzymes, and growth factors, and expression of associated genes have been evaluated via quantitative PCR, mass spectrometry, and RNA sequencing. These techniques have identified regulatory factors, age-dependent metabolic activity, and novel biomarkers of OA[118–120]. Experimental metabolomic data has been combined with computational modeling to analyze and predict the metabolic response of chondrocytes to dynamic compression[121]. Effects of loading have also been evaluated by monitoring mitochondrial respiration, depolarization, and release of reactive oxygen species, all by commercially available kits[79,107,109]. Calcium signaling and transient receptor potential vanilloid (TRPV) channel activity, nonspecific indicators of metabolic activity, have been monitored in situ to gain further insight into the process of cartilage mechanotransduction[122].

Although informative, previous methods of evaluating chondrocyte metabolism do not allow real-time, non-destructive evaluation of specific metabolic pathways, and are therefore limited in their capacity to analyze longitudinal mechanobiological activity. Conversely, OMI does meet these criteria and has been successfully applied to other tissues[114,123–125]. Innovation and adaptation of methods such as these for use in cartilage are key to gaining a better understanding of the

interplay between cartilage metabolism, function, and pathology.

1.3. Objectives

The overarching aim of this dissertation was to establish models capable of determining the relationships between maturation, mechanical loading, metabolism, and tissue health in cartilage. This work was conducted through three specific objectives:

Objective 1: Determine the consequences of maturation on chondrocyte identity and activity. Progenitor cell marker expression, anabolic gene expression, and baseline metabolic redox activity were analyzed in porcine cartilage samples representing a broad maturation spectrum ranging from neonatal to aged. *Chapter 2* and *Chapter 5* report differential anabolic gene and progenitor cell marker expression, as well as differential baseline metabolic activity across the maturation spectrum, with aged samples demonstrating redox activity reminiscent of pre-adolescence.

Objective 2: Develop an experimental system capable of observing the real-time effects of loading on cartilage metabolism and analyze loading rate- and age-dependent sensitivity to compression with respect to redox ratio metrics, gene expression, and progenitor functionality. OMI was adapted for use in cartilage to assess the real-time effects of mechanical loading following delivery of both slow, non-injurious and rapid, injurious loading. Progenitor cell marker expression and anabolic gene expression were also analyzed in samples subjected to a fast-rate load. *Chapter 2* describes enhanced sensitivity to mechanically induced changes in gene expression in pre-adolescent samples compared to older tissues. *Chapter 3* demonstrates the ability of optical redox imaging to capture temporary metabolic flux in cartilage explants immediately following application of a slow physiological compression. *Chapter 4* builds upon this work by imaging the metabolic effects of a fast-rate injurious impact load, detecting time- and dose-dependent effects different from those resulting from slow non-injurious compression.

Objective 3: Identify the downstream implications of metabolic redox activity for tissue health. Baseline metabolic redox status was imaged in cartilage ranging from neonatal to aged maturation status, and samples were then histologically scored for overall tissue health. The effects of metabolic inhibition, and thereby shifted redox activity, on gene expression were assessed for a suite of anabolic and catabolic genes pertinent to cartilage maintenance. *Chapter 5* presents data showing suppressed expression of select cartilage maintenance genes, both anabolic and catabolic in nature, as a result of glycolysis inhibition.

1.4. References

1. Sophia Fox AJ, Bedi A, Rodeo SA. 2009. The basic science of articular cartilage: structure, composition, and function. Sports Health 1(6):461–8.
2. Boettcher K, Kienle S, Nachtsheim J, et al. 2016. The structure and mechanical properties of articular cartilage are highly resilient towards transient dehydration.
3. Hayes WC, Mockros LF. 1971. Viscoelastic properties of human articular cartilage. Appl. Physiol. 4.
4. Han G, Hess C, Eriten M, Henak CR. 2018. Uncoupled poroelastic and intrinsic viscoelastic dissipation in cartilage. J. Mech. Behav. Biomed. Mater. 84:28–34.
5. Jadin KD, Wong BL, Bae WC, et al. 2005. Depth-varying density and organization of chondrocytes in immature and mature bovine articular cartilage assessed by 3d imaging and analysis. J. Histochem. Cytochem. 53(9):1109–19.
6. Bartell LR, Xu MC, Bonassar LJ, Cohen I. 2018. Local and global measurements show that damage initiation in articular cartilage is inhibited by the surface layer and has significant rate dependence. J. Biomech. 72:63–70.

7. Monsour JM. 2013. Biomechanics of Cartilage. In: Lupash EJ, Klingler AM, Carmen M, et al., editors. Kinesiology: The Mechanics and Pathomechanics of Human Movement, 2nd ed. Baltimore, MD: Lippincott Williams & Wilkins. p 69–83.

8. Luo Y, Sinkeviciute D, He Y, et al. 2017. The minor collagens in articular cartilage. Protein Cell 8(8):560–572.

9. Alexopoulos LG, Setton LA, Guilak F. 2005. The biomechanical role of the chondrocyte pericellular matrix in articular cartilage. Acta Biomater. 1(3):317–325.

10. Peters HC, Otto TJ, Enders JT, et al. 2011. The protective role of the pericellular matrix in chondrocyte apoptosis. Tissue Eng. Part A 17(15–16):2017–24.

11. Goldring MB. 2012. Chondrogenesis, chondrocyte differentiation, and articular cartilage metabolism in health and osteoarthritis. Ther. Adv. Musculoskelet. Dis. 4(4):269–85.

12. Singh P, Marcu KB, Goldring MB, Otero M. 2018. Phenotypic instability of chondrocytes in osteoarthritis: on a path to hypertrophy. Ann. N. Y. Acad. Sci. .

13. Tchetina E V., Markova GA. 2018. Regulation of energy metabolism in the growth plate and osteoarthritic chondrocytes. Rheumatol. Int. 38:1–12.

14. Fukui N, Ikeda Y, Ohnuki T, et al. 2008. Regional differences in chondrocyte metabolism in osteoarthritis: A detailed analysis by laser capture microdissection. Arthritis Rheum. 58(1):154–163.

15. Bevill SL, Boyer KA, Andriacchi TP. 2014. The regional sensitivity of chondrocyte gene expression to coactive mechanical load and exogenous TNF-α stimuli. J. Biomech. Eng. 136(9):091005.

16. Waller K a, Zhang LX, Elsaid K a, et al. 2013. Role of lubricin and boundary lubrication in the prevention of chondrocyte apoptosis. Proc. Natl. Acad. Sci. U. S. A. 110(15).

17. Jay GD, Waller KA. 2014. The biology of Lubricin: Near frictionless joint motion. Matrix Biol. 39:17–24.

18. Schmidt TA, Gastelum NS, Han EH, et al. 2008. Differential regulation of proteoglycan 4 metabolism in cartilage by IL-1α, IGF-I, and TGF-β1. Osteoarthr. Cartil. 16(1):90–97.

19. Kozhemyakina E, Zhang M, Ionescu A, et al. 2015. Identification of a Prg4 -expressing articular cartilage progenitor cell population in mice. Arthritis Rheumatol. 67(5):1261–1273.

20. Jørgensen AEM, Kjær M, Heinemeier KM. 2017. The effect of aging and mechanical loading on the metabolism of articular cartilage. J. Rheumatol. :jrheum.160226.

21. Loeser RF, Goldring SR, Scanzello CR, Goldring MB. 2012. Osteoarthritis: A disease of the joint as an organ. Arthritis Rheum. 64(6):1697–1707.

22. Sokolove J, Lepus CM. 2013. Role of inflammation in the pathogenesis of osteoarthritis: Latest findings and interpretations. Ther. Adv. Musculoskelet. Dis. 5(2):77–94.

23. Kloppenburg M, Berenbaum F. 2020. Osteoarthritis year in review 2019: epidemiology and therapy. Osteoarthr. Cartil. 28(3):242–248.

24. Litwic A, Edwards MH, Dennison EM, Cooper C. 2013. Epidemiology and burden of osteoarthritis. Br. Med. Bull. 105(1):185–199.

25. Cross M, Smith E, Hoy D, et al. 2014. The global burden of hip and knee osteoarthritis: estimates from the Global Burden of Disease 2010 study. Ann. Rheum. Dis. 73(7):1323–1330.

26. Mence Palazzo C, Ravaud J-F, Papelard A, et al. 2014. The burden of musculoskeletal conditions.

27. Woolf AD, Pfleger B. 2003. Burden of major musculoskeletal conditions. Bull. World

Health Organ. 81(9):646–656.

28. Wallace IJ, Worthington S, Felson DT, et al. 2017. Knee osteoarthritis has doubled in prevalence since the mid-20th century. Proc. Natl. Acad. Sci. U. S. A. 114(35):9332–9336.
29. Abhishek A, Doherty M. 2013. Diagnosis and clinical presentation of osteoarthritis. Rheum. Dis. Clin. North Am. 39(1):45–66.
30. Nieminen MT, Casula V, Nevalainen MT, Saarakkala S. 2019. Osteoarthritis year in review 2018: imaging. Osteoarthr. Cartil. 27(3):401–411.
31. Swagerty DL, Hellinger D. 2001. Radiographic assessment of osteoarthritis. Am. Fam. Physician 64(2):279–286.
32. Parsons C, Fuggle NR, Edwards MH, et al. 2018. Concordance between clinical and radiographic evaluations of knee osteoarthritis. Aging Clin. Exp. Res. 30(1):17–25.
33. Kaukinen P, Podlipská J, Guermazi A, et al. 2017. Magnetic resonance imaging (MRI)-defined cartilage degeneration and joint pain are associated with poor physical function in knee osteoarthritis – the Oulu Knee Osteoarthritis study. Osteoarthr. Cartil. 25(11):1829–1840.
34. Bashir A, Gray ML, Hartke J, Burstein D. 1999. Nondestructive imaging of human cartilage glycosaminoglycan concentration by MRI. Magn. Reson. Med. 41(5):857–865.
35. Ike RW. 1993. The role of arthroscopy in the differential diagnosis of osteoarthritis of the knee. Rheum. Dis. Clin. North Am. 19(3):673–96.
36. Von Engelhardt L V., Lahner M, Klussmann A, et al. 2010. Arthroscopy vs. MRI for a detailed assessment of cartilage disease in osteoarthritis: Diagnostic value of MRI in clinical practice. BMC Musculoskelet. Disord. 11(1):75.
37. Zhang Y, Jordan JM. 2008. Epidemiology of osteoarthritis. Rheum Dis Clin North Am

34(3):515–529.

38. Paradowski PT, Englund M, Lohmander LS, Roos EM. 2005. The effect of patient characteristics on variability in pain and function over two years in early knee osteoarthritis. Health Qual. Life Outcomes 3:59.

39. Leopoldino AO, MacHado GC, Ferreira PH, et al. 2019. Paracetamol versus placebo for knee and hip osteoarthritis. Cochrane Database Syst. Rev. 2019(2).

40. Baigent C, Bhala N, Emberson J, et al. 2013. Vascular and upper gastrointestinal effects of non-steroidal anti-inflammatory drugs: Meta-analyses of individual participant data from randomised trials. Lancet 382(9894):769–779.

41. Bennell KL, Hunter DJ, Paterson KL. 2017. Platelet-rich plasma for the management of hip and knee osteoarthritis. Curr. Rheumatol. Rep. 19(5):1–10.

42. Muchedzi TA, Roberts SB. 2018. A systematic review of the effects of platelet rich plasma on outcomes for patients with knee osteoarthritis and following total knee arthroplasty. Surgeon 16(4):250–258.

43. Xing D, Wang Q, Yang Z, et al. 2018. Mesenchymal stem cells injections for knee osteoarthritis: a systematic overview. Rheumatol. Int. 38(8):1399–1411.

44. Yen YM, Cascio B, O'Brien L, et al. 2008. Treatment of osteoarthritis of the knee with microfracture and rehabilitation. Med. Sci. Sports Exerc. 40(2):200–205.

45. Lee JJ, Lee SJ, Lee TJ, et al. 2013. Results of microfracture in the osteoarthritic knee with focal full-thickness articular cartilage defects and concomitant medial meniscal tears. Knee Surg. Relat. Res. 25(2):71–76.

46. Kraeutler MJ, Belk JW, Purcell JM, McCarty EC. 2017. Microfracture versus autologous chondrocyte implantation for articular cartilage lesions in the knee: A systematic review of

5-year outcomes. Am. J. Sports Med. :036354651770191.

47. Gou G-H, Tseng F-J, Wang S-H, et al. 2019. Autologous Chondrocyte Implantation Versus Microfracture in the Knee: A Meta-Analysis and Systematic Review. Arthrosc. J. Arthrosc. Relat. Surg. .

48. De Bari C, Roelofs AJ. 2018. Stem cell-based therapeutic strategies for cartilage defects and osteoarthritis. Curr. Opin. Pharmacol. 40:74–80.

49. Mandl LA. 2019. Osteoarthritis year in review 2018: clinical. Osteoarthr. Cartil. 27(3):359–364.

50. Julkunen P, Iivarinen J, Brama PA, et al. 2010. Maturation of collagen fibril network structure in tibial and femoral cartilage of rabbits. Osteoarthr. Cartil. 18(3):406–415.

51. Julkunen P, Harjula T, Iivarinen J, et al. 2009. Biomechanical, biochemical and structural correlations in immature and mature rabbit articular cartilage. Osteoarthr. Cartil. 17:1628–1638.

52. Oinas J, Ronkainen AP, Rieppo L, et al. 2018. Composition, structure and tensile biomechanical properties of equine articular cartilage during growth and maturation. Sci. Rep. 8(1):1–12.

53. Rieppo J, Hyttinen MM, Halmesmaki E, et al. 2009. Changes in spatial collagen content and collagen network architecture in porcine articular cartilage during growth and maturation. Osteoarthr. Cartil. 17(4):448–455.

54. Meachim G. 1971. Effect of age on the thickness of adult articular cartilage at the shoulder joint. Ann. Rheum. Dis. 30(1):43–46.

55. Singh M, Detamore MS. 2008. Tensile properties of the mandibular condylar cartilage. J. Biomech. Eng. 130(1).

56. Tanaka E, Yamano E, Dalla-Bona DA, et al. 2006. Dynamic compressive properties of the mandibular condylar cartilage. J. Dent. Res. 85(6):571–575.

57. Mansfield JC, Bell JS, Winlove CP. 2015. The micromechanics of the superficial zone of articular cartilage. Osteoarthr. Cartil. 23(10):1806–1816.

58. Otsuki S, Grogan SP, Miyaki S, et al. 2010. Tissue neogenesis and STRO-1 expression in immature and mature articular cartilage. J. Orthop. Res. 28(1):96–102.

59. Mukoyama S, Sasho T, Akatsu Y, et al. 2015. Spontaneous repair of partial thickness linear cartilage injuries in immature rats. Cell Tissue Res. 359(2):513–20.

60. Brown S, Hornyak J, Jungels R, et al. 2019. Characterization of post-traumatic osteoarthritis in rats following ACL rupture by non-invasive knee injury (NIKI). J. Orthop. Res. :jor.24470.

61. Dare D, Rodeo S. 2014. Mechanisms of post-traumatic osteoarthritis after ACL injury. Curr. Rheumatol. Rep. 16(10):448.

62. Barton KI, Shekarforoush M, Heard BJ, et al. 2017. Use of pre-clinical surgically induced models to understand biomechanical and biological consequences of PTOA development. J. Orthop. Res. 35(3):454–465.

63. Rai MF, Duan X, Quirk JD, et al. 2017. Post-Traumatic Osteoarthritis in Mice Following Mechanical Injury to the Synovial Joint. Sci. Rep. 7:45223.

64. Culley KL, Dragomir CL, Chang J, et al. 2015. Mouse models of osteoarthritis: Surgical model of posttraumatic osteoarthritis induced by destabilization of the medial meniscus. Methods Mol. Biol. 1226:143–173.

65. Bolam CJ, Hurtig MB, Cruz A, McEwen BJE. 2006. Characterization of experimentally induced post-traumatic osteoarthritis in the medial femorotibial joint of horses. Am. J. Vet.

Res. 67(3):433–447.

66. Carter TE, Taylor KA, Spritzer CE, et al. 2015. In vivo cartilage strain increases following medial meniscal tear and correlates with synovial fluid matrix metalloproteinase activity. J. Biomech. 48(8):1461–8.

67. Takahashi I, Matsuzaki T, Kuroki H, Hoso M. 2018. Induction of osteoarthritis by injecting monosodium iodoacetate into the patellofemoral joint of an experimental rat model. PLoS One 13(4):e0196625.

68. Jiang L, Li L, Geng C, et al. 2013. Monosodium iodoacetate induces apoptosis via the mitochondrial pathway involving ROS production and caspase activation in rat chondrocytes in vitro. J. Orthop. Res. 31(3):364–369.

69. Liu H, Zhao Z, Clarke RB, et al. 2013. Enhanced tissue regeneration potential of juvenile articular cartilage. Am. J. Sports Med. 41(11):2658–2667.

70. Ribitsch I, Mayer RL, Egerbacher M, et al. 2018. Fetal articular cartilage regeneration versus adult fibrocartilaginous repair: secretome proteomics unravels molecular mechanisms in an ovine model. Dis. Model. Mech. 11(7):dmm033092.

71. Tran-Khanh N, Hoemann CD, McKee MD, et al. 2005. Aged bovine chondrocytes display a diminished capacity to produce a collagen-rich, mechanically functional cartilage extracellular matrix. J. Orthop. Res. 23(6):1354–62.

72. Adkisson HD, Martin JA, Amendola RL, et al. 2010. The potential of human allogeneic juvenile chondrocytes for restoration of articular cartilage. Am. J. Sports Med. 38(7):1324–33.

73. Martin JA, Buckwalter JA. 2002. Aging, articular cartilage chondrocyte senescence and osteoarthritis. Biogerontology 3(5):257–264.

74. Vinatier C, Domínguez E, Guicheux J, Caramés B. 2018. Role of the inflammation-autophagy-senescence integrative network in Osteoarthritis. Front. Physiol. 9(JUN).

75. Samsudin EZ, Kamarul T. 2016. The comparison between the different generations of autologous chondrocyte implantation with other treatment modalities: a systematic review of clinical trials. Knee Surgery, Sport. Traumatol. Arthrosc. 24(12):3912–3926.

76. DiDomenico CD, Lintz M, Bonassar LJ. 2018. Molecular transport in articular cartilage — what have we learned from the past 50 years? Nat. Rev. Rheumatol. 14(7):393–403.

77. Zhang L, Szeri AZ. 2008. Transport of neutral solute in articular cartilage: Effect of microstructure anisotropy. J. Biomech. 41(2):430–437.

78. Salinas D, Mumey BM, June RK. 2018. Physiological dynamic compression regulates central energy metabolism in primary human chondrocytes. Biomech. Model. Mechanobiol. :1–9.

79. Brouillette MJ, Ramakrishnan PS, Wagner VM, et al. 2014. Strain-dependent oxidant release in articular cartilage originates from mitochondria. Biomech. Model. Mechanobiol. 13(3):565–72.

80. Madden RMJ, Han S-K, Herzog W. 2015. The effect of compressive loading magnitude on in situ chondrocyte calcium signaling. Biomech. Model. Mechanobiol. 14(1):135–142.

81. Repo RU, Finlay JB. 1977. Survival of articular cartilage after controlled impact. J. Bone Joint Surg. Am. 59(8):1068–76.

82. Finlay JB, Repo RU. 1978. Impact characteristics of articular cartilage. ISA Trans. 17(1):29–34.

83. Vrahas MS, Smith GA, Rosler DM, Baratta R V. 1997. Method to impact in vivo rabbit femoral cartilage with blows of quantifiable stress. J. Orthop. Res. 15(2):314–317.

84. Jeffrey JE, Thomson LA, Aspden RM. 1997. Matrix loss and synthesis following a single impact load on articular cartilage in vitro. Biochim. Biophys. Acta 1334(2–3):223–32.

85. Kaplan JT, Neu CP, Drissi H, et al. 2017. Cyclic loading of human articular cartilage: The transition from compaction to fatigue. J. Mech. Behav. Biomed. Mater. 65:734–742.

86. Riemenschneider PE, Rose MD, Giordani M, McNary SM. 2019. Compressive fatigue and endurance of juvenile bovine articular cartilage explants. J. Biomech. :109304.

87. Vazquez KJ, Andreae JT, Henak CR. 2019. Cartilage-on-cartilage cyclic loading induces mechanical and structural damage. J. Mech. Behav. Biomed. Mater. 98:262–267.

88. Verteramo A, Seedhom BB. 2007. Effect of a single impact loading on the structure and mechanical properties of articular cartilage. J. Biomech. 40(16):3580–3589.

89. Burgin L V., Aspden RM. 2008. Impact testing to determine the mechanical properties of articular cartilage in isolation and on bone. J. Mater. Sci. Mater. Med. 19(2):703–711.

90. Duda GN, Eilers M, Loh L, et al. 2001. Chondrocyte death precedes structural damage in blunt impact trauma. Clin. Orthop. Relat. Res. (393):302–9.

91. Aspden RM, Jeffrey JE, Burgin LV. 2002. Letter to the editor. Osteoarthr. Cartil. 10(7):588–589.

92. Radin EL, Paul IL, Lowy M. 1970. A comparison of the dynamic force transmitting properties of subchondral bone and articular cartilage. J. Bone Joint Surg. Am. 52(3):444–56.

93. Delco ML, Goodale M, Talts JF, et al. 2020. Integrin α10β1-selected mesenchymal stem cells mitigate the progression of osteoarthritis in an equine talar impact model. Am. J. Sports Med. 48(3):612–623.

94. Milentijevic D, Rubel IF, Liew ASL, et al. 2005. An in vivo rabbit model for cartilage

trauma: A preliminary study of the influence of impact stress magnitude on chondrocyte death and matrix damage. J. Orthop. Trauma :466–473.

95. Kuyinu EL, Narayanan G, Nair LS, Laurencin CT. 2016. Animal models of osteoarthritis: classification, update, and measurement of outcomes. J. Orthop. Surg. Res. 11(1):19.

96. Christiansen BA, Guilak F, Lockwood KA, et al. 2015. Non-invasive mouse models of post-traumatic osteoarthritis. Osteoarthr. Cartil. 23(10):1627–1638.

97. Waldstein W, Perino G, Gilbert SL, et al. 2016. OARSI osteoarthritis cartilage histopathology assessment system: A biomechanical evaluation in the human knee. J. Orthop. Res. 34(1).

98. McIlwraith CW, Frisbie DD, Kawcak CE, et al. 2010. The OARSI histopathology initiative – recommendations for histological assessments of osteoarthritis in the horse. Osteoarthr. Cartil. 18:S93–S105.

99. Agathocleous M, Harris WA. 2013. Metabolism in physiological cell proliferation and differentiation. Trends Cell Biol. 23(10):484–492.

100. Warburg O. 1956. On the origin of cancer cells. Science 123(3191):309–14.

101. Alhallak K, Rebello LG, Muldoon TJ, et al. 2016. Optical redox ratio identifies metastatic potential-dependent changes in breast cancer cell metabolism. Biomed. Opt. Express 7(11):4364–4374.

102. Hou J, Wright HJ, Chan N, et al. 2016. Correlating two-photon excited fluorescence imaging of breast cancer cellular redox state with seahorse flux analysis of normalized cellular oxygen consumption. J. Biomed. Opt. 21(6):60503.

103. Ballock RT, O'Keefe RJ. 2003. Physiology and pathophysiology of the growth plate. Birth Defects Res. Part C Embryo Today Rev. 69(2):123–143.

104. Drevet S, Gavazzi G, Grange L, et al. 2018. Reactive oxygen species and NADPH oxidase 4 involvement in osteoarthritis. Exp. Gerontol. 111:107–117.

105. Nishida T, Kubota S, Aoyama E, Takigawa Yz M. 2013. Impaired glycolytic metabolism causes chondrocyte hypertrophy-like changes via promotion of phospho-Smad1/5/8 translocation into nucleus. Osteoarthr. Cartil. .

106. Mobasheri A, Vannucci SJ, Bondy CA, et al. 2002. Glucose transport and metabolism in chondrocytes: a key to understanding chondrogenesis, skeletal development and cartilage degradation in osteoarthritis. Histol. Histopathol. 17(4):1239–67.

107. Delco ML, Bonnevie ED, Bonassar LJ, Fortier LA. 2017. Mitochondrial dysfunction is an acute response of articular chondrocytes to mechanical injury. J. Orthop. Res. 36(2):739–750.

108. Martin JA, McCabe D, Walter M, et al. 2009. N-Acetylcysteine inhibits post-impact chondrocyte death in osteochondral explants. J. Bone Jt. Surgery-American Vol. 91(8):1890–1897.

109. Coleman MC, Ramakrishnan PS, Brouillette MJ, Martin JA. 2016. Injurious loading of articular cartilage compromises chondrocyte respiratory function. Arthritis Rheumatol. 68(3):662–671.

110. Yagi R, McBurney D, Laverty D, et al. 2005. Intrajoint comparisons of gene expression patterns in human osteoarthritis suggest a change in chondrocyte phenotype. J. Orthop. Res. 23(5):1128–1138.

111. Kirsch T, Swoboda B, Nah HD. 2000. Activation of annexin II and V expression, terminal differentiation, mineralization and apoptosis in human osteoarthritic cartilage. Osteoarthr. Cartil. 8(4):294–302.

112. Robertson CM, Pennock AT, Harwood FL, et al. 2006. Characterization of pro-apoptotic and matrix-degradative gene expression following induction of osteoarthritis in mature and aged rabbits. Osteoarthr. Cartil. 14(5):471–476.

113. Pullig O, Weseloh G, Ronneberger DL, et al. 2000. Chondrocyte differentiation in human osteoarthritis: Expression of osteocalcin in normal and osteoarthritic cartilage and bone. Calcif. Tissue Int. 67(3):230–240.

114. Skala M, Ramanujam N. 2010. Multiphoton redox ratio imaging for metabolic monitoring in vivo. Methods Mol. Biol. 594:155–62.

115. Shah AT, Heaster TM, Skala MC. 2017. Metabolic imaging of head and neck cancer organoids. PLoS One 12(1):1–17.

116. Walsh AJ, Castellanos JA, Nagathihalli NS, et al. 2016. Optical imaging of drug-induced metabolism changes in murine and human pancreatic cancer organoids reveals heterogeneous drug response. Pancreas 45(6):863–9.

117. Adavallan K, Gurushankar K, Nazeer SS, et al. 2017. Optical redox ratio using endogenous fluorescence to assess the metabolic changes associated with treatment response of bioconjugated gold nanoparticles in streptozotocin-induced diabetic rats. Laser Phys. Lett. 14(6):065901.

118. Dai J, Yu D, Wang Y, et al. 2017. Kdm6b regulates cartilage development and homeostasis through anabolic metabolism. Ann. Rheum. Dis. 76(7):1295–1303.

119. Kahn MK, Coverdale JA, Leatherwood JL, et al. 2017. Age-related effects on markers of inflammation and cartilage metabolism in response to an intra-articular lipopolysaccharide challenge in horses. J. Anim. Sci. 95(2):671.

120. Sanchez C, Bay-Jensen A-C, Pap T, et al. 2017. Chondrocyte secretome: a source of novel

insights and exploratory biomarkers of osteoarthritis. Osteoarthr. Cartil. .

121. Salinas D, Minor CA, Carlson RP, et al. 2017. Combining targeted metabolomic data with a model of glucose metabolism: toward progress in chondrocyte mechanotransduction. PLoS One 12(1):e0168326.

122. Han S-K, Wouters W, Clark A, Herzog W. 2012. Mechanically induced calcium signaling in chondrocytes in situ. J. Orthop. Res. 30(3):475–481.

123. Rice WL, Kaplan DL, Georgakoudi I. 2010. Two-photon microscopy for non-invasive, quantitative monitoring of stem cell differentiation. PLoS One 5(4):e10075.

124. Quinn KP, Bellas E, Fourligas N, et al. 2012. Characterization of metabolic changes associated with the functional development of 3D engineered tissues by non-invasive, dynamic measurement of individual cell redox ratios. Biomaterials 33(21):5341–8.

125. Frikha-Benayed D, Basta-Pljakic J, Majeska RJ, Schaffler MB. 2016. Regional differences in oxidative metabolism and mitochondrial activity among cortical bone osteocytes. Bone 90:15–22.

Chapter 2: Maturity-Dependent Cartilage Cell Plasticity and Sensitivity to External Perturbation*

Shannon K. Walsh, Stephanie E. Schneider, Laura A. Amundson, PhD,

Corey P. Neu, PhD, Corinne R. Henak, PhD

*(*Reprinted with permission from the Journal of Mechanical Behavior of Biomedical Materials)*

2.1. Abstract

OBJECTIVE: Articular cartilage undergoes biological and morphological changes throughout maturation. The prevalence of osteoarthritis in the aged population suggests that maturation predisposes cartilage to degradation and/or impaired regeneration, but this process is not fully understood. Therefore, the objective of this study was to characterize the cellular and genetic profile of cartilage, as well as biological plasticity in response to mechanical and culture time stimuli, as a function of animal maturity. METHODS/DESIGN: Porcine articular cartilage explants were harvested from stifle joints of immature (2-4 weeks), adolescent (5-6 months), and mature (1-5 years) animals. Half of all samples were subjected to a single compressive mechanical load. Loaded samples were paired with unloaded controls for downstream analyses. Expression of cartilage progenitor cell markers CD105, CD44, and CD29 were determined via flow cytometry. Expression of matrix synthesis genes Col1, Col2, Col10, ACAN, and SOX9 were determined via qPCR. Tissue morphology and matrix content were examined histologically. Post-loading assays were performed immediately and following 7 days in culture. RESULTS: CD105 and CD29 expression decreased with maturity, while CD44 expression was upregulated in cartilage from mature animals. Expression of matrix synthesis genes were generally upregulated in cartilage from mature animals, and adolescent animals showed the lowest expression of several matrix

synthesizing genes. Culture time and mechanical loading analyses revealed greater plasticity to mechanical loading and culture time in cartilage from younger animals. Histology confirmed distinct structural and biochemical profiles across maturity. CONCLUSION: This study demonstrates differential, nonlinear expression of chondroprogenitor markers and matrix synthesis genes as a function of cartilage maturity, as well as loss of biological plasticity in aged tissue. These findings have likely implications for age-related loss of regeneration and osteoarthritis progression.

Keywords: articular cartilage, plasticity, progenitor cells, aging, osteoarthritis

2.2. Introduction

Articular cartilage, a mechanically loaded tissue, is at high risk for degeneration and ultimately osteoarthritis (OA). OA can result from a single traumatic mechanical overload, but more commonly results from chronic overload over decades[1,2]. Once damaged, cartilage from skeletally mature animals is unable to regenerate. However, cartilage in juvenile animals has some capacity for self-repair, demonstrated by tissue neogenesis at damage sites not observed in mature samples[3,4]. Current OA treatments serve to ameliorate symptoms such as pain and immobility but are unable to prevent or reverse disease progression[5]. Understanding the biological underpinnings of this maturity-dependent regeneration disparity is an important first step in developing effective OA therapies. Mechanical loading is inherent in the synovial joints where cartilage resides and cartilage is mechanosensitive, thus, mechanical loading serves as a potentially important target for enhancing therapies.

Articular cartilage undergoes changes during maturation that likely hinder tissue regeneration in mature animals. Skeletally immature cartilage is thicker, softer and less structurally organized with relatively higher proteoglycan content and lower collagen content than mature cartilage[4,6,7 8–11]. Chondrocytes experience phenotype changes throughout maturation as cells from immature tissue favor expression of genes associated with growth and expansion while mature tissue cells favor relatively greater expression of genes associated with matrix structural integrity[4]. Unsurprisingly, previous studies have provided evidence of immature tissue containing more cells considered to be chondrogenic progenitor cells than mature tissue[3,12]. Furthermore, comparisons of chondrocytes from juvenile and aged individuals have demonstrated maturity-dependent tissue regeneration capability, attributed in part to differential expression of genes and proteins associated with stem and progenitor cell maintenance[4,13,14]. Plasticity, which describes the ability of cells to respond to various environmental stimuli including mechanical loading, has also demonstrated age-related reduction in articular chondrocytes[15–18]. Several studies have associated enhanced chondrocyte plasticity with heightened regenerative capacity both in vitro and in vivo, suggesting alterations in plasticity could have important implications in how cartilage from older animals is able to respond to therapeutic intervention[16,19,20].

Although several maturity-dependent properties of cartilage have been described, the specific properties responsible for loss of regenerative function in aged cartilage remain unknown[3,4,6,12]. Thus, the present study evaluated cartilage from three distinct maturity groups to test the following hypotheses: a) chondrocytes exhibit distinct maturity-dependent patterns of progenitor cell markers and matrix synthesis genes, and b) cartilage demonstrates maturity-dependent plasticity in response to the stimuli of mechanical loading and culture time. Cartilage explants were subjected to mechanical loading followed by immediate and day 7 analyses of post-loading

activity, including expression of select chondrogenic progenitor cell markers and matrix protein-related genes. Chondrocyte progenitor surface markers CD44 and CD29 are cell adhesion molecules, and CD105, also known as endoglin, is a component of the transforming growth factor beta (TGF-β) receptor complex[21–23].

2.3. Methods

2.3.1. Sample Harvest

Samples were harvested from immature (n=5, 2-4 weeks), adolescent (n=7, 5-6 months), and mature (n=6, 1-5 years) pigs. For simplicity, the remainder of this manuscript will use immature, adolescent, and mature cartilage to refer to the cartilage and cells from animals of these respective maturity groups. All samples were obtained following euthanasia (IACUC protocol A005856) or from a local abattoir. Full-thickness 6 mm diameter samples were harvested from the articular cartilage of the stifle joint using a biopsy punch and a scalpel. From each adolescent and mature joint, approximately 6 retropatellar samples and 10 femoral samples were harvested. From each immature joint, approximately 2 retropatellar samples, 3 femoral samples, and 3 tibial samples were harvested. The number of assays performed required sample harvest from multiple joint surfaces, and surface area constraints of immature animals necessitated inclusion of tibial samples to achieve sufficient sample numbers. Samples were stored in chondrocyte media containing Ham's F-12 media (Mediatech, Inc., Manassas, VA), 10% fetal bovine serum (Hyclone, GE Healthcare Bio-Sciences, Pittsburgh, PA), 50 μg/ml ascorbic acid (Amresco, LLC., Solon, OH), 30 μg/ml alpha-ketoglutaric acid (Thermo Fisher Scientific Chemicals, Inc., Waltham, MA), 300 μg/ml L-glutamine, 100 IU/ml penicillin G, 100 μg/ml streptomycin, and 6 mg/ml HEPES buffer (Corning, Inc., Corning, NY) at 4°C until use. All samples were used within 10 hours of collection. Immature samples (typically greater than 2 mm thick) were trimmed to 2 mm to remove

subchondral bone and create an even loading surface. Similarly, uneven adolescent and mature samples (typically less than 2 mm thick) greater than 1 mm were trimmed to a thickness of 1 mm to provide an even surface for loading without disruption of the deep zone.

2.3.2. Mechanical Loading

Samples were randomly designated to be mechanically loaded or unloaded controls (Figure 1). Loaded samples were paired with controls from the same articular surface. Samples were removed from media, sample thickness was measured using digital calipers, and samples were adhered on the subchondral side to a metal backplate with cyanoacrylate. The backplate was inserted into a well and submerged in Dulbecco's phosphate buffered saline (DPBS). This process took less than 5 minutes, and samples were given a 5-minute recovery period once submerged. A glass loading platen spanning the entire sample surface was used to deliver a single compressive load via tabletop test machine (TA Instruments 3230-AT Series III); load was detected by a 100 lb load cell (TA Instruments, 100 lbf/50.6 in-lb). Once in contact with the sample, determined by detection of a load greater than 0 N (< 0.1 N), samples were subjected to a target waveform of 0.6 strain at 10 s^{-1} strain rate. Loading parameters were chosen to model a single superphysiological load without causing the level of macroscopic damage associated with traumatic impact[24,25]. Control samples were glued next to loaded samples but were not under the loading platen. Loaded samples received compressive strain ranging from 0.11-0.52 and 0.08-5.27 MPa stress.

Following mechanical loading, cell viability was assessed in a subset of samples to confirm mechanical loading was not causing substantial cell death that would preclude interpretation of downstream analyses. Loaded samples exhibited a greater percentage of cell death than unloaded samples averaged across maturity groups and time points (27.4% ± 20.0% vs. 15.7% ± 12.3%)

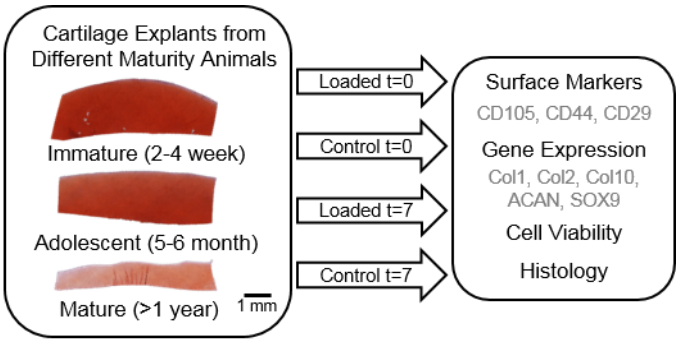

Figure 2-1. Schematic overview of study design.

(Supplementary Figure 1). Additionally, samples cultured for t=7 days demonstrated greater cell death than t=0 samples (31.3% ± 19.2% vs. 15.0% ± 12.9%) (Supplementary Figure 1).

2.3.3. Flow Cytometry

Cell phenotypes were characterized using flow cytometry. Three to four pairs of samples per animal were designated for flow cytometry analysis and were pooled by loading condition and subjected to a 15-hour digest at 37°C to isolate cells immediately post-loading. Three to four additional pairs of samples were incubated for 1 week (37°C, 5% CO_2) post-loading prior to cell isolation. Digest media consisted of 0.75% type IV collagenase (MP Biomedicals, LLC, Santa Ana, CA) in chondrocyte media. After digestion, each cell suspension was passed through a 40 μm cell strainer and incubated with 1% Ghost Dye Violet 510 (Tonbo Biosciences, Inc., San Diego, CA) for exclusion of dead cells. Samples were then stained with the following fluorophore-conjugated antibodies: 2.5 ng ml^{-1} CD45 PerCP-Cy5.5 (clone: HI30), 2 μg ml^{-1} CD44 APC-Cy7 (clone: IM7), 5 μg ml^{-1} CD34 FITC (clone: 581, BioLegend, San Diego, CA), 2.5% CD105 PE (clone: MEM-229, Abcam, Cambridge, MA), 2 μg ml^{-1} CD29 Alexa647 (clone: NaM160-1A3, BD Biosciences, San Jose, CA), and 2 μg ml^{-1} Stro-1 Alexa405 (clone: STRO-1, Novus

Biologicals, LLC., Littleton, CO). Porcine reactivity of all antibodies was confirmed by the manufacturer. Samples were run through a MACSQuant10 cytometer and data were processed using FlowJo software v10 (FlowJo, LLC, Ashland, OR). Data were gated to exclude debris, cell aggregates, dead cells, and $CD34^+$ or $CD45^+$ hematopoietic cells. Flow cytometry yielded two types of data: percent of total cells positive for each marker, and median fluorescence intensity (MFI) of each positive population, indicative of degree of marker expression. Stro-1 fluorescence was minimal in all samples; whether this was due to naturally low expression or poor antibody affinity was not confirmed. Stro-1 was included in all flow cytometry panels for consistency, but expression was excluded from final analyses.

2.3.4. Quantitative PCR

Chondrocyte gene expression was quantified using real time RT-qPCR (reverse transcription-quantitative polymerase chain reaction). Primers were custom designed from known porcine gene sequences when possible and predicted sequences when necessary using NCBI Primer-BLAST (Table 1)[26]. Sequences were chosen to span an intron when possible to minimize genomic DNA contamination and to produce a sequence of 50-200 base pairs. Primer pairs with the lowest self-affinity were chosen to reduce likelihood of primer dimer formation.

Two pairs of samples per animal were designated for RT-qPCR analysis, performed immediately post-loading and following 1-week incubation (37°C, 5% CO_2). Samples were snap frozen in liquid nitrogen and stored at -80°C until processing. To isolate total RNA, samples were manually crushed and homogenized in TRIzol (Thermo Fisher Scientific, Waltham, MA) with a handheld tissue homogenizer (Omni International, Kennesaw, GA). Phase separation protein extraction was performed using chloroform (Thermo Fisher Scientific, Waltham, MA) and RNA was extracted using the E.Z.N.A. Tissue RNA Kit column system (Omega Bio-tek, Inc., Norcross,

Table 2-1. Custom-designed qPCR primer sequences.

Gene (Identification)	Forward (f) and Reverse (r) Primer
Col1a1 (XM_013981006.1)	f: TGCTGTTGGTGCTAAGGGTG r: GAGCACCAGCAATACCAGGA
Col2a1 (NC_010447.5)	f: CACAACCCGAACTCAGGACT r: CTCCAATCCGGGCAGAACTC
Col10a1 (NM_001005153.1)	f: GCTCCCAACATCCAGAATCCA r: TGGTGGGCCTTTTATGCCTG
ACAN (NM_001164652.1)	f: AGGTCGTGGTCAAAGGCATC r: TCCAGGGTGTAGCGTGTAGA
SOX9 (NM_213843.1)	f: GGCAAACTCTGGAGACTGCTG r: GATGGCGTTGGGAGAGATGT
PPIA (NM_214353.1)	f: CATGGTTAACCCCACCGTCT r: TCTGCAAACAGCTCGAAGGA
SDHA (DQ402993.1)	f: CCAGGAACACTGTTGTCGCT r: GTAGGGTGGAACTGCACGAA

GA). Complimentary DNA (cDNA) was synthesized from template RNA at a reaction concentration of 0.5 ng/μl using qScript cDNA SuperMix (Quantabio, Beverly, MA) according to manufacturer instructions and stored at -20°C until use. Gene expression analysis was performed using PerfeCTa SYBR Green Fastmix (Quantabio, Beverly, MA) according to manufacturer instructions. A three-step cycling protocol was performed in an Applied Biosystems StepOne Plus (Thermo Fisher Scientific, Inc., Waltham, MA) according to detection kit instructions. Gene expression data (C_T) were standardized to the geometric mean of two housekeeping genes (ΔC_T) and calculated as fold change ($2^{-\Delta\Delta CT}$) from average gene expression of control group. Genes measured for cartilage matrix proteins included collagen type I (Col1), type II (Col2), type X (Col10), and aggrecan (ACAN), and SOX9 was measured as a transcriptional regulator of collagen synthesis[27–30].

Preliminary experiments were conducted to analyze the expression of four candidate housekeeping genes: ACTB, GAPDH, PPIA, and SDHA. Chondrocyte GAPDH mRNA expression was unstable across the 12 sample conditions (3 maturities × 2 loading conditions × 2 time points) and eliminated as a suitable housekeeping gene for this experiment. Chondrocyte

PPIA and SDHA mRNA expression were the most stable across the 12 sample conditions and therefore were the most suitable housekeeping genes for this study. Protocol verification was performed via qPCR analysis of serially-diluted template cDNA to confirm primer and SYBR specificity.

2.3.5. Histology

Qualitative cartilage integrity was histologically evaluated. After loading, one pair of samples per animal was bisected into hemicylinders for histological analysis. One hemicylinder of each sample was immediately fixed in 10% formalin in PBS prior to being processed, embedded, and sectioned onto slides in 4 μm-thick slices. The remaining halves were incubated in chondrocyte media (37°C, 5% CO_2) and fixed one week later. Samples were stained with Hematoxylin (Electron Microscopy Sciences, Hatfield, PA) and Eosin (VWR International, Radnor, PA) (H&E) for gross structural analysis, and with Safranin-O (Thermo Fisher Scientific, Waltham, MA) and Fast Green FCF (MP Biomedicals, LLC, Santa Ana, CA) for proteoglycan content analysis, both according to standard protocols[31]. Stained samples were imaged via bright field microscopy, and were used to assign tissue damage scores on a scale of 0-20 to each sample according to the OARSI microscopic grading system for cell necrosis, chondrone formation, fibrillation and fissuring, focal cell loss, and Safranin O/Fast Green stain uptake[32].

2.3.6. Statistics

The dependence of differential progenitor cell marker and gene expression on animal maturity, sample culture time, and loading condition was evaluated. Percentage and MFI cell marker data and gene expression data were not normally distributed and thus were subjected to nonparametric two-step analyses. For each cell marker of interest, an initial Aligned Rank Transformation (ART) analysis of variance (ANOVA) was performed on both percentage and MFI

data to test the hypothesis that samples would demonstrate differential marker expression as a function of maturity. For each gene of interest, an ART ANOVA was performed on $2^{-\Delta\Delta CT}$ values normalized to the average gene expression of immature samples to test the hypothesis that samples would demonstrate differential gene expression as a function of maturity. Tukey pairwise comparisons were performed post-hoc on significant age effects. A secondary ART ANOVA of time and loading condition within each maturity was then performed on cell marker percentage and MFI data within each maturity group to test the hypotheses that time and loading condition would have an effect on marker expression, and these effects may differ depending on tissue maturity. Likewise, a secondary ART ANOVA of time and loading condition within each maturity was performed on $2^{-\Delta\Delta CT}$ values normalized to the average gene expression of either time=0 or unloaded samples within each maturity group to test the hypotheses that time and loading condition, respectively, would have an effect on gene expression, and these effects may differ depending on tissue maturity.

Histological scoring data were not normally distributed and, thus, were subjected to nonparametric analysis. Total scores were subject to aligned rank transformation and an ART ANOVA was performed to test for the effect of age on cumulative OARSI scores. Tukey post-hoc tests were employed to determine significant pairwise comparisons.

2.4. Results

Cartilage maturity affected cell surface marker expression, gene expression, and matrix content. Of the surface markers, CD105 expression was the most variable between sample groups (Figure 2). Both $CD105^{+}$ percentage and MFI data showed greatest marker expression in immature samples, followed by adolescent and then mature samples. Expression of CD44 and CD29 also

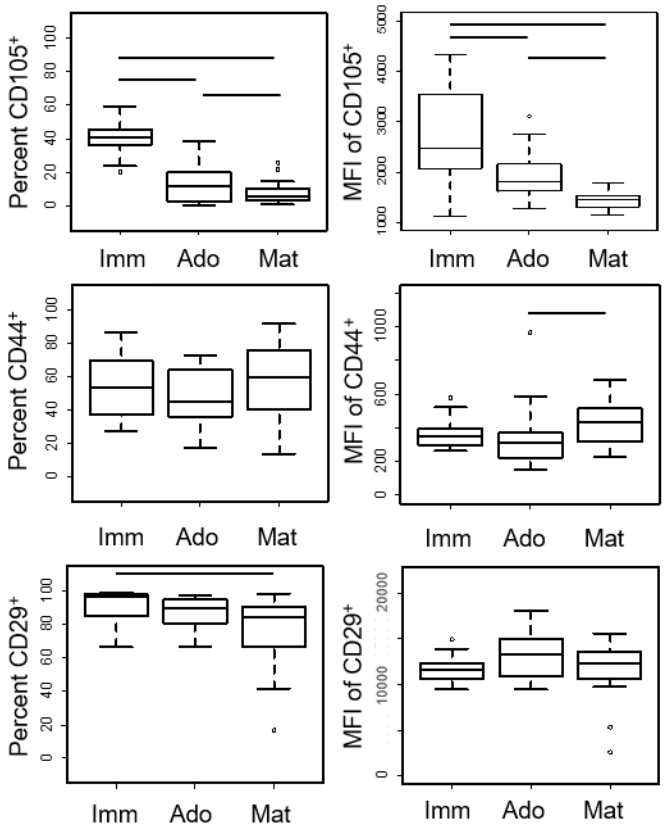

Figure 2-2. Expression of cartilage progenitor cell markers varied with animal maturity. Expression was pooled over timepoint and loading condition within each maturity group. Significance bars indicate $P < 0.05$, n=5 immature (imm), 5 adolescent (ado), 6 mature (mat) animals.

varied across groups with mature samples having a higher $CD44^+$ MFI compared to adolescent samples, and lower percentage of CD29 expression than immature samples.

Gene expression analysis revealed maturity-dependent differential expression of all five genes of interest (Figure 3). Adolescent samples showed decreased Col1 and Col2 mRNA expression compared to both immature and mature samples. Immature samples demonstrated drastically

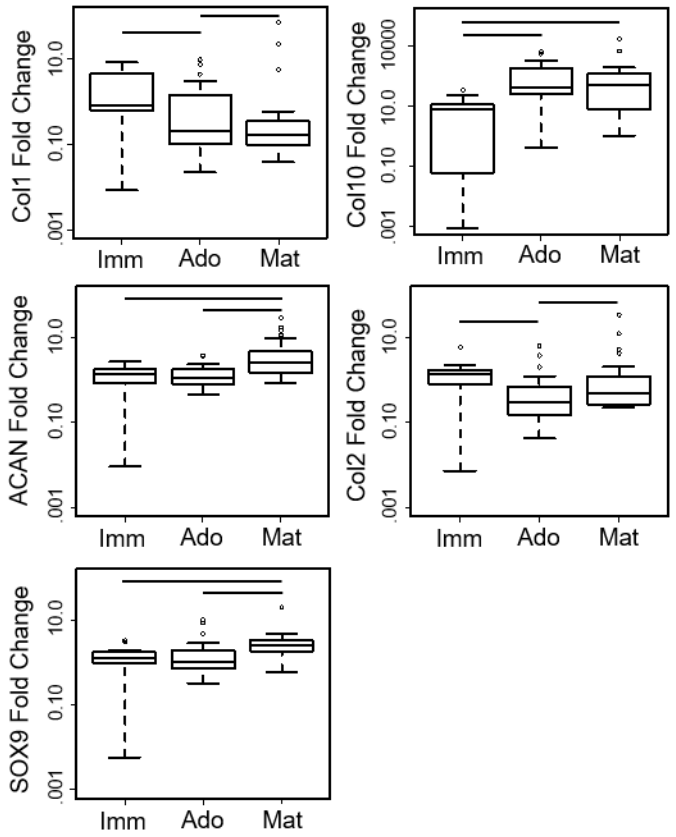

Figure 2-3. Maturity-dependent expression of matrix synthesis genes expressed as $2^{-\Delta\Delta CT}$ values plotted on a logarithmic scale. Data were normalized to average expression of immature samples. Note the varying y-axis scales. Expression was pooled over timepoint and loading condition within each maturity group. Significance bars indicate $P < 0.05$; n=5 immature (imm), 7 adolescent (ado), 6 mature (mat) animals.

lower expression of Col10 ($2^{-\Delta\Delta CT}$ = 5.96 ± 6.61) than adolescent (118.08 ± 159.03) and mature (155.50 ± 363.48) samples. Chondrocyte ACAN and SOX9 mRNA expression both increased with maturity.

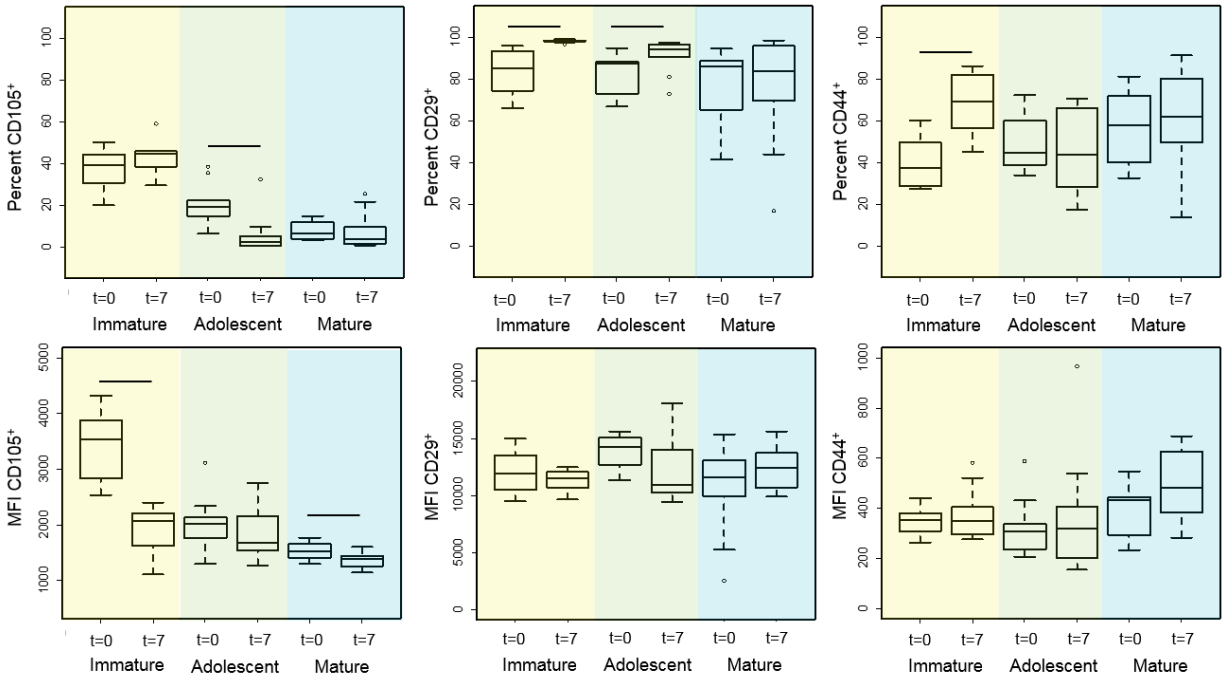

Figure 2-4. Expression of progenitor cell surface markers demonstrated maturity-dependent differential sensitivity to culture time. Significance bars indicate $P < 0.05$ between time points within age; n=5 immature (yellow), 5 adolescent (green), 6 mature (blue) animals.

Time in culture affected cell surface marker expression and gene expression. In the maturity-dependent analysis, percentage of adolescent cells expressing CD105 decreased to nearly 0% between t=0 and t=7 days, while immature and mature $CD105^+$ MFI decreased over 7 days in culture (Figure 4). This analysis also revealed an increase in percentage of immature cells expressing CD44 and CD29 over 7 days in culture, as well as an increase in CD29 percentage expression in adolescent samples. Culture time was a significant factor for Col1 expression within immature and adolescent groups, with greater culture time corresponding with decreased Col1 expression in both groups (Figure 5). Culture time was also a significant factor in ACAN and

SOX9 expression, as immature and adolescent samples, respectively, exhibited a decrease in gene expression over time.

Mechanical loading only affected immature samples. Specifically, loading caused samples to exhibit lower expression of Col1 and ACAN (Figure 6). No effects of loading were seen on gene expression in the adolescent or mature groups.

Analysis of OARSI scores revealed significantly greater cumulative scores in mature samples compared to immature and adolescent samples (Supplementary Figure 2).

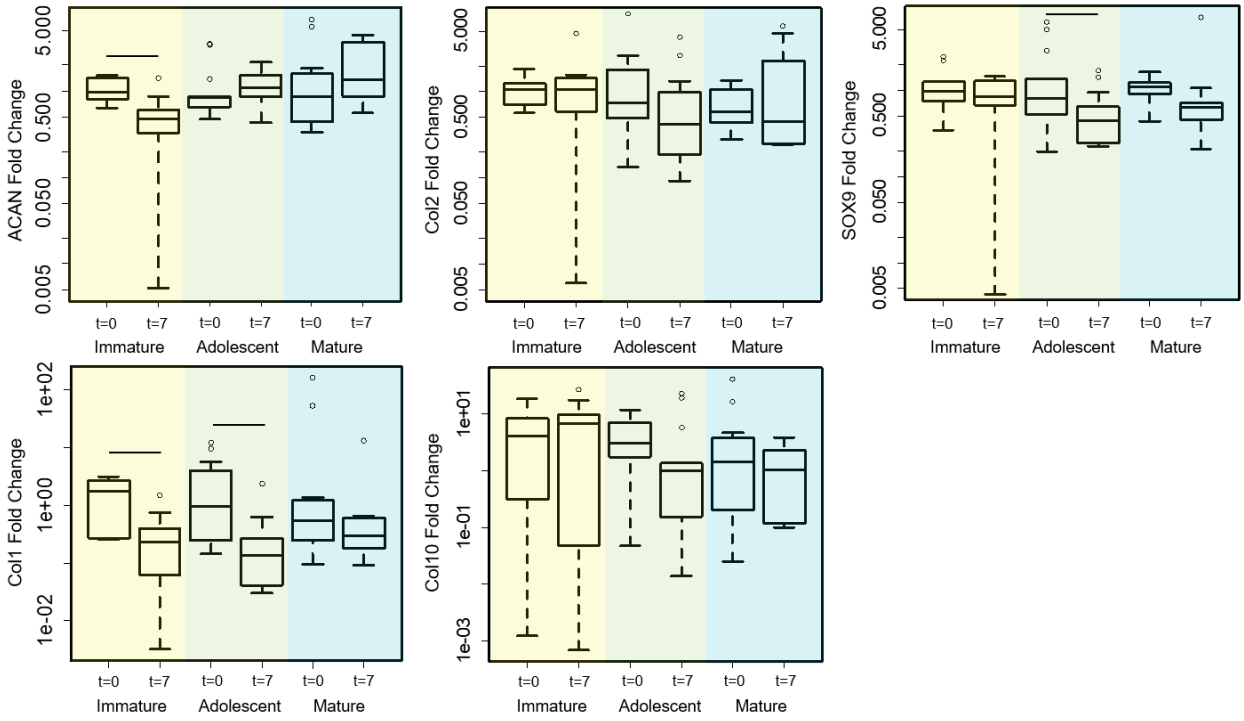

Figure 2-5. Expression of matrix synthesis genes expressed as $2^{-\Delta\Delta CT}$ values plotted on a logarithmic scale demonstrated maturity-dependent differential sensitivity to culture time. Data were pooled across loading condition and normalized to average expression of t=0 samples within each age. Note the varying axis scales. Significance bars indicate $P < 0.05$, n=5 immature (yellow), 7 adolescent (green), 6 mature (blue) animals.

2.5. Discussion

This study supports the hypothesis that cartilage demonstrates maturity-dependent plasticity in response to mechanical load and culture time (Figure 7). Significant effects of loading and culture time on gene and surface marker expression were detected exclusively in cartilage from non-mature animals. Results suggest that expression of Col1, ACAN, and SOX9 may be particularly sensitive to mechanical loading and culture time. This is consistent with previous studies demonstrating chondrocyte mechanosensitivity, with mild downregulation in response to mildly injurious loads[33,34]. Furthermore, culture time had mixed effects on progenitor marker expression. Percent of cells expressing CD105 decreased almost entirely in t=7-day adolescent samples compared to t=0, and $CD105^+$ MFI of cartilage from immature animals followed suit. However, culture time had a positive effect on CD44 and CD29 expression in immature samples. The loss of CD105 expression in adolescent samples over culture time is intriguing, as this is contradictory to the general expectation that *in vitro* culture conditions promote cell stemness[35,36]. Though dedifferentiation is often attributed to two-dimensional monolayer cell conformation as opposed to the three-dimensional explants in the current study, bioactive factors in fetal bovine serum present in incubation media may be a contributing factor of phenotypic change. The upregulation of migratory chondrocyte progenitor markers CD44 and CD29 coupled with the time-dependent downregulation of matrix synthesis genes Col1, ACAN and SOX9 detected in this study support the notion of promoted dedifferentiation via artificial culture conditions. Taken together, these data suggest enhanced inherent plasticity of immature and adolescent chondrocytes compared to mature tissue chondrocytes. These results are consistent with previous studies that found juvenile articular chondrocytes to be better suited for regenerative applications than adult cells, due in part to enhanced sensitivity to environmental perturbations in vitro[4,13,37]. In addition,

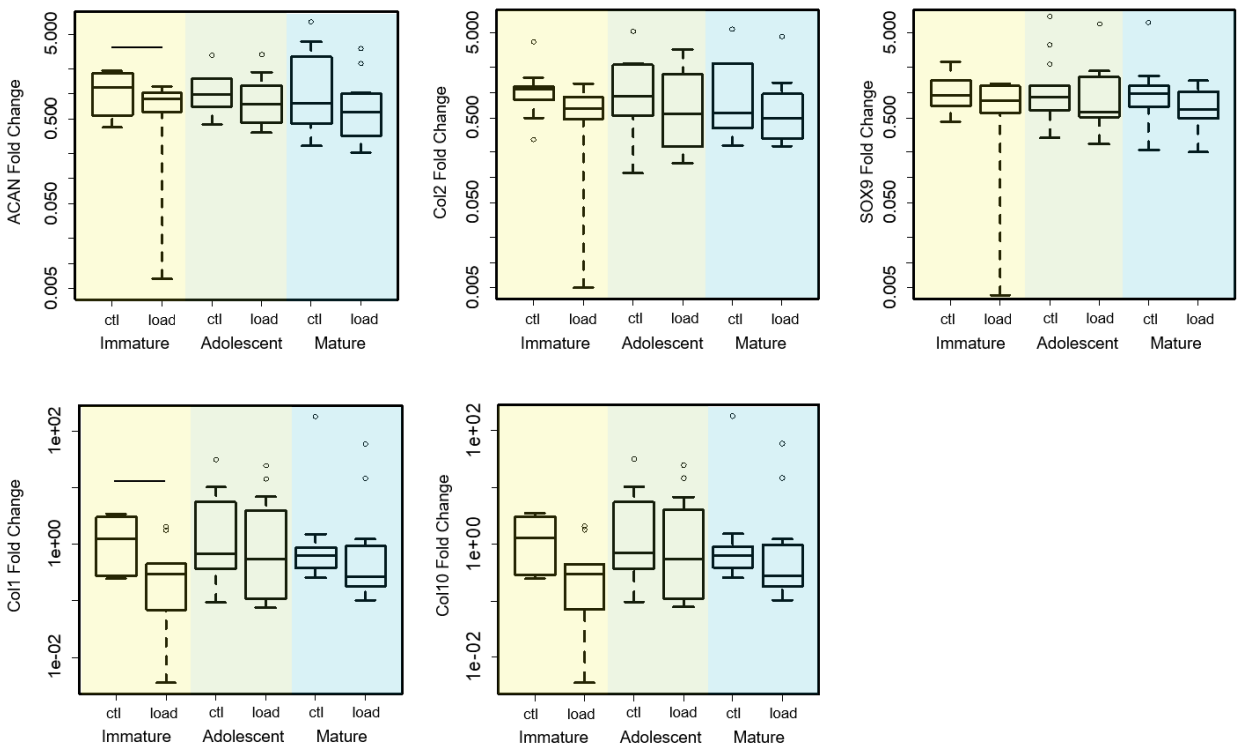

Figure 2-6. Expression of matrix synthesis genes expressed as $2^{-\Delta\Delta CT}$ values shows evidence of maturity-dependent differential sensitivity to mechanical loading. Data were pooled across culture time and normalized to average expression of unloaded control (ctl) samples within each age. Significance bars indicate $P < 0.05$, n=5 immature, 7 adolescent, 6 mature animals.

these results suggest that mechanomedicine approaches could target maturity-dependent plasticity in response to mechanical stimuli.

Baseline gene and surface marker expression data from this study support the hypothesis that chondrocyte phenotype is maturity-dependent (Figure 7). As expected, expression of chondrocyte progenitor markers CD105, a component of the TGF-β receptor complex, and CD29, a cell adhesion molecule, decreased with maturity, changes that may play a key role in the lack of

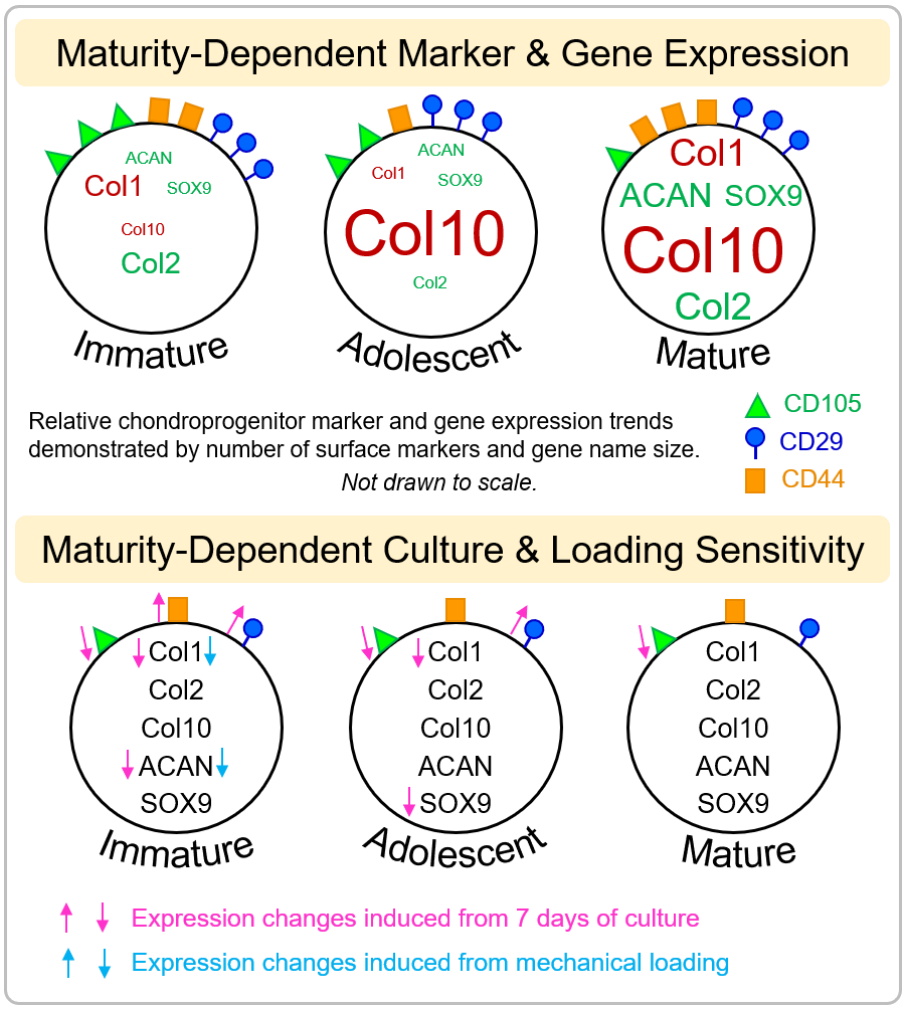

Figure 2-7. Schematic of results demonstrating maturity-dependent baseline expression of genes and progenitor markers of interest (top), and differential sensitivity of these expression patterns to artificial tissue culture and mechanical loading across age groups (bottom).

regenerative potential in mature tissue[3,12,22,23]. However, CD44, another cell adhesion molecule, showed the highest MFI in mature tissue[21]. This discrepancy is surprising given the overlapping migratory functionality of CD44 and CD29[21,22]. Furthermore, mature tissue exhibited relatively high expression of all matrix protein genes of interest compared to younger groups—an interesting

result given the non-regenerative nature of mature cartilage. Mature chondrocytes may inherently reside in a more differentiated state than immature cells, resulting in greater expression of synthetic genes. This explanation is supported by evidence that mature cartilage contains a smaller population of progenitor cells than immature cartilage, as progenitor cells are historically thought to possess proliferative and migratory capabilities at the expense of synthetic capacity[3,12]. Alternatively, these findings may indicate that mature tissue is attempting to mount a biosynthetic pre-OA response to prevent tissue degeneration[28,29,38]. Interestingly, Col1 and Col2 expression in adolescent tissue were significantly lower than both mature and immature expression of these genes. Following similar rationale, immature tissue may be mounting developmental biosynthetic activity; a process which subsides by adolescence[6,7,39].

Counterintuitive results in mature tissue coupled with large variance in this group may indicate variable health status of samples from mature animals. While several of the mature animals included in this study presented with some degree of lameness, and some mature joints did have lesions, all samples were harvested several millimeters away from any visible lesions. Histological scoring revealed enhanced, but highly variable, tissue degradation in mature samples. Col1 and Col10 mRNA expression in the mature tissue group was widely scattered. This is consistent with tissue health disparity amongst the mature samples, as these collagens are associated with fibrotic and hypertrophic phenotypes, respectively, and are expected to be upregulated in OA[28,40]. The mild increase in MFI among $CD44^{+}$ cells observed in mature tissue also supports the notion of early stage damage because CD44 expression has been shown to increase progressively with increasing OA severity[41,42]. CD44 binds to hyaluronic acid (HA), a major component of proteoglycans, which decrease throughout maturity[3,4]. While chondrocyte ACAN mRNA expression was upregulated in cartilage from mature animals, Safranin O staining

qualitatively demonstrated proteoglycan loss. This suggests that upregulated ACAN expression did not translate into successful aggrecan synthesis; mature cartilage is notoriously ill-equipped to produce full-size proteoglycan aggregates[43]. Rather, upregulated ACAN expression in cartilage from mature animals likely indicates early degenerative changes instead of a truly osteoarthritic state, wherein matrix synthesis gene expression is often downregulated[38]. A similar paradigm of translational failure may also apply to all other genes observed to be upregulated in cartilage from mature animals. Interestingly, Col2, the main collagen in articular cartilage, and Col1, a maladaptive collagen, also demonstrated greater expression in cartilage from immature animals than in that from adolescent animals. Taken together, the gene expression profiles observed across maturity groups in this study allude to cartilage from mature animals exhibiting early yet disparate signs of degeneration wherein Col2, Col10, and ACAN are upregulated, rather than late-stage osteoarthritic degeneration wherein expression of these genes is downregulated[38,40]. Distinguishing healthy cartilage aging from degenerative aging and understanding the mechanisms and implications of each is an ongoing challenge in OA research.

There are several established relationships between chondrogenic progenitor cells and matrix synthesis genes that aid interpretation of the present study. For instance, Col2 synthesis is upregulated in cartilage cells as they differentiate and lose their progenitor status[44–47]. Thus, the progenitor cells targeted in this study are unexpected to have contributed to Col2 expression. Rather, it is expected that non-progenitors co-expressed Col2 and SOX9, a transcription factor with an established role as a regulator of collagen synthesis that has been shown to correlate to robust Col2 synthesis[29,30,48]. In the present study, SOX9 expression followed the same patterns of maturity- and time-dependence as Col2 and ACAN, suggesting SOX9 may have been acting as a master regulator of both collagen and aggrecan synthesis[29,30,49,50]. Like Col2, ACAN demonstrates

progressive upregulation with chondrocyte differentiation[38,44,46]. Thus, the loss of ACAN expression in cartilage from immature animals with culture time and mechanical loading in the present study is aligned with the concurrent increase in CD44 and CD29 expression in these samples, providing further supporting evidence of increased phenotypic plasticity amongst younger tissue[21,22]. Col10 is produced by terminally differentiated hypertrophic chondrocytes, therefore it is highly unexpected that Col10 was expressed by any cells expressing progenitor surface markers in the present study[27,28,44,46]. Indeed, drastic upregulation of Col10 in cartilage from adolescent and mature animals was detected in the present study compared to immature. A possible explanation of this result is that cartilage from immature animals fosters a more progenitor-oriented cell population, while mature cartilage takes on a more matrix-synthetic phenotype. The concurrent changes in cellular profile and matrix composition observed throughout maturation raise questions regarding cell-matrix interactions, and the consequences of such interactions on regenerative capacity. Uncovering the interplay between the extracellular matrix and cell phenotype and function is critical for development of cartilage regeneration strategies, as both cell and matrix properties need to be carefully considered in order to achieve optimal and sustainable tissue performance.

Meaningful trends can be drawn from synthesizing the full suite of reported results beyond individual statistics. As previously alluded to, the loss of CD105 expression in tissues as early as adolescence is striking, indicating that $CD105^+$ cells could represent a key progenitor population responsible for regeneration that is lost throughout maturation. Additionally, the uptick in CD44 expression in mature samples and cultured immature samples may speak to the wound-healing functionality of $CD44^+$ cells demonstrated in other tissues, as these samples may have been responding appropriately to perceived vulnerability due to their inherent health status, in the case

of mature tissue, or external environment, in the case of artificial culture[51]. However, according to the predominant paradigm, progenitor cell functionality, which is often associated with wound healing and regeneration, is inversely correlated with chondrogenic biosynthesis, a key component of tissue maintenance, casting doubt on the importance of progenitor cell maintenance for cartilage health. Similarly, age-related differences in synthetic gene expression are expected, as cartilage is known to develop throughout maturation, particularly with respect to the collagen matrix. Thus, maturity-dependent trends on their own are difficult to interpret as representative of definitively advantageous or disadvantageous to tissue health. Conversely, in the context of culture time and mechanical loading, it is difficult to conceive of a scenario in which reduced plasticity to external perturbation would be an advantage to mature tissue. *In vivo* exposure to environmental cues such as those applied in the present study, high-rate mechanical loading in particular, would be expected to warrant some level of biological response in order to maintain homeostasis; a response which appears muted if not entirely absent in mature tissue in the present study. Beyond natural physiology, the loss of sensitivity observed in mature tissue has implications for orthopedic medicine and may help to explain why development of preventative or regenerative therapies for degenerative aged cartilage has thus far been unsuccessful.

There are several limitations to the current study. Anatomical origin of samples was not accounted for; samples were pooled across locations due to the number of assays performed and low cellularity. While these assays demonstrated meaningful maturity-dependent tissue properties, analyzing regional variation between and across joint surfaces would likely reveal additional pertinent information. Additionally, although interesting changes were captured at 7 days post-loading, alternative time points on the order of hours to weeks would likely reveal additional maturity-dependent responses to mechanical loading. Finally, loading was analyzed as a binary

treatment due to variations in loading because of sample variation, thus, load-differential effects may not have been captured by the current statistical model[25].

Cartilage degeneration is a common and burdensome condition, affecting a large portion of the population in a predictably age-dependent manner. Key mechanisms associated with enhanced regenerative capacity of immature cartilage are incompletely understood. The current study evaluated maturity-dependent synthetic activity of chondrocytes pre- and post-compressive loading. Mature tissue exhibited reversion toward pre-adolescent gene expression levels, and sample groups demonstrated maturity-dependent plasticity in response to the stimuli of mechanical loading and culture time. These results help to elucidate mechanisms of cartilage regeneration and failure, which is a critical step to developing effective mechanomedicine therapies for the prevention and reversal of OA.

2.6. References

1. Riordan EA, Little C. 2014. Pathogenesis of post-traumatic OA with a view to intervention. Best Pract. Res. Clin. Rheumatol. 28(1):17–30.
2. Shane Anderson A, Loeser RF. 2010. Why is osteoarthritis an age-related disease? Best Pract. Res. Clin. Rheumatol. 24(1):15–26.
3. Otsuki S, Grogan SP, Miyaki S, et al. 2010. Tissue neogenesis and STRO-1 expression in immature and mature articular cartilage. J. Orthop. Res. 28(1):96–102.
4. Liu H, Zhao Z, Clarke RB, et al. 2013. Enhanced tissue regeneration potential of juvenile articular cartilage. Am. J. Sports Med. 41(11):2658–2667.
5. Nelson AE. 2018. Osteoarthritis year in review 2017: clinical. Osteoarthr. Cartil. 26:319–325.

6. Jadin KD, Wong BL, Bae WC, et al. 2005. Depth-varying density and organization of chondrocytes in immature and mature bovine articular cartilage assessed by 3d imaging and analysis. J. Histochem. Cytochem. 53(9):1109–19.

7. Julkunen P, Harjula T, Iivarinen J, et al. 2009. Biomechanical, biochemical and structural correlations in immature and mature rabbit articular cartilage. Osteoarthr. Cartil. 17:1628–1638.

8. Charlebois M, McKee MD, Buschmann MD. 2004. Nonlinear tensile properties of bovine articular cartilage and their variation with age and depth. J. Biomech. Eng. 126(2):129–37.

9. Stolz M, Gottardi R, Raiteri R, et al. 2009. Early detection of aging cartilage and osteoarthritis in mice and patient samples using atomic force microscopy. Nat. Nanotechnol. 4(3):186–192.

10. Chen AC, Temple MM, Ng DM, et al. 2002. Induction of advanced glycation end products and alterations of the tensile properties of articular cartilage. Arthritis Rheum. 46(12):3212–3217.

11. Verzijl N, DeGroot J, Zaken C Ben, et al. 2002. Crosslinking by advanced glycation end products increases the stiffness of the collagen network in human articular cartilage: A possible mechanism through which age is a risk factor for osteoarthritis. Arthritis Rheum. 46(1):114–123.

12. Mukoyama S, Sasho T, Akatsu Y, et al. 2015. Spontaneous repair of partial thickness linear cartilage injuries in immature rats. Cell Tissue Res. 359(2):513–20.

13. Taylor SEB, Lee J, Smeriglio P, et al. 2016. Identification of human juvenile chondrocyte-specific factors that stimulate stem cell growth. Tissue Eng. Part A .

14. Tran-Khanh N, Hoemann CD, McKee MD, et al. 2005. Aged bovine chondrocytes display

a diminished capacity to produce a collagen-rich, mechanically functional cartilage extracellular matrix. J. Orthop. Res. 23(6):1354–62.

15. Loeser RF, Im H-J, Richardson B, et al. 2009. Methylation of the OP-1 promoter: potential role in the age-related decline in OP-1 expression in cartilage. Osteoarthr. Cartil. 17(4):513–517.

16. Blaney Davidson E, Scharstuhl A, Vitters E, et al. 2005. Reduced transforming growth factor-beta signaling in cartilage of old mice: role in impaired repair capacity. Arthritis Res. Ther. 7(6):R1338.

17. Shanmugaapriya S, van Caam A, de Kroon L, et al. 2016. Expression of TGF-β Signaling Regulator RBPMS (RNA-Binding Protein With Multiple Splicing) Is Regulated by IL-1β and TGF-β Superfamily Members, and Decreased in Aged and Osteoarthritic Cartilage. Cartilage 7(4):333–345.

18. Madej W, van Caam A, Blaney Davidson EN, et al. 2016. Ageing is associated with reduction of mechanically-induced activation of Smad2/3P signaling in articular cartilage. Osteoarthr. Cartil. 24(1):146–157.

19. Varela-Eirín M, Varela-Vázquez A, Guitián-Caamaño A, et al. 2018. Targeting of chondrocyte plasticity via connexin43 modulation attenuates cellular senescence and fosters a pro-regenerative environment in osteoarthritis. Cell Death Dis. 9(12):1166.

20. Pelttari K, Pippenger B, Mumme M, et al. 2014. Adult human neural crest–derived cells for articular cartilage repair. Sci. Transl. Med. 6(251).

21. Ishida O, Tanaka Y, Morimoto I, et al. 1997. Chondrocytes are regulated by cellular adhesion through CD44 and hyaluronic acid pathway. J. Bone Miner. Res. 12(10):1657–63.

22. Ode A, Kopf J, Kurtz A, et al. 2011. CD73 and CD29 concurrently mediate the mechanically

induced decrease of migratory capacity of mesenchymal stromal cells. Eur. Cell. Mater. 22:26–42.

23. Cheifetz S, Bellón T, Calés C, et al. 1992. Endoglin is a component of the transforming growth factor-beta receptor system in human endothelial cells. J. Biol. Chem. 267(27):19027–30.

24. Carter TE, Taylor KA, Spritzer CE, et al. 2015. In vivo cartilage strain increases following medial meniscal tear and correlates with synovial fluid matrix metalloproteinase activity. J. Biomech. 48(8):1461–8.

25. Aspden RM, Jeffrey JE, Burgin LV. 2002. Letter to the editor. Osteoarthr. Cartil. 10(7):588–589.

26. Ye J, Coulouris G, Zaretskaya I, et al. 2012. Primer-BLAST: a tool to design target-specific primers for polymerase chain reaction. BMC Bioinformatics 13(1):134.

27. Rahmati M, Nalesso G, Mobasheri A, Mozafari M. 2017. Aging and osteoarthritis: Central role of the extracellular matrix. Ageing Res. Rev. 40:20–30.

28. Luo Y, Sinkeviciute D, He Y, et al. 2017. The minor collagens in articular cartilage. Protein Cell 8(8):560–572.

29. Hino K, Saito A, Kido M, et al. 2014. Master regulator for chondrogenesis, Sox9, regulates transcriptional activation of the endoplasmic reticulum stress transducer BBF2H7/CREB3L2 in chondrocytes. J. Biol. Chem. 289(20):13810–20.

30. Yao B, Zhang M, Liu M, et al. 2018. Sox9 functions as a master regulator of antler growth by controlling multiple cell lineages. DNA Cell Biol. 37(1):15–22.

31. Schmitz N, Laverty S, Kraus VB, Aigner T. 2010. Basic methods in histopathology of joint tissues. Osteoarthritis Cartilage 18 Suppl 3:S113-6.

32. McIlwraith CW, Frisbie DD, Kawcak CE, et al. 2010. The OARSI histopathology initiative – recommendations for histological assessments of osteoarthritis in the horse. Osteoarthr. Cartil. 18:S93–S105.

33. Scholtes S, Krämer E, Weisser M, et al. 2018. Global chondrocyte gene expression after a single anabolic loading period: Time evolution and re-inducibility of mechano-responses. J. Cell. Physiol. 233(1):699–711.

34. Jeon JE, Schrobback K, Hutmacher DW, Klein TJ. 2012. Dynamic compression improves biosynthesis of human zonal chondrocytes from osteoarthritis patients. Osteoarthr. Cartil. 20(8):906–915.

35. Schnabel M, Marlovits S, Eckhoff G, et al. 2002. Dedifferentiation-associated changes in morphology and gene expression in primary human articular chondrocytes in cell culture. Osteoarthr. Cartil. 10(1):62–70.

36. Shao X, Duncan NA, Lin L, et al. 2013. Serum-free media for articular chondrocytes in vitro expansion. Chin. Med. J. (Engl). 126(13):2523–9.

37. Adkisson HD, Martin JA, Amendola RL, et al. 2010. The potential of human allogeneic juvenile chondrocytes for restoration of articular cartilage. Am. J. Sports Med. 38(7):1324–33.

38. Fukui N, Ikeda Y, Ohnuki T, et al. 2008. Regional differences in chondrocyte metabolism in osteoarthritis: A detailed analysis by laser capture microdissection. Arthritis Rheum. 58(1):154–163.

39. Julkunen P, Iivarinen J, Brama PA, et al. 2010. Maturation of collagen fibril network structure in tibial and femoral cartilage of rabbits. Osteoarthr. Cartil. 18(3):406–415.

40. Brew CJ, Clegg PD, Boot-Handford RP, et al. 2010. Gene expression in human

chondrocytes in late osteoarthritis is changed in both fibrillated and intact cartilage without evidence of generalised chondrocyte hypertrophy. Ann. Rheum. Dis. 69(01):234–240.

41. Tibesku CO, Szuwart T, Ocken SA, et al. 2006. Expression of the matrix receptor CD44v5 on chondrocytes changes with osteoarthritis: an experimental investigation in the rabbit. Ann. Rheum. Dis. 65(1):105–8.

42. Zhang F-J, Luo W, Gao S-G, et al. 2013. Expression of CD44 in articular cartilage is associated with disease severity in knee osteoarthritis. Mod. Rheumatol. 23(6):1186–91.

43. Verbruggen G, Cornelissen M, Almqvist KF, et al. 2000. Influence of aging on the synthesis and morphology of the aggrecans synthesized by differentiated human articular chondrocytes. Osteoarthr. Cartil. 8(3):170–179.

44. Jiang Y, Cai Y, Zhang W, et al. 2016. Human cartilage-derived progenitor cells from committed chondrocytes for efficient cartilage repair and regeneration. Stem Cells Transl. Med. 5(6):733–44.

45. Varela-Eirin M, Loureiro J, Fonseca E, et al. 2018. Cartilage regeneration and ageing: Targeting cellular plasticity in osteoarthritis. Ageing Res. Rev. 42:56–71.

46. Seol D, McCabe DJ, Choe H, et al. 2012. Chondrogenic progenitor cells respond to cartilage injury. Arthritis Rheum. 64(11):3626–3637.

47. Lin Y Z S, Lee WYW, Xu L, et al. 2017. Stepwise preconditioning enhances mesenchymal stem cell-based cartilage regeneration through epigenetic modification. Osteoarthr. Cartil. 25:1541–1550.

48. Grogan SP, Miyaki S, Asahara H, et al. 2009. Mesenchymal progenitor cell markers in human articular cartilage: normal distribution and changes in osteoarthritis. Arthritis Res. Ther. 11(3):R85.

49. Bar Oz M, Kumar A, Elayyan J, et al. 2016. Acetylation reduces SOX9 nuclear entry and ACAN gene transactivation in human chondrocytes. Aging Cell 15(3):499–508.

50. Zwickl H, Niculescu-Morzsa E, Halbwirth F, et al. 2016. Correlation analysis of SOX9, -5, and -6 as well as COL2A1 and aggrecan gene expression of collagen I implant-derived and osteoarthritic chondrocytes. Cartilage 7(2):185–92.

51. Jordan AR, Racine RR, Hennig MJP, Lokeshwar VB. 2015. The Role of CD44 in Disease Pathophysiology and Targeted Treatment. Front. Immunol. 6:182.

Chapter 3: Real-Time Optical Redox Imaging of Cartilage Metabolic Response to Mechanical Loading*

Shannon K. Walsh, Melissa C. Skala, Corinne R. Henak

*(*Reprinted from Osteoarthritis & Cartilage with permission from Elsevier)*

3.1. Abstract

OBJECTIVE Metabolic dysregulation has recently been identified as a key feature of osteoarthritis. Mechanical overloading has been postulated as a primary cause of this metabolic response. Current methods of real-time metabolic activity analysis in cartilage are limited and challenging. However, optical redox imaging leverages the autofluorescence of co-enzymes NAD(P)H and FAD to provide dye-free real-time analysis of metabolic activity. This technique has not yet been applied to cartilage. This study aimed to assess the effects of a compressive load on cartilage using optical redox imaging. METHOD Cartilage samples were excised from porcine femoral condyles. To validate this imaging modality in cartilage, glycolysis was inhibited via 2-deoxy-D-glucose (2DG) and oxidative phosphorylation was inhibited by rotenone. Optical redox images were collected pre- and post-inhibition. To assess the effects of mechanical loading, samples were subjected to a compressive load and imaged for approximately 30 minutes. Load and strain parameters were determined using high-speed camera images in Matlab. A range of loading magnitudes and rates were applied across samples. RESULTS 2DG and rotenone demonstrated the expected inhibitory effects on fluorescence intensity in the channels corresponding to NAD(P)H and FAD, respectively. Mechanical loading induced an increase in NAD(P)H channel fluorescence which subsided by 30 minutes post-loading. Magnitude of loading

parameters had mixed effects on metabolites. CONCLUSIONS Optical redox imaging provides an opportunity to assess real-time metabolic activity in cartilage. This approach revealed a metabolic response to a single load and can be used to provide insight into the role of metabolism in mechanically-mediated cartilage degradation.

Keywords: articular cartilage, metabolism, glycolysis, oxidative phosphorylation, redox, mechanical loading

3.2. Introduction

Metabolic dysregulation occurs in many diseases and has recently been implicated as a feature of mechanically-mediated articular cartilage damage. Broadly, metabolism serves to generate energy in the form of adenosine triphosphate (ATP) via glycolysis, which occurs in the cytosol, and oxidative phosphorylation, which occurs in the mitochondria[1]. A shift in metabolic balance between energetic reliance on glycolysis and oxidative phosphorylation, respectively, can occur in disease states as a maladaptive response, or as a return to a more embryonic phenotype. For example, the Warburg effect is a well-established marker of cancer phenotype[2]. The resulting upregulation of glycolysis results either from mitochondrial dysfunction or from demand for secondary products required for cellular proliferation and extracellular matrix formation[3]. Compared to healthy articular cartilage, growth plate cartilage exhibits a Warburg-like metabolic phenotype, with greater relative reliance on glycolysis[1,4]. Osteoarthritic cartilage has been shown to revert to a metabolic phenotype similar to that of the growth plate, demonstrating greater relative glycolytic activity and lower oxidative phosphorylation activity than healthy articular cartilage[1,5,6].

Recent evidence suggests articular cartilage metabolism is also altered in response to mechanical load, with extreme cases leading to tissue damage via multiple mechanisms. Superphysiological loading alters basal and maximal respiration, repetitive cyclic loading exacerbates stress-dependent metabolic dysfunction, and mitochondrial damage precedes osteoarthritis-like macroscopic cartilage damage[7–9]. Additionally, non-pathway-specific metabolic activity has shown sensitivity to mechanical loading, including changes over less than one hour after superphysiological loading[10–15]. Despite this body of associative evidence, the role of short term mechanically-mediated metabolic flux, defined here as a detectable increase or decrease in metabolic activity, in long term metabolic dysregulation and cartilage degradation remain unclear. This is in part due to limited methods established for nondestructively evaluating short-term metabolic flux in cartilage.

There are several established techniques for evaluating metabolism in cartilage. Metabolic biomarkers and regulatory factors associated with cartilage damage have been identified by qPCR, mass spectrometry, and RNA sequencing[16–18]. Computational modeling has been combined with experimental metabolomic data to predict metabolic response to dynamic loading on the cellular level[19]. Commercially available kits have allowed for functional analysis of mitochondria, including respiration, depolarization, and ROS release[8,9,20,21]. Intracellular calcium flux has been imaged in real-time under axial compression to indicate immediate metabolic response to mechanotransduction[10,11,22]. Though informative, these techniques are limited to single time points, exogenous dyes, non-specific evaluation, or sample-destructive methods. Thus, non-destructive methods capable of longitudinally analyzing specific metabolic activity in cartilage tissue have not been established.

Conversely, a real-time imaging technique for evaluation of relative oxidative phosphorylation and glycolysis activity has been established for other tissues[23–25]. Optical redox imaging leverages the autofluorescence of flavin adenine dinucleotide (FAD) and nicotinamide adenine dinucleotide (NADH), which are electron acceptors and donors, respectively, in an array of metabolic reactions. Fluorescence intensity of each metabolite is correlated with its concentration. Intensity changes in the fluorescence channels corresponding to these respective metabolites can be interpreted as congruous changes in the accumulation of these metabolites, and, thus, altered activity of the metabolic processes that created them[23,26]. Additionally, optical redox ratio, a measure of the oxidative-reduction status of the mitochondrial matrix, can be calculated from the fluorescence intensities of FAD and NADH, and changes in optical redox ratio can be interpreted as changes in relative activity levels of mitochondrial and nonmitochondrial metabolic activity, respectively. It should be noted that fluorescence properties of NADH are identical to nicotinamide adenine dinucleotide phosphate (NADPH), so the fluorescence in this channel includes a contribution from both metabolites. The combined fluorescence is denoted as NAD(P)H.

Optical redox imaging has been employed in cancer and stem cell research, and is sensitive to relative changes in glycolysis and oxidative phosphorylation, but has not yet been applied to cartilage[23,24,27–30]. However, previous studies have directly and indirectly measured activity of glycolysis and oxidative phosphorylation in cartilage via alternative techniques, reporting metabolic flux as a notable feature of disease and mechanotransduction[12,31–34]. This line of research would benefit substantially from development of a label-free, nondestructive technique capable of detecting time- and mechanical load-dependent shifts in metabolic activity of whole tissue explants. Therefore, the objectives of this study were to validate real-time optical redox imaging

in articular cartilage, then to use this method to detect metabolic flux in response to a single compressive load.

3.3. Methods

3.3.1. Sample Collection & Preparation

Cartilage samples were collected from femoral condyles of 5-6-month-old pigs at a local abattoir within 6 hours of sacrifice. Full-thickness cylindrical plugs were excised using a 4 mm diameter biopsy punch and scalpel. Samples were stored in chondrocyte media containing Ham's F-12 media (Mediatech, Inc., Manassas, VA), 10% fetal bovine serum (Hyclone, GE Healthcare Bio-Sciences, Pittsburgh, PA), 50 ug/ml ascorbic acid (Amresco, LLC., Solon, OH), 30 ug/ml alpha-ketoglutaric acid (Thermo Fisher Scientific Chemicals, Inc., Waltham, MA), 300 ug/ml L-glutamine, 100 IU/ml penicillin G, 100 ug/ml streptomycin, and 6 mg/ml HEPES buffer (Corning, Inc., Corning, NY) at room temperature for same-day use, or otherwise incubated at 37 °C and 5% CO_2 for up to 6 days. Days spent in culture did not affect baseline metabolic values. Subchondral bone was removed with a razor blade to create a deep surface parallel to the articular surface. Cylindrical plugs were then bisected into hemicylinders for imaging.

3.3.2. Metabolic Imaging

Metabolic imaging was performed on an inverted epifluorescent microscope (Olympus IX-71, Tokyo, Japan) with a metal halide fluorescent lamp (X-Cite 120 Fluorescence Illumination System, Exfo Inc., Quebec, Canada). A DAPI filter cube (excitation 361-389 nm, emission 435-485 nm) was used to measure fluorescence in channel 1, in which NAD(P)H fluoresces (160-250 ms exposure time) (Figure 1D), and a green filter cube (excitation 470-490 nm, emission 500-550 nm) was used to measure fluorescence in channel 2, in which FAD fluoresces (1.5-6 s exposure time) (Figure 1E). All images were captured at 40× using a 1.6× extender. Fluorescence intensities

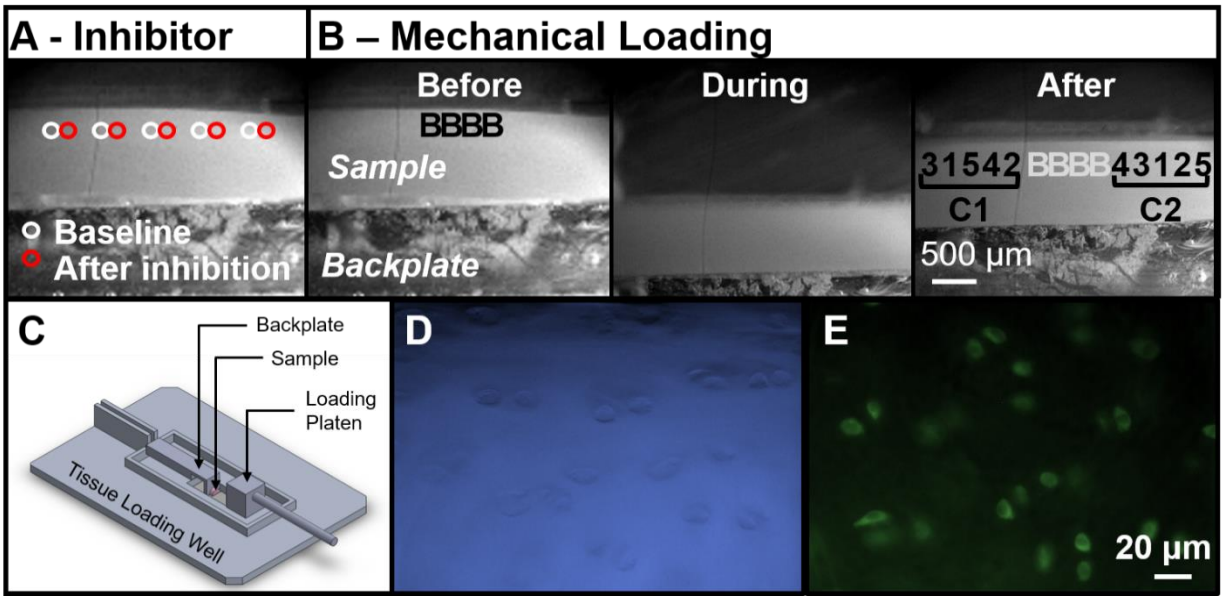

Figure 3-1. Schematic overview of imaging setup. Imaging locations for chemical inhibitor validation (A) and mechanical loading (B). Imaging fields are distributed across the sample to avoid photobleaching effect. 'B' indicates the locations of baseline images, 'C1' and 'C2' indicate two clusters used for time-course analysis, and numbers indicate time post-loading bin (1=0-5 min, 2=5-10 min, 3=10-15 min, 4=15-20 min, 5=30-35 min). Mechanical loading tissue well (C) in which sample was submerged in PBS throughout loading and imaging. Representative metabolic images in NAD(P)H-capturing channel 1 (D) and FAD-capturing channel 2 (E). Images were captured at 40×.

of channel 1 and channel 2 images were measured with a monochrome camera (DP80, Olympus, Tokyo, Japan), and ImageJ software was used to calculate the optical redox ratio, defined here as ORR = [FAD channel]/[NAD(P)H channel + FAD channel][24,35,36].

3.3.3. Imaging Validation

To validate the sensitivity and specificity of this metabolic imaging method, samples were imaged before and after exposure to established metabolic inhibitors of oxidative phosphorylation and glycolysis (Figure 1A). 2-deoxy-D-glucose (2-DG) (Alfa Aesar, Haverhill, MA) is a glucose analog and inhibits glycolysis, while rotenone (Sigma-Aldrich, St. Louis, MO) is an inhibitor of mitochondrial complex I electron transport and downregulates oxidative phosphorylation[24,34]. Samples were imaged on a coverslip along the articular edge of the cross section. Preliminary cell viability imaging was performed on the cut surface of cartilage samples and revealed minimal cell death due to sample sectioning (data not shown). Control images were first taken in chondrocyte media at room temperature, and samples were then incubated for either 24 hours in 10 mM 2-DG (n=8 samples from 3 animals, 4 locations per sample) or for 30 minutes in 20 μM rotenone (n=9 samples from 3 animals, 4 locations per sample) in chondrocyte media at 37°C prior to re-imaging baseline-paired locations at room temperature (Figure 1A).

To confirm that the observed metabolic effects were caused by mechanical loading, a series of control experiments were performed. Unloaded samples were imaged 30 minutes apart with the intermediate imaging protocol applied to loaded samples to ensure time and fluorescent exposure were not causing the metabolic effects observed in loaded samples. Mechanical loading control data showed minimal metabolic changes over time compared to loaded samples (Supplementary Figure S1). Additionally, optical redox imaging was performed every five minutes up to 30 minutes on a thermal probe in place of a sample to detect temperature increase as a function of light exposure. Thermal monitoring revealed a total increase of 0.2°C from the 30 minute imaging protocol applied to mechanically loaded samples (Supplementary Figure S1).

3.3.4. Mechanical Loading

Samples were mechanically loaded on a custom-built microscope-top loading apparatus (Figure 1C). The loading apparatus consists of a custom well and backplate that sits on top of inverted microscope, with a custom loading platen that interfaces with an actuator (Aerotech ACT165D, Aerotech, Pittsburgh, PA). Twenty-eight samples from 10 animals were bisected into hemicylinders and adhered to a backplate on the subchondral side via cyanoacrylate with the tissue cross section flush with the imaging coverslip. While chemical inhibitor studies required submersion in chondrocyte media due to prolonged incubation, mechanical loading and subsequent imaging took place in under an hour. Thus, mechanical loading samples were submerged in PBS throughout testing and were given sufficient time to equilibrate to room temperature prior to loading and imaging. Normalization of fluorescence data to baseline intensity within each sample was assumed to account for any baseline differences in metabolism attributable to varied media between these two studies. Further, a subset of samples was subjected to the adhesion process and imaged without mechanical loading to ensure that cyanoacrylate had no significant effect on metabolism. Samples underwent a single compression using a metal platen spanning the entire articular surface; a variety of displacements and rates were applied using the actuator to achieve a range of peak strain, strain rate, force, and force rate. Mechanical loading was imaged using a high-speed camera at 100 frames per second (Phantom v1211, Vision Research, Wayne, NJ), which was sufficient to capture the displacement rates achieved. Metabolic imaging was completed pre- and post-loading. Pre-loading images were collected at the center of the sample (Figure 1B). In order to account for variation in thickness of uneven samples and resulting variation in experienced deformation, post-loading time series images were collected at randomly selected locations in two imaging clusters, one on either side of the centered baseline image cluster, up to 30 minutes following loading.

Metabolic image intensities were determined. For time series analysis, post-loading image intensities were normalized to average baseline fluorescence per sample. Achieved mechanical loading parameters were then determined. High-speed camera images were downsampled to 10 frames per second in Matlab (Mathworks, version R2015a). Full-thickness, 1 mm wide segments were cropped at the center location of each imaging cluster in ImageJ, and bulk compressive strain was calculated in each of these cropped sections. Custom Matlab code tracked the displacement of the platen and backplate based on image intensity[37]. Strain was calculated based on the length of the sample at each time point (distance between backplate and platen) in comparison to the length before loading began. Force was calculated based on the behavior of the backplate as a leaf spring, with a calibration constant determined by fitting an experimentally-obtained force versus displacement curve. Peak compressive strain (ε) and peak force (F) were obtained. Strain rate ($\dot{\varepsilon}$) and force rate ($\dot{F}$) were determined by fitting the segment of 30 data points immediately preceding maximum values on the strain versus time and force versus time curves, respectively, and applying a Savitzky-Golay noise-smoothing filter using open-access Matlab code[38]. In order to visualize mechanical loading time-course metabolic data comprehensively, three-dimensional plots were created in Matlab (Figure 2, Supplementary Figures S2 and corresponding mp4 files)[39].

3.3.5. Statistical Analysis

Validation and mechanical loading data were not normally distributed and were therefore analyzed nonparametrically in R software (version 3.2.5). Pre- and post-inhibitor validation data were compared via paired Wilcoxon rank-sum tests.

Post-loading time and mechanical loading parameters were binned to statistically test for interactions between these covariates beyond individual regressions. Time post-loading was binned into five groups, and mechanical loading parameters (peak strain, peak force, peak strain

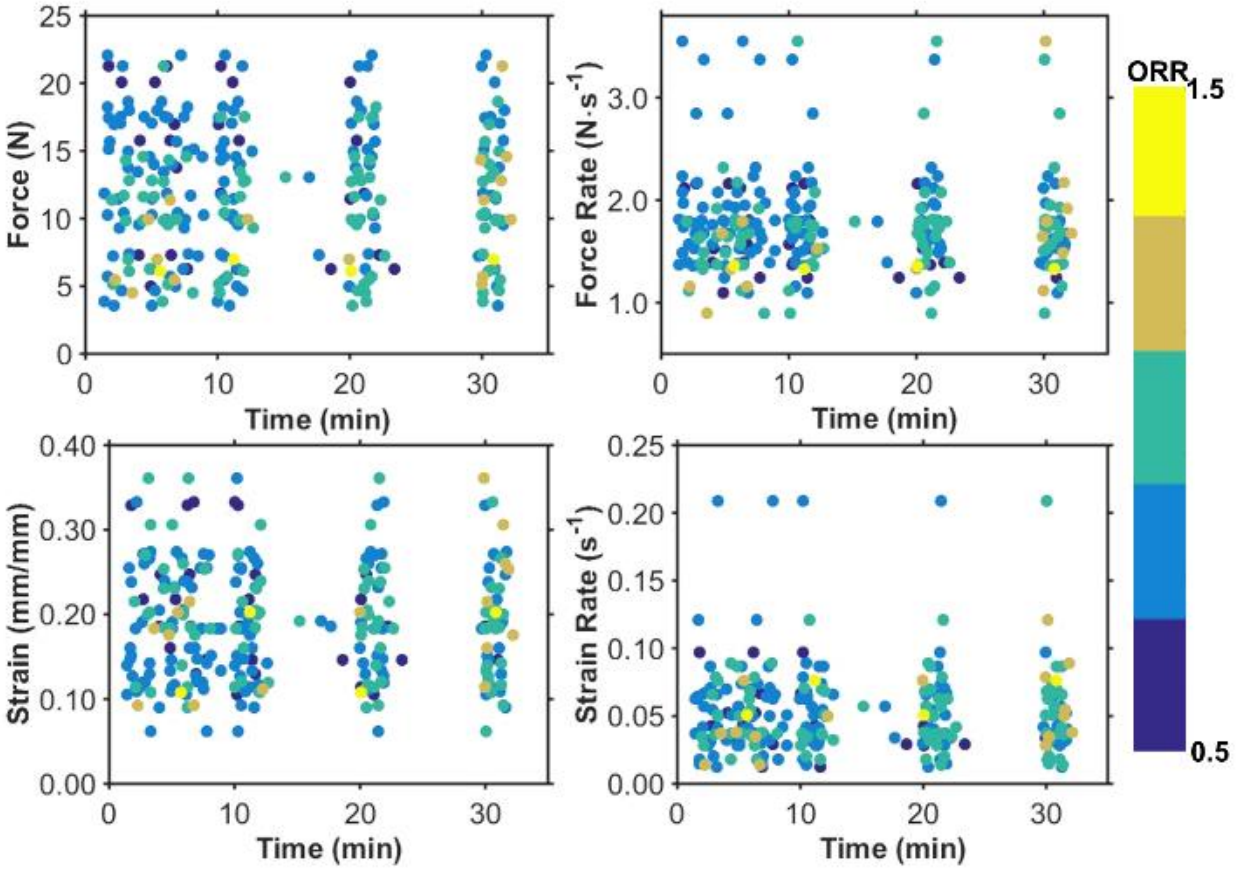

Figure 3-2. Optical redox ratio as a function of time and mechanical load. Qualitative trends with time and loading are visible. Full three-dimensional results are available in the supplementary data.

rate, and peak force rate) were each binned into three groups: low, medium, and high loading magnitude. Mechanical bin intervals were chosen to yield comparable n-values between bins. A two-way aligned rank transformation analysis of variance (ART ANOVA) was used to assess the effects of loading parameter magnitudes and time post-loading, both main effects and the interaction, on each respective metabolic output (channel 1, channel 2, and redox ratio). Significant

factors from each ANOVA were analyzed post-hoc via Tukey Honest Significant Difference (HSD) pairwise comparisons for detection of differences between binned groups.

3.4. Results

Inhibitors caused the expected changes in channels 1 and 2, validating the use of these imaging methods for cartilage (Figure 3). 2-DG, a glucose analog intended to inhibit glycolysis, decreased channel 1 (NAD(P)H) fluorescence (-13.0%) as expected, and increased channel 2 (FAD) fluorescence (+31.8%) and optical redox ratio ([FAD]/[FAD+NAD(P)H]) (+51.2%). Rotenone, an oxidative phosphorylation complex I inhibitor, caused the expected decrease of channel 2 fluorescence (-16.0%) as well as optical redox ratio (-5.4%), and also decreased channel 1 fluorescence (-5.4%). Wilcoxon rank-sum tests revealed statistically significant changes in all three metabolic outputs by both chemical inhibitors at $p<0.05$.

A range of peak strain, force, strain rate and force rate was achieved. Peak strain ranged from 0.06 to 0.36 (average = 0.19 ± 0.07). Peak force ranged from 3.6 to 22.0 N (average = 11.9 ± 5.0 N). Peak strain rate ranged from 0.01 to 0.21 s^{-1} (average = 0.05 ± 0.03 s^{-1}). Peak force rate ranged from 0.90 to 3.56 $N \cdot s^{-1}$ (average = 1.75 ± 0.48 $N \cdot s^{-1}$).

Post-loading time and loading magnitude had significant independent effects on all three metabolic measurements (Figures 4 and 5). However, none of the interactions between mechanical loading and post-loading time point were significant in the two-way ANOVAs. Channel 1 (NAD(P)H) fluorescence was consistently affected by time in all models, with an initial increase in fluorescence post-loading (+10.0% maximum) that subsided by 30 minutes post-loading, while channel 2 (FAD) fluorescence was unaffected by time point (Figure 4). Peak force magnitude had significant bearing on channel 1 fluorescence, with greater force showing greater intensity (+11.2% difference maximum) (Figure 5). Applied strain rate showed the opposite pattern, as

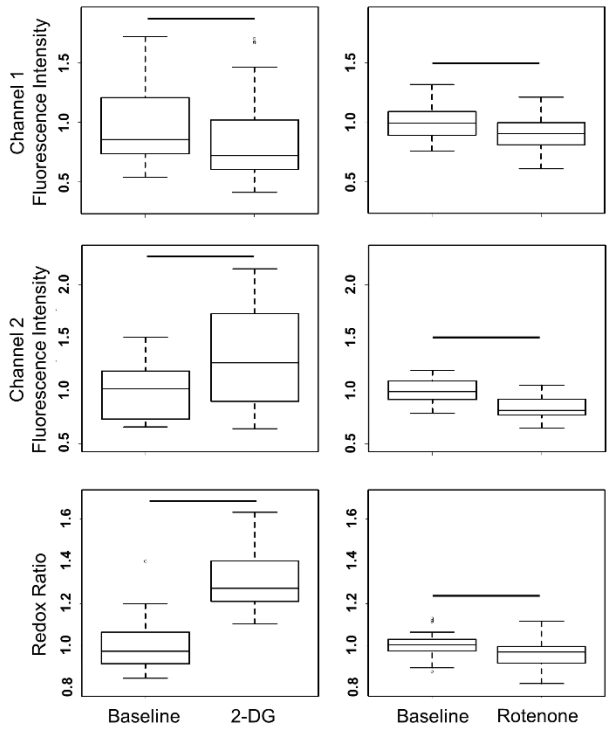

Figure 3-3. Imaging results of 2-DG (n = 32 imaging regions from 8 samples representing 3 animals) and rotenone metabolic inhibition (n = 36 imaging regions from 9 samples representing 3 animals). Data are expressed as median values (lines), interquartile range (box hinges), and data range constrained to total data range multiplied by interquartile range or less (whiskers) with outliers (circles). Fluorescence intensities were normalized to average baseline values within each sample. Pre- and post-inhibitor data were compared nonparametrically via Wilcoxon rank-sum tests. Significance bars = $p \leq 0.05$.

samples subjected to high strain rate showed significantly lower channel 1 fluorescence (-5.5%) than those subjected to low strain rate (Figure 5). However, peak strain and force rate had similar effects on channel 2 activity as on channel 1, with greater peak strain and force rate associating with greater channel 2 intensity (+6.3% and +3.7% maximum differences, respectively) (Figure

5). Redox ratio was affected by both time and loading magnitude (Figures 2, 4-5). Redox ratio was higher at later time points than earlier time points (+6.2%) (Figure 4). Higher peak force resulted in lower redox ratio (-6.9% maximum difference), and higher strain rate resulted in higher redox ratio (+3.28% maximum difference) (Figure 5). Statistical redox ratio trends were primarily governed by changes in channel 1 (NAD(P)H) fluorescence (Figures 4 and 5).

3.5. Discussion

Inhibition of glycolysis and oxidative phosphorylation demonstrated the validity of using optical redox imaging to evaluate metabolic activity in articular cartilage. Although slight in magnitude, rotenone caused a decrease in channel 2 fluorescence intensity as well as redox ratio, and 2-DG caused a decrease in channel 1 fluorescence intensity and increased redox ratio. Previous studies have demonstrated similarly mild effects of these inhibitors[24,34]. The pleiotropic actions of these compounds on both metabolites of interest, though seemingly off-target, are unsurprising given the inevitable interplay between metabolic processes. For example, rotenone has demonstrated an inhibitory effect on NAD(P)H production similar to that of 2-DG[34]. Conversely, short-term NADH photobleaching has been shown to cause an immediate sharp increase in FAD fluorescence intensity, perhaps as a compensatory mechanism to maintain ATP production[40]. In cartilage, glycolysis and mitochondrial respiration have demonstrated unique coupling such that glycolytic activity relies upon reactive oxygen species generated by oxidative phosphorylation[34,41]. It is possible that the higher concentration of glycolytic inhibitor 2-DG applied in the present study than previous studies (10 mM vs. 3 mM) stimulated a compensatory mechanism responsible for the apparent increase in oxidative phosphorylation activity following 24-hour incubation. Though the underlying mechanisms are not fully understood, the perturbation of both fluorescence

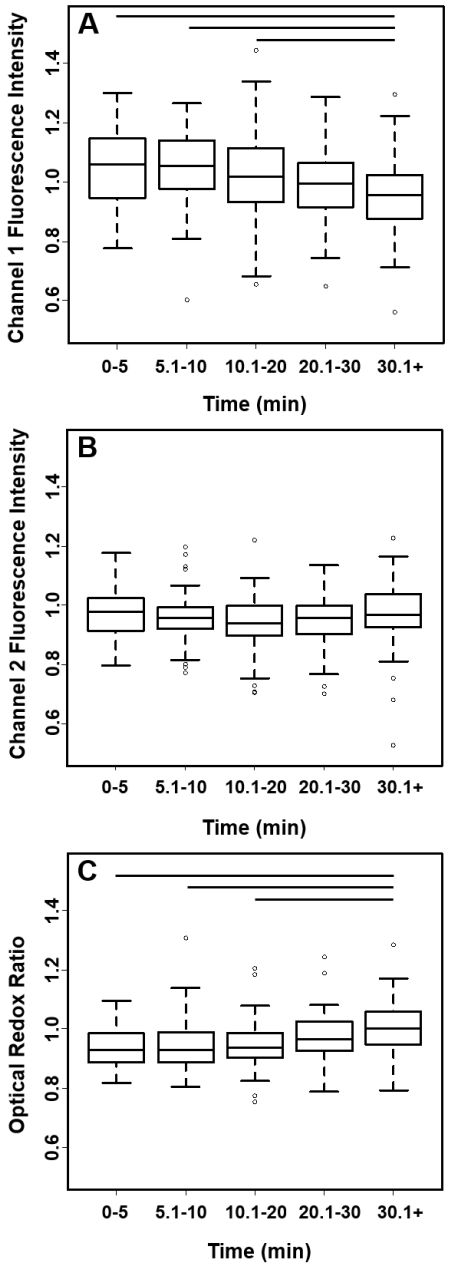

Figure 3-4. Metabolic outputs as a function of time. NAD(P)H fluorescence intensity is captured by channel 1 (A), FAD intensity is captured by channel 2 (B), and redox ratio (C) is calculated as [FAD]/[NAD(P)H + FAD]. Fluorescence intensities were normalized to baseline values averaged within each sample (per time bin: n=49-58 images from 25-27 samples representing 10 animals). Significance bars = $p \leq 0.05$.

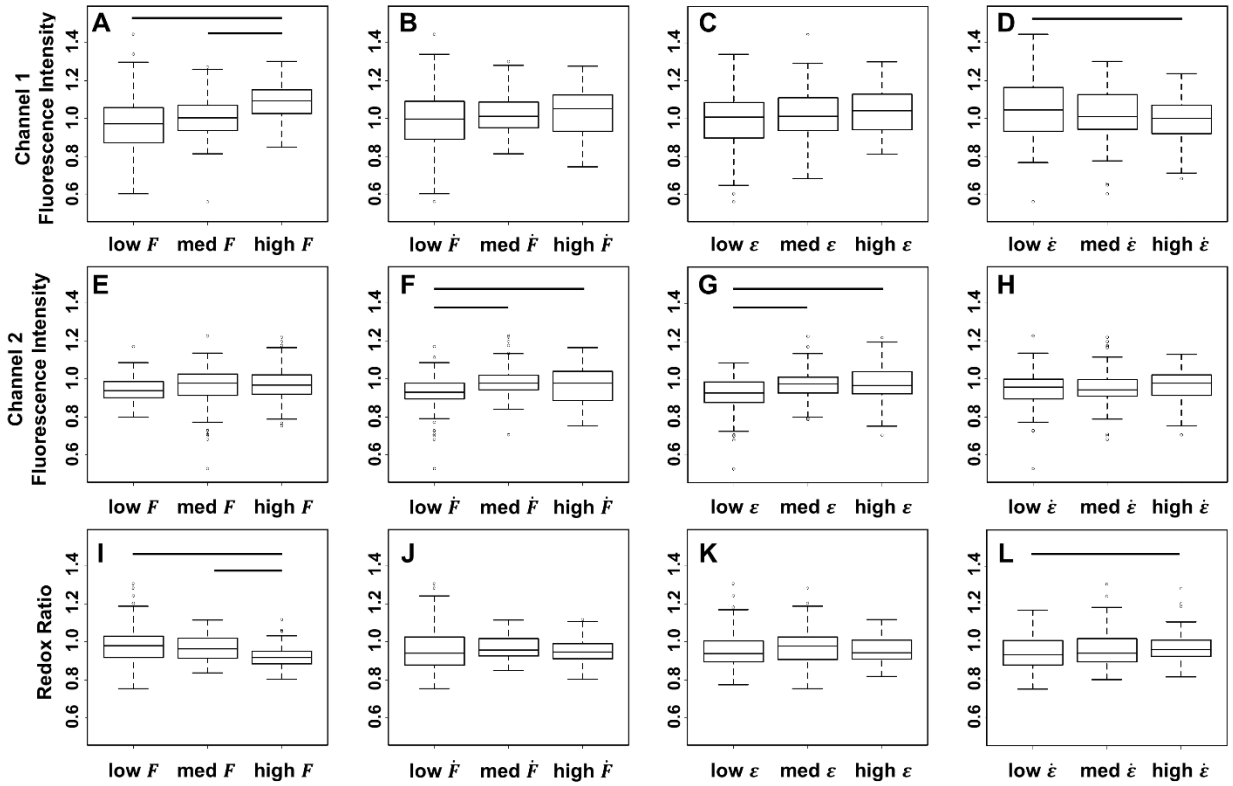

Figure 3-5. Metabolic response to mechanical loading. NAD(P)H fluorescence intensity is captured by channel 1 (A-D), FAD fluorescence intensity is captured by channel 2 (E-H) and redox ratio (I-L) is calculated as [FAD]/[NAD(P)H + FAD]. Metabolic output is displayed as a function of force (A, E, F), force rate (B, F, J), strain (C, G, K) and strain rate (D, H, L). Fluorescence intensities were normalized to baseline values averaged within each sample (per mechanical bin: n=75-107 images from 12-21 samples representing 10 animals). Significance bars = $p \leq 0.05$.

channels observed from sustained chemical inhibition in the present study is ultimately not unexpected.

Metabolic imaging revealed a time-dependent response immediately following a single physiological load. The loading applied in this study was maintained below the superphysiological range, with maximum peak strain values akin to estimated strains in vivo during dynamic loading activities, and loading rates were several orders of magnitude below the suggested criteria for impact loading[42,43]. Increased force, strain, and force rate corresponded with increased metabolic activity. Specifically, channel 1 fluorescence was significantly increased by greater force, and channel 2 fluorescence was increased by greater strain and force rate. This is consistent with previous research showing that moderate compressive loading of healthy chondrocytes stimulates an anabolic response that increases the cells' energy requirement and necessitates an increase in metabolic activity[44,45]. Conversely, increased strain rate corresponded with significantly decreased channel 1 fluorescence and a trend of decreased channel 2 fluorescence. While these mechanical loading effects may seem contradictory, they likely arise due to rate-dependent cartilage behavior that result from poroelasticity[46,47]. Compressive strain rate is often associated with fluid flow in cartilage, which subjects chondrocytes to shear, thus inducing metabolic flux[48,49]. Though bulk strain rates in the present study were physiological, resulting in minimal fluid flow across the whole tissue, metabolic imaging evaluated a local region of cartilage just beneath a cut sample edge where fluid flow may have played a nontrivial role in the observed metabolic changes[50]. Further, additional research could clarify whether the loads applied in this study, which were highly unlikely to be injurious, could induce a healthy inhibitory effect on anabolic activity as a physiological process by which metabolic homeostasis is maintained[51,52].

Time had a significant effect on channel 1 fluorescence in all two-way ANOVAs, consistently showing greatest intensity at early time. This result provides additional confidence that the metabolic changes observed resulted from mechanical loading, as metabolic activity induced

simply by time in non-physiological conditions alone would be expected to be minimal in the early time points. The same reasoning applied to the effect of mechanical loading magnitude, wherein compression stimulates anabolism, may pertain to time effect as well, as the stimulatory response observed early after loading appears to dissipate within 30 minutes. The decrease in channel 1 fluorescence by 30 minutes provides further evidence of the mild nature of the compression and in this study and confirms that the chosen time points capture the early effects of a single load. Indeed, it is prudent that the present study results are not overinterpreted on a mechanistic level given the limitations of the metabolic analysis method employed and as well as the simplicity of the applied loading regime. Rather, the present study reveals short-term variation in metabolic response to mechanical loading, leaving future studies with additional questions and a useful tool to tease out the mechanical thresholds that result in healthy and unhealthy cartilage response.

It is worth noting that the statistical model employed was chosen to allow for two-way ANOVA using nonparametric data. This model is unable to accommodate inclusion of individual animal source as a third covariate in addition to timepoint and mechanical input. However, animal-dependent variations were of interest, as samples from the same animal are not truly independent. Therefore, using the current statistical model, two-way ANOVAs were conducted with timepoint and animal as covariates against all three metabolic outputs (channel 1, channel 2, redox ratio) with post-hoc Tukey-corrected pairwise comparisons. Channel 1 and redox ratio showed no statistically significant pairwise comparisons between animal sources and very few approaching significance, and channel 2 output showing relatively few significant differences between animal sources (at $p<0.05$). Given the random distribution of mechanical bins, sample numbers did not allow for further two-way ANOVAs testing animal source against mechanical input as the two covariates. However, in light of the results of timepoint by animal interaction analyses and the

known consistency of animal source with respect to age, breed, approximate weight, housing conditions, and macroscopic tissue health, interpreting statistical analyses in which individual animal factor is omitted was considered to be appropriate for the current study.

Given that channel 2 (FAD) showed minimal changes compared to channel 1 (NAD(P)H), it is unsurprising that redox ratio appeared to be largely governed by channel 1 trends, mirroring all findings of statistical significance of this channel. It is well known that glycolysis is a faster method of ATP production than oxidative phosphorylation[3,53]. As such, it follows that these pathways would exhibit differential sensitivity to environmental perturbations with glycolysis likely showing earlier and possibly more robust effects, and that the byproducts of these processes would reflect this discrepancy. It is also unsurprising that channel 1 and channel 2 intensities were affected in largely the same direction by all mechanical parameters. A shift in metabolic preference indicated by a lasting increase or decrease in redox ratio, as observed in osteoarthritic chondrocytes, would signal a meaningful change in biological phenotype unlikely to be incited by a single load well below suggested thresholds for mechanical injury induction[5,6,43]. It should be noted that it is possible that mechanical loading such as that applied in the current study could have functional consequences on cell signaling and gene expression without necessarily demonstrating a shift in biological phenotype[54]. Such downstream effects have not yet been studied using the current imaging technique in cartilage.

Though optical redox imaging overcomes many challenges associated with current metabolic analyses, this technique does not come without limitations. Testing conditions differed from physiological joint conditions such that we cannot completely rule out differential metabolic activity driven by ambient temperature, oxygen concentration, and biochemical environment in the present study. This further motivates conservative interpretation of results, as additional studies

controlling for such environmental factors are warranted in order to derive mechanistic insights into truly physiological chondrocyte function. Furthermore, in addition to NAD(P)H and FAD, collagen cross-links are autofluorescent, with excitation and emission spectra that overlap with those of NAD(P)H[55]. The present study assumed consistent collagen fluorescence within and between samples because all samples were taken from animals of the same age and all metabolic images were collected when cartilage was in an unloaded state. Temperature was deemed to have no effect on collagen fluorescence in the present study, as the imaging protocol employed induced a thermal increase well below the threshold at which temperature-dependent change in collagen fluorescence becomes a concern (Supplementary Figure S1)[56]. Future studies including more variable tissue sources, particularly those of varied maturity, or significant temperature variation should seek to account for the contribution of collagen fluorescence in the NAD(P)H channel. Similarly, while the present study assumed equal cell counts across samples, future studies including samples of varying ages and/or depth-wise analysis should account for variance in cellularity across these parameters. Additionally, preliminary data demonstrated the presence of a photobleaching effect on NAD(P)H when samples were imaged multiple times at the same location. This finding tailored the design of the present study, which imaged regionally-grouped locations without re-imaging tissue that had already been exposed to fluorescent light. Previous studies have confirmed that NADH is subject to photobleaching and have elucidated the possibility of redox flux as a biological consequence of this process[40,57]. Lastly, cartilage imaging in the present study was confined to the superficial zone due to restricted light penetration through the middle and deep zones, while mechanical analyses determined bulk properties. Imaging across the sample cross section and coupling fluorescence results with local mechanics would likely yield new insights into cartilage metabolism as chondrocyte response to mechanical loading varies

between tissue zones[58]. The present study opted to image 4 mm diameter hemicylinders for the sake of mechanical loading; imaging thinly sliced cartilage cross sections could likely circumnavigate this limitation.

The present study demonstrated metabolic consequences of a single compressive load at varying physiological magnitudes in cartilage. The ability of optical redox imaging to detect mechanically-induced metabolic flux below the threshold of injury motivates the future application of this technique to various pathological models. Although multiphoton and confocal imaging, the modalities previously used for optical redox imaging, could reduce issues of imaging penetration and collagen fluorescence interference to some degree, the use of an epifluorescent microscope in the present study was motivated by access and mechanical adaptability. Indeed, these findings can be built upon by determining the immediate and long-term metabolic effects of alternative loading regimes such as cyclic loading or crack nucleation, and comparing load-induced metabolic flux between healthy and degrading cartilage can provide new insight into the mechanisms of OA progression. Furthermore, this is the first study, to the authors' knowledge, to describe adaptation of an epifluorescent microscope for optical redox imaging of FAD and NAD(P)H. The accessibility and simplicity of this technique is anticipated to attract a variety of research groups as it provides a more cost effective and easier method to assess metabolic changes relative to existing techniques.

Cartilage redox imaging provides a solution to several fundamental limitations of previous methods of metabolic analysis. This novel application of an existing technique opens a host of opportunities for studying the intermediate cellular activity between external perturbation and altered gene expression in cartilage, a time frame which has historically been difficult to capture.

Ultimately, optical redox imaging provides a simple yet powerful metric of chondrocyte metabolic phenotype, a benchmark with promising applications in OA research.

3.6. Acknowledgments

Funding from the UW-Madison VCGRE is gratefully acknowledged. Technical assistance with backplate calibration from Jack Fahy and imaging from Alexandra Ciolko is gratefully acknowledged.

3.7. References

1. Tchetina E V., Markova GA. 2018. Regulation of energy metabolism in the growth plate and osteoarthritic chondrocytes. Rheumatol. Int. 38:1–12.
2. Warburg O. 1956. On the origin of cancer cells. Science 123(3191):309–14.
3. Zheng J. 2012. Energy metabolism of cancer: Glycolysis versus oxidative phosphorylation (Review). Oncol. Lett. 4(6):1151–1157.
4. Stambough JL, Brighton CT, Iannotti JP, Storey BT. 1984. Characterization of growth plate mitochondria. J. Orthop. Res. 2(3):235–246.
5. Blanco FJ, López-Armada MJ, Maneiro E. 2004. Mitochondrial dysfunction in osteoarthritis. Mitochondrion 4(5-6 SPEC. ISS.):715–728.
6. Yang X, Chen W, Zhao X, et al. 2018. Pyruvate kinase M2 modulates the glycolysis of chondrocyte and extracellular matrix in osteoarthritis. DNA Cell Biol. 37(3):271–277.
7. Goetz JE, Coleman MC, Fredericks DC, et al. 2017. Time-dependent loss of mitochondrial function precedes progressive histologic cartilage degeneration in a rabbit meniscal destabilization model. J. Orthop. Res. 35(3):590–599.
8. Delco ML, Bonnevie ED, Bonassar LJ, Fortier LA. 2017. Mitochondrial dysfunction is an

acute response of articular chondrocytes to mechanical injury. J. Orthop. Res. 36(2):739–750.

9. Coleman MC, Ramakrishnan PS, Brouillette MJ, Martin JA. 2016. Injurious loading of articular cartilage compromises chondrocyte respiratory function. Arthritis Rheumatol. 68(3):662–671.

10. Han S-K, Wouters W, Clark A, Herzog W. 2012. Mechanically induced calcium signaling in chondrocytes in situ. J. Orthop. Res. 30(3):475–481.

11. Madden RMJ, Han S-K, Herzog W. 2015. The effect of compressive loading magnitude on in situ chondrocyte calcium signaling. Biomech. Model. Mechanobiol. 14(1):135–142.

12. Zignego DL, Hilmer JK, June RK. 2015. Mechanotransduction in primary human osteoarthritic chondrocytes is mediated by metabolism of energy, lipids, and amino acids. J. Biomech. 48(16):4253–4261.

13. Jutila AA, Zignego DL, Hwang BK, et al. 2014. Candidate mediators of chondrocyte mechanotransduction via targeted and untargeted metabolomic measurments. Arch. Biochem. Biophys. 545:116–123.

14. Jutila AA, Zignego DL, Schell WJ, June RK. 2014. Encapsulation of Chondrocytes in High-Stiffness Agarose Microenvironments for In Vitro Modeling of Osteoarthritis Mechanotransduction. Ann. Biomed. Eng. 43(5):1132–1144.

15. Adams SB, Setton LA, Kensicki E, et al. 2012. Global metabolic profiling of human osteoarthritic synovium. Osteoarthr. Cartil. 20(1):64–67.

16. Dai J, Yu D, Wang Y, et al. 2017. Kdm6b regulates cartilage development and homeostasis through anabolic metabolism. Ann. Rheum. Dis. 76(7):1295–1303.

17. Sanchez C, Bay-Jensen A-C, Pap T, et al. 2017. Chondrocyte secretome: a source of novel

insights and exploratory biomarkers of osteoarthritis. Osteoarthr. Cartil. .

18. Kahn MK, Coverdale JA, Leatherwood JL, et al. 2017. Age-related effects on markers of inflammation and cartilage metabolism in response to an intra-articular lipopolysaccharide challenge in horses. J. Anim. Sci. 95(2):671.

19. Salinas D, Minor CA, Carlson RP, et al. 2017. Combining targeted metabolomic data with a model of glucose metabolism: toward progress in chondrocyte mechanotransduction. PLoS One 12(1):e0168326.

20. Martin JA, McCabe D, Walter M, et al. 2009. N-Acetylcysteine inhibits post-impact chondrocyte death in osteochondral explants. J. Bone Jt. Surgery-American Vol. 91(8):1890–1897.

21. Brouillette MJ, Ramakrishnan PS, Wagner VM, et al. 2014. Strain-dependent oxidant release in articular cartilage originates from mitochondria. Biomech. Model. Mechanobiol. 13(3):565–72.

22. Lv M, Zhou Y, Chen X, et al. 2017. Calcium Signaling of in situ Chondrocytes in Articular Cartilage under Compressive Loading: Roles of Calcium Sources and Cell Membrane Ion Channels. J. Orthop. Res. .

23. Skala M, Ramanujam N. 2010. Multiphoton redox ratio imaging for metabolic monitoring in vivo. Methods Mol. Biol. 594:155–62.

24. Alhallak K, Rebello LG, Muldoon TJ, et al. 2016. Optical redox ratio identifies metastatic potential-dependent changes in breast cancer cell metabolism. Biomed. Opt. Express 7(11):4364–4374.

25. Quinn KP, Bellas E, Fourligas N, et al. 2012. Characterization of metabolic changes associated with the functional development of 3D engineered tissues by non-invasive,

dynamic measurement of individual cell redox ratios. Biomaterials 33(21):5341–8.

26. Quinn KP, Sridharan G V., Hayden RS, et al. 2013. Quantitative metabolic imaging using endogenous fluorescence to detect stem cell differentiation. Sci. Rep. 3(1):3432.

27. Hou J, Wright HJ, Chan N, et al. 2016. Correlating two-photon excited fluorescence imaging of breast cancer cellular redox state with seahorse flux analysis of normalized cellular oxygen consumption. J. Biomed. Opt. 21(6):60503.

28. Walsh AJ, Castellanos JA, Nagathihalli NS, et al. 2016. Optical imaging of drug-induced metabolism changes in murine and human pancreatic cancer organoids reveals heterogeneous drug response. Pancreas 45(6):863–9.

29. Shah AT, Heaster TM, Skala MC. 2017. Metabolic imaging of head and neck cancer organoids. PLoS One 12(1):1–17.

30. Rice WL, Kaplan DL, Georgakoudi I. 2010. Two-photon microscopy for non-invasive, quantitative monitoring of stem cell differentiation. PLoS One 5(4):e10075.

31. Nishida T, Kubota S, Aoyama E, Takigawa Yz M. 2013. Impaired glycolytic metabolism causes chondrocyte hypertrophy-like changes via promotion of phospho-Smad1/5/8 translocation into nucleus. Osteoarthr. Cartil. .

32. Mobasheri A, Vannucci SJ, Bondy CA, et al. 2002. Glucose transport and metabolism in chondrocytes: a key to understanding chondrogenesis, skeletal development and cartilage degradation in osteoarthritis. Histol. Histopathol. 17(4):1239–67.

33. Wang C, Silverman RM, Shen J, O'Keefe RJ. 2018. Distinct metabolic programs induced by TGF-β1 and BMP2 in human articular chondrocytes with osteoarthritis. J. Orthop. Transl. 12:66–73.

34. Martin JA, Martini A, Molinari A, et al. 2012. Mitochondrial electron transport and

glycolysis are coupled in articular cartilage. Osteoarthr. Cartil. 20(4):323–9.

35. Schneider CA, Rasband WS, Eliceiri KW. 2012. NIH Image to ImageJ: 25 years of image analysis. Nat. Methods 9(7):671–675.

36. Adavallan K, Gurushankar K, Nazeer SS, et al. 2017. Optical redox ratio using endogenous fluorescence to assess the metabolic changes associated with treatment response of bioconjugated gold nanoparticles in streptozotocin-induced diabetic rats. Laser Phys. Lett. 14(6):065901.

37. Henak CR, Bartell LR, Cohen I, Bonassar LJ. 2017. Multiscale strain as a predictor of impact-induced fissuring in articular cartilage. J. Biomech. Eng. 139(3).

38. Losada R. 2009. Savitzky-Golay Filtering. MathWorks, Inc. [cited 2018 May 6] Available from: https://www.mathworks.com/help/signal/ref/sgolayfilt.html.

39. [Date unknown]. scatter3: 3-D scatter plot. MathWorks, Inc. [cited 2019 Jan 23] Available from: https://www.mathworks.com/help/matlab/ref/scatter3.html?searchHighlight=scatter3&s_tid=doc_srchtitle#btrui17-1_seealso.

40. Combs CA, Balaban RS. 2001. Direct Imaging of Dehydrogenase Activity within Living Cells Using Enzyme-Dependent Fluorescence Recovery after Photobleaching (ED-FRAP). Biophys. J. 80(4):2018–2028.

41. Wolff KJ, Ramakrishnan PS, Brouillette MJ, et al. 2013. Mechanical stress and ATP synthesis are coupled by mitochondrial oxidants in articular cartilage. J. Orthop. Res. 31(2):191–6.

42. Sanchez-Adams J, Leddy HA, McNulty AL, et al. 2014. The mechanobiology of articular cartilage: bearing the burden of osteoarthritis. Curr. Rheumatol. Rep. 16(10):451.

43. Aspden RM, Jeffrey JE, Burgin LV. 2002. Letter to the editor. Osteoarthr. Cartil. 10(7):588–589.

44. Vincent TL, McLean CJ, Full LE, et al. 2007. FGF-2 is bound to perlecan in the pericellular matrix of articular cartilage, where it acts as a chondrocyte mechanotransducer. Osteoarthr. Cartil. 15(7):752–763.

45. Millward-Sadler SJ, Wright MO, Davies LW, et al. 2000. Mechanotransduction via integrins and interleukin-4 results in altered aggrecan and matrix metalloproteinase 3 gene expression in normal, but not osteoarthritic, human articular chondrocytes. Arthritis Rheum. 43(9):2091–2099.

46. Párraga Quiroga JM, Wilson W, Ito K, van Donkelaar CC. 2017. The effect of loading rate on the development of early damage in articular cartilage. Biomech. Model. Mechanobiol. 16(1):263–273.

47. Li LP, Herzog W. 2004. Strain-rate dependence of cartilage stiffness in unconfined compression: the role of fibril reinforcement versus tissue volume change in fluid pressurization. J. Biomech. 37(3):375–82.

48. Gemmiti C V, Guldberg RE. 2009. Shear stress magnitude and duration modulates matrix composition and tensile mechanical properties in engineered cartilaginous tissue. Biotechnol. Bioeng. 104(4):809–20.

49. Lane Smith R, Trindade MC, Ikenoue T, et al. 2000. Effects of shear stress on articular chondrocyte metabolism. Biorheology 37(1–2):95–107.

50. Han G, Hess C, Eriten M, Henak CR. 2018. Uncoupled poroelastic and intrinsic viscoelastic dissipation in cartilage. J. Mech. Behav. Biomed. Mater. 84:28–34.

51. Huber M, Trattnig S, Lintner F. 2000. Anatomy, biochemistry, and physiology of articular

cartilage. Invest. Radiol. 35(10):573–80.

52. Sophia Fox AJ, Bedi A, Rodeo SA. 2009. The basic science of articular cartilage: structure, composition, and function. Sports Health 1(6):461–8.

53. Pfeiffer T, Schuster S, Bonhoeffer S. 2001. Cooperation and Competition in the Evolution of ATP-Producing Pathways. Science (80-.). 292(5516):504–507.

54. Salinas D, Mumey BM, June RK. 2018. Physiological dynamic compression regulates central energy metabolism in primary human chondrocytes. Biomech. Model. Mechanobiol. :1–9.

55. Croce AC, Bottiroli G. 2014. Autofluorescence spectroscopy and imaging: a tool for biomedical research and diagnosis. Eur. J. Histochem. 58(4):2461.

56. Menter JM. 2006. Temperature dependence of collagen fluorescence. Photochem. Photobiol. Sci. 5(4):403.

57. Tiede LM, Nichols MG. 2006. Photobleaching of Reduced Nicotinamide Adenine Dinucleotide and the Development of Highly Fluorescent Lesions in Rat Basophilic Leukemia Cells During Multiphoton Microscopy. Photochem. Photobiol. 82(3):656.

58. Vanderploeg EJ, Wilson CG, Levenston ME. 2008. Articular chondrocytes derived from distinct tissue zones differentially respond to in vitro oscillatory tensile loading. Osteoarthr. Cartil. 16(10):1228–36.

Chapter 4: Mechanobiology of Cartilage Impact via Real-Time Metabolic Imaging*

Shannon K. Walsh, Joshua C. Shelley, Corinne R. Henak

*(*Manuscript under revision for publication in the Journal of Biomechanical Engineering)*

4.1. Abstract

Cartilage loading is important in both structural and biological contexts, with overloading known to cause osteoarthritis. Cellular metabolism, which can be evaluated through the relative measures of glycolysis and oxidative phosphorylation, is important in disease processes across tissues. Details of structural damage coupled with cellular metabolism in cartilage have not been evaluated. Therefore, the aim of this study was to characterize the time- and location-dependent metabolic response to traumatic impact loading in articular cartilage. Cartilage samples from porcine femoral condyles underwent a single traumatic injury that created cracks in most samples. Before and up to 30 minutes after loading, samples underwent optical metabolic imaging (OMI). OMI measures the fluorescent intensity of byproducts of the two metabolic pathways, FAD for oxidative phosphorylation and NAD(P)H for glycolysis, as well as the redox ratio between them. Images were taken at varied distances from the center of the impact. Time after impact, distance from impact center, contact pressure and compressive strain significantly affected the measured metabolic response. Shortly after impact, fluorescence intensity in both channels decreased, while redox ratio was unchanged. The most dramatic metabolic response was measured closest to the impact center, with both channels decreased following impact relative to baseline. Redox ratio was also affected by distance from the impact. Finally, both strain and contact pressure affected each

channel, with some different effects by magnitude. In conclusion, this study demonstrated that articular cartilage responds metabolically to traumatic impact loading in a time-, distance-, and load-dependent manner.

Keywords: mechanobiology, cartilage fracture, metabolism, optical redox imaging, impact

4.2. Introduction

Osteoarthritis (OA) primarily originates from two mechanically-mediated processes: consistent cyclic overload or single traumatic impact. High body mass index, obesity, and manual labor are known risk factors for OA, demonstrating the physiological cost of repetitive overload on cartilage health[1–5]. In the absence of repetitive overload, single traumatic impact injuries, such as intra-articular fracture, often also lead to accelerated post-traumatic OA[1,2,6–8].

Despite low cell density in cartilage, cellular behavior is important as a driver of both proper tissue function and dysfunction. Cellular behavior can be characterized in a variety of ways, including cell death, gene expression, protein production, and metabolic state. Cellular metabolism has recently been of increasing interest in cartilage. Cellular metabolism is a key marker of health, as well as a key determinant of regeneration, repair and cellular proliferation. Adenosine triphosphate (ATP), the main energy source for cells, is derived primarily from anaerobic glycolysis, which occurs in the cytosol, and aerobic oxidative phosphorylation (oxphos), which occurs in the mitochondria[9]. Mounting evidence shows cellular metabolism and mitochondrial function are altered in OA[10–16]. The timing of these changes, and whether they promote or indicate disease, are not understood.

While mechanical overloading is known to cause OA, some level of loading is required for maintenance of joint health. Animal models have demonstrated the adverse effects of complete cartilage unloading[17–20]. Because tissue failure occurs with both sub- and super-physiological loading, establishing the link between loading and cellular response, mechanobiology, is crucial for advancing our understanding of cartilage health and disease. Our recent study evaluated the effect of a single, physiological compression on the short-term metabolic response of articular cartilage[21]. In that study, we adapted optical metabolic imaging to demonstrate that cartilage exhibits temporary responses in oxphos and glycolysis activity within five minutes of experiencing a relatively slow, low-magnitude load. While an exciting step, that study naturally opened questions about the short-term metabolic response of cartilage to traumatic superphysiological loading.

Although both cartilage mechanobiology and cartilage failure following impact loading are well-studied individually, the connection of the two is ripe for further understanding. This is particularly important in the broader context of OA for evaluating how cells accelerate or intervene in the damage process. Following impact injury, gross fissuring, fibrillation, and mechanical softening occur[22–29]. The most commonly measured cellular response to traumatic impact loading is cell death. Generally, cell death occurs around cracks or other gross failure, the extent of cell death increases with increasing peak strain and strain rate, and cell death increases over time post-impact[24,30–34]. When evaluated in a matched experimental setup, cell death occurred at lower strain magnitudes than required to induce fissuring[23,35]. Altered gene expression and protein production also follow impact loading[34]. Relatedly, metabolic processes have been shown to respond to impact injury. For example, impact injury causes immediate mitochondrial depolarization as well as

longer-term reductions in metabolic activity[36–38]. Together, these studies strongly suggest the merit of evaluating metabolic pathway-specific outcomes following traumatic impact injury.

The present study leveraged our recent adaptation of optical metabolic imaging to evaluate the biological consequence of cartilage overloading. The specific objective of this study was to characterize the time- and location-dependent metabolic response to traumatic impact loading in articular cartilage.

4.3. Methods

Cartilage samples underwent a multi-step experimental protocol in order to create impact injury and capture the short-term metabolic response (Figure 1).

4.3.1. Sample Collection & Preparation

Articular cartilage samples were harvested from porcine stifles at a local abattoir within 4 hours of sacrifice. Cylindrical samples were excised from the weight-bearing region of bilateral medial femoral condyles from 8 animals using a 6 mm diameter biopsy punch and scalpel (sex unknown and assumed random). Any residual subchondral bone was removed from cartilage cylinders prior to storage or testing. Samples were stored in chondrocyte media containing Ham's F-12 media (Mediatech, Inc., Manassas, VA), 10% fetal bovine serum (Hyclone, GE Healthcare Bio-Sciences, Pittsburgh, PA), 50 μg/ml ascorbic acid (Amresco, LLC., Solon, OH), 30 μg/ml alpha-ketoglutaric acid (Thermo Fisher Scientific Chemicals, Inc., Waltham, MA), 300 μg/ml L-glutamine, 100 IU/ml penicillin G, 100 μg/ml streptomycin, and 6 mg/ml HEPES buffer (Corning, Inc., Corning, NY) at 37ºC, 5% CO_2 until use. All samples were tested within three days of harvest.

For testing, samples were prepared using a custom trimming fixture (Figure 1). Sixteen hemicylinders were created, each from a distinct explant, with two hemicylinders from each

animal. Samples were trimmed to approximately 1.5 mm thick to allow for the isolation of the articular cartilage from the subchondral bone and for the visibility of both impact tip and backplate

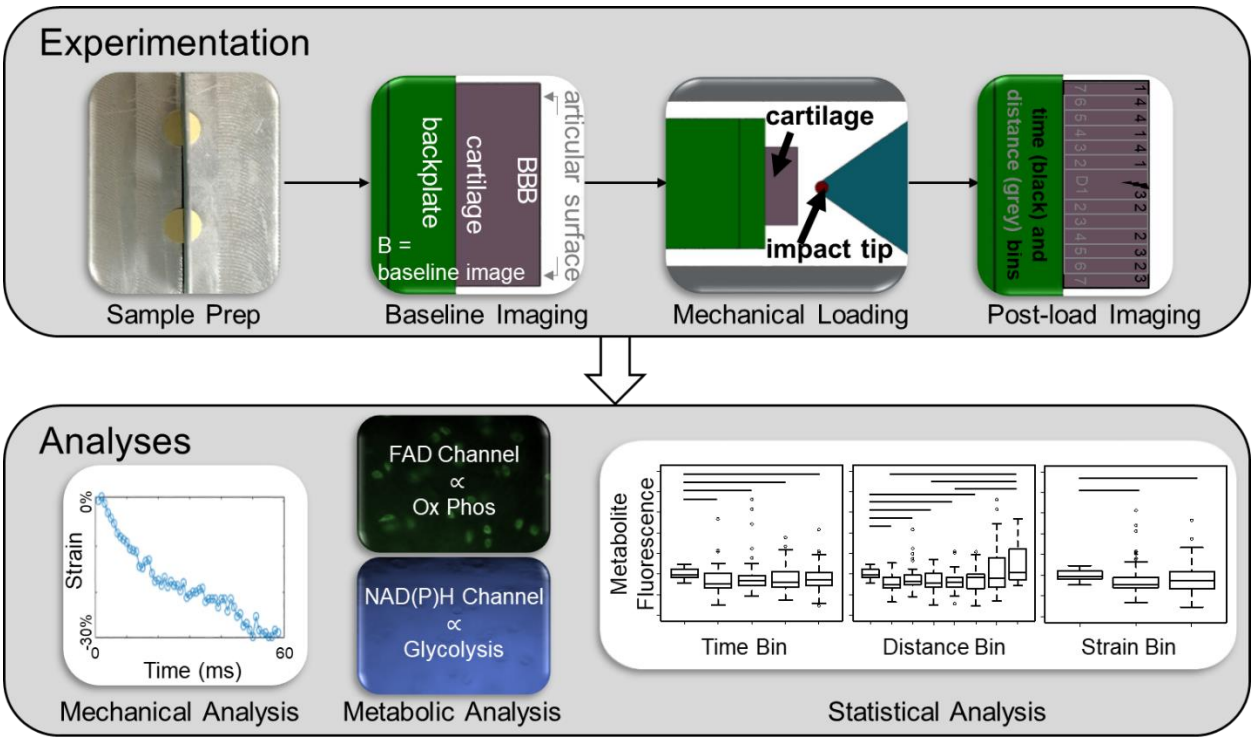

Figure 4-1. Overview of experimental and analysis methods. Samples were prepared, underwent baseline metabolic imaging, were impacted, then underwent imaging as a function of distance from the crack and time after impact. Following data acquisition, data were analyzed mechanically, metabolically, then statistically.

during impact. Samples were trimmed using a custom aluminum template that enabled consistent sizing and mitigated cartilage damage from surface abrasion. After trimming, samples were attached to the impact device backplate using a small amount of cyanoacrylate with cut surfaces in-line and planar with the bottom edge of the backplate. Samples were oriented with articular

surfaces facing outward. The backplate was then placed in the testing well at a height that enabled the microscope to focus on the cut surface.

4.3.2. Mechanical Loading & Imaging

Cartilage samples underwent impact loading on a custom-built microscope-top loading apparatus[21] (Figure 2 A,B). Briefly, the system consists of a custom well, backplate, and indenter which sit on an inverted brightfield and epiflourescent microscope (Olympus IX-71). The indenter was actuated (Aerotech ACT165D, Aerotech, Pittsburgh, PA), and deformation during loading was captured at 10,000 frames per second and at 4× magnification using a high-speed camera (Phantom v1211, Vision Research, Wayne, NJ) (Figure 2 C). The indenter was comprised of a 1 mm diameter cylindrical rod on a triangular cross-section. In the 2D projection captured by the camera, this resulted in an indenter geometry that appeared as a spheroconical indenter with a 500 μm radius and a 35° half angle. Samples were impacted at consistent input strains and strain rates. Once placed in the custom well, sample thickness (t) was measured optically. A target displacement of 80% strain at 1000 s^{-1} was then applied.

Metabolic imaging was performed as previously described[21]. Briefly, filter cubes were applied to an epifluorescent microscope to capture the autofluorescence of metabolites NAD(P)H and FAD in the green and DAPI channels, respectively[39]. All images were taken along the articular edge of the sample cross section to ensure ample light penetration. Prior to mechanical loading, three baseline images were taken at the center of each sample (Figure 1). Following loading, images were taken at randomized distances from the impacted site. No two images were taken at the same location so as to prevent photobleaching effect. A total of 12 post-impact images were taken per sample, with images temporally clustered into four time bins spanning from 0 to 30 minutes post-load (Figure 1).

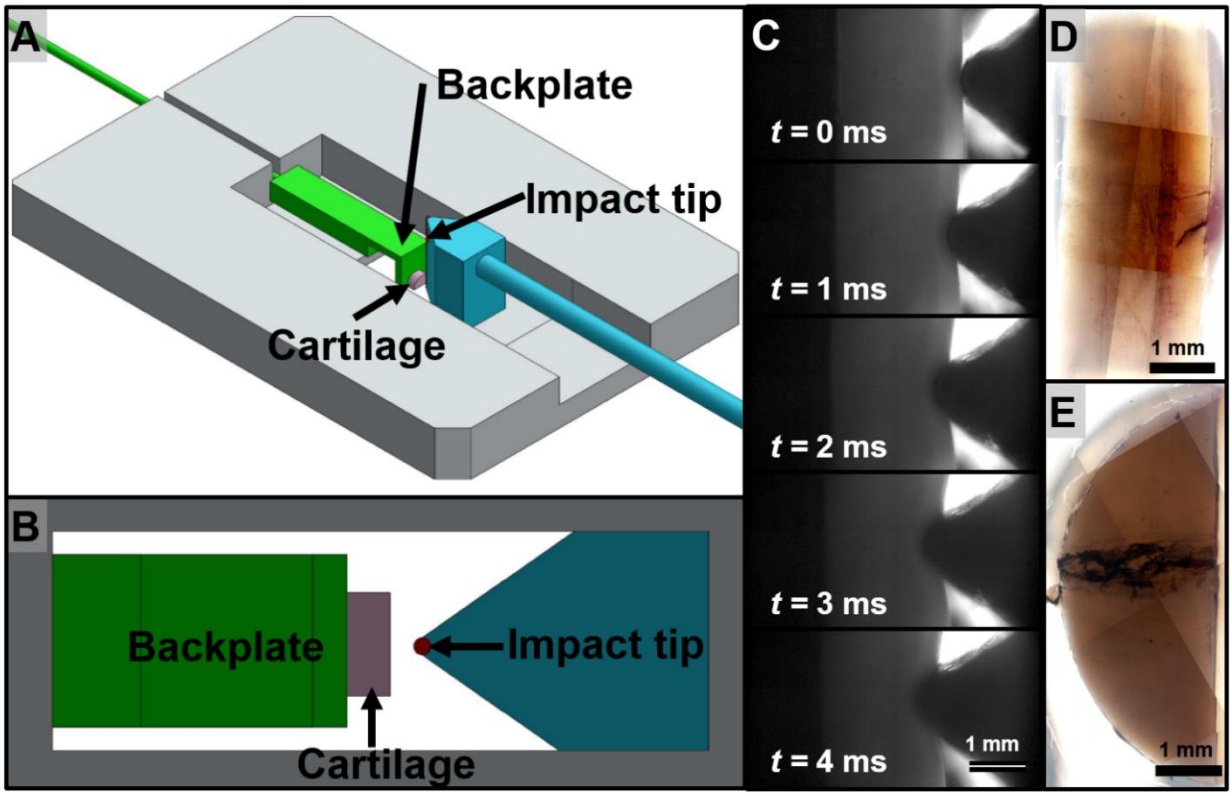

Figure 4-2. Impact device and methods, including (A) overview of whole impact device, (B) view as seen through the inverted microscope, (C) time series for a representative sample during impact, (D) crack as seen from the cut surface, and (E) crack as seen from the articular surface.

4.3.3. Post-Processing

Evaluation of fracture was performed on each sample following post-impact metabolic imaging (Figure 2D,E). Articular and cut surfaces of each sample were stained with India ink to highlight the fractures. Samples were then imaged using an inverted brightfield microscope at 4×.

Strain under the indenter tip and force applied to the samples were determined from camera images. Sample impact videos were cropped to include the area just under the impact tip. Custom

Matlab code tracked the displacement of the platen and backplate based on image intensity[21,23]. Engineering strain was calculated based on the length of the sample at each time point (distance between backplate and platen) in comparison to the reference length. Force was calculated based on the behavior of the backplate as a leaf spring, with a calibration constant determined by fitting an experimentally-obtained force versus displacement curve. Peak force (F) and strain (ε) at peak force were obtained. In order to estimate contact pressure, Hertzian contact solutions for spheroconical contact were used [40]. First, indentation depth (h) was calculated:

$$h = t \cdot \varepsilon \tag{1}$$

Along with the dimensions of the indenter, this was then used to estimate the contact radius (a) at the time of peak force using the expression:

$$h + \frac{a}{R}\left[\sqrt{a^2 - (R\cos(\theta))^2} - a\right] - \frac{a}{\tan(\theta)}\left[\frac{\pi}{2} - \arcsin\left(\frac{R\cos(\theta)}{a}\right)\right] = 0 \tag{2}$$

Where R is the radius of the indenter and θ is the angle of the conical portion of the indenter. Because all samples were cut as 6 mm diameter hemicylinders and impacted in approximately the center of the hemicylinder, the total contact area (A) at the time of peak force was calculated:

$$A = 2a \cdot (3\ \text{mm}) \tag{3}$$

This allowed the average contact pressure (p_{avg}) to be calculated:

$$p_{avg} = \frac{F}{A} \tag{4}$$

Metabolic images were analyzed as previously described[21]. Briefly, median fluorescence intensities for each image were determined using ImageJ software, and optical redox ratio was calculated [39,41]:

$$\text{Redox ratio} = \frac{\text{FAD channel}}{\text{FAD channel} + \text{NAD(P)H channel}} \tag{5}$$

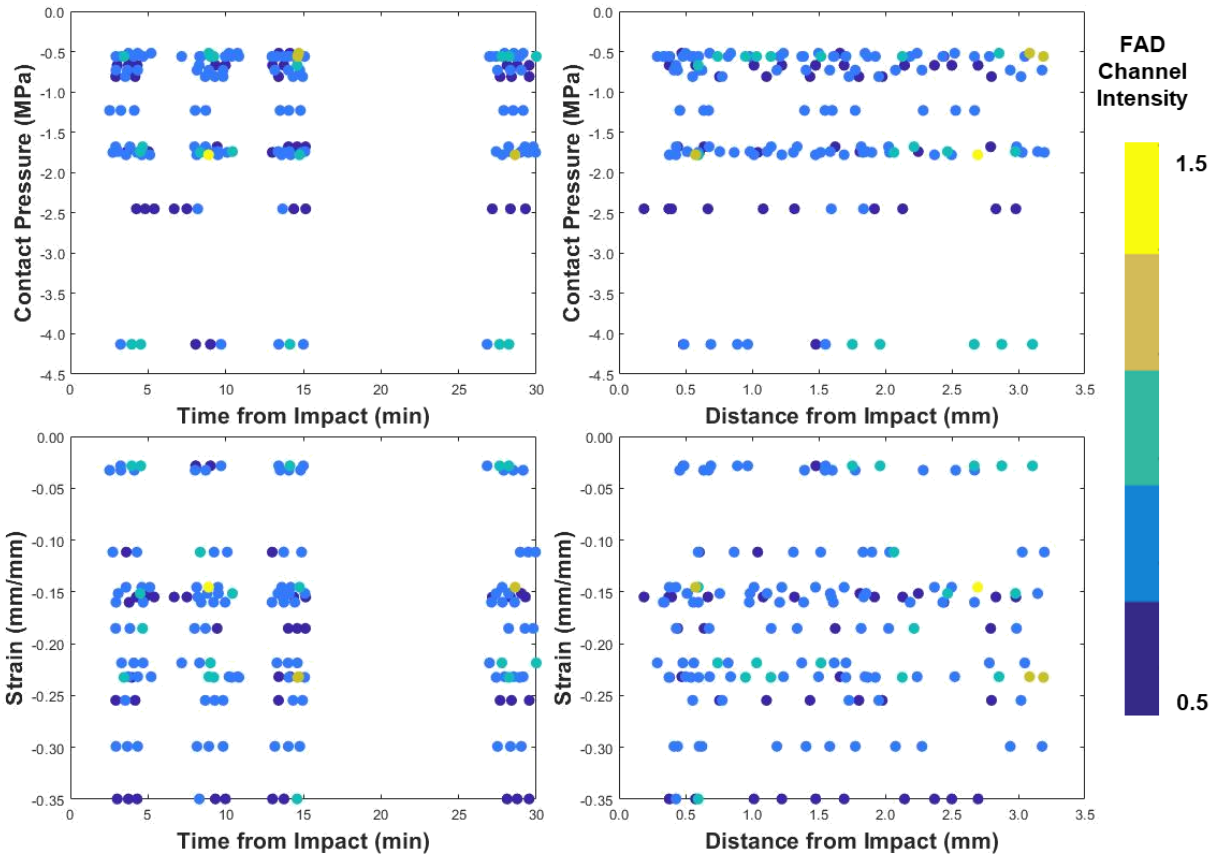

Figure 4-3. A subset of three-dimensional data depicting the effects of post-impact time and contact pressure (top left), time and strain (bottom left), distance from impact and contact pressure (top right), and distance and strain (bottom right) on FAD channel fluorescence intensity.

4.3.4. Statistical Analysis

Post-impact metabolic imaging yielded multi-dimensional data, all combinations of which were reviewed qualitatively via 3-dimensional plots generated in Matlab (Figure 3). Data were not normally distributed and therefore were analyzed nonparametrically. To assess the effects of time from impact, distance from impact, strain at peak load, and peak contact pressure on the metabolic outputs NAD(P)H channel fluorescence intensity, FAD channel fluorescence intensity, and redox

ratio, each of these predictor variables was binned into discrete groups. An Aligned Rank Transformation (ART) ANOVA was first performed to test for interaction effects between time and distance on both peak contact pressure and strain at peak load, respectively. Following the absence of significant interactions, a secondary set of ART ANOVA tests were performed to assess the effects of each individual predictor variable (time, distance, strain, contact pressure) on each of the three metabolic outputs, respectively. Significant main effects were further analyzed by post-hoc Tukey-corrected pairwise comparisons between predictor variable bins.

4.4. Results

4.4.1. Achieved Impact Loads

A range of impacts were delivered to the samples. The majority of samples (13/17) had visible fractures after testing. Three samples could not be analyzed due to lost videos or poor video contrast, leaving 14 samples for the remainder of the mechanical analysis, of which 11 fractured. The strain at maximum force was -18.3 ± 9.1% (range, -2.8% to -35.0%). Peak contact pressure was -1.37 ± 1.01 MPa (range, -0.52 MPa to -4.13 MPa).

4.4.2. Effect of Post-Impact Time on Metabolism

Time after impact affected both fluorescence channels individually but did not affect redox ratio (Figure 4 A, E, I). Averaged across distances, later time bins (>11 minutes post-impact) in the NAD(P)H channel showed lower median intensity than both baseline images and the 6-11 minute time bin, respectively, but not the 0-6 minute bin (Figure 4A). In the FAD channel, all post-impact time bins showed lower median fluorescence intensities than baseline images (Figure 4E).

4.4.3. Effect of Distance from Impact Center on Metabolism

Distance from impact affected all metabolic outputs (Figure 4 B, F, J). Averaged across time post-impact, NAD(P)H channel fluorescence bins 0.0-1.0 mm and 2.0-2.5 mm away from the site

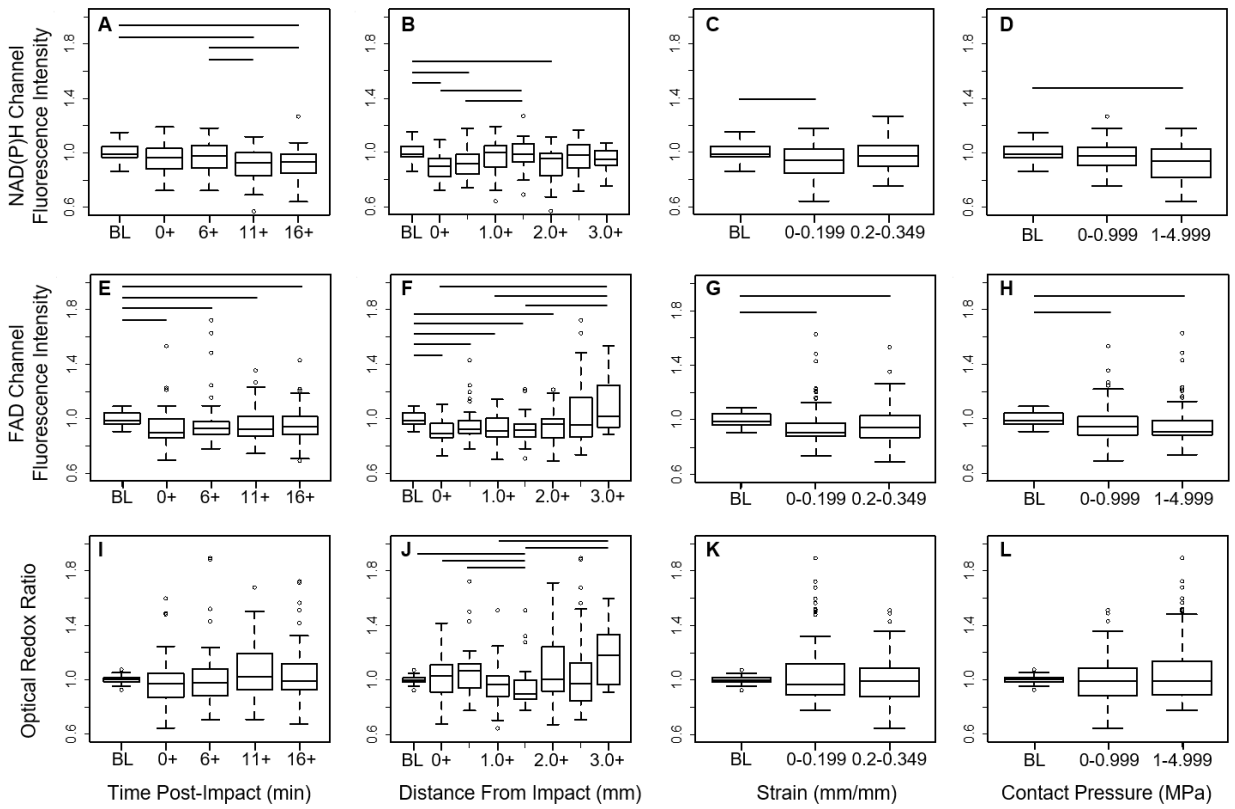

Figure 4-4. Metabolic response to impact loading. Boxplots represent the response of NAD(P)H channel fluorescence intensity (A-D), FAD channel fluorescence intensity (E-F), and redox ratio (I-L), a ratio of relative intensity contribution of both metabolites. Metabolic measurements were normalized to baseline measurements collected prior to loading (BL). The effects of predictor variables post-impact time (A, E, I), spatial distance from impact (B, F, J), mechanical strain at peak impact load (C, G, K) and estimated contact pressure at peak load (D, H, J) on metabolic response metrics were binned and evaluated nonparametrically. Note that distance from impact was binned into equal groups spanning 0.5 mm each. Significance bars indicate $p<0.05$.

of impact all showed decreased median intensities compared to baseline, while the median intensity from 1.5-2.0 mm was elevated from bins spanning 0.0-1.0 mm. The FAD channel saw decreased median fluorescence intensities in all bins spanning 0.0-2.5 mm from impact compared to pre-load baseline fluorescence, while images in this channel taken greater than 3.0 mm from impact showed greater fluorescence intensity than distance bins 0.0-0.5 mm and 1.0-2.0 mm, respectively. Median redox ratio was lowest at 1.5-2.0 mm from impact, showing significant deviation from baseline, 0.0-1.0 mm, and 3.0+ mm distance bins. Images taken farthest away from the impact site also demonstrated a greater redox ratio than those taken 1.0-1.5 mm away from impact.

4.4.4. Effect of Loading on Metabolism

Strain and contact pressure affected both fluorescence channels individually but did not affect redox ratio (Figure 4 C,D,G,H,K,L). Both low- and high-strain impact decreased fluorescence intensity in the FAD channel compared to baseline, and low-strain impact decreased intensity from baseline in the NAD(P)H channel. Similar effects were observed as a result of variable contact pressure. Both low- and high-pressure loading resulted in decreased FAD channel intensity, while only high-pressure loading decreased intensity in the NAD(P)H channel.

4.4.5. Interaction Effects on Metabolism

The interaction effects of mechanical loading and distance from impact were significant on the FAD channel and redox ratio (Figure 5). Specifically, the interaction between distance from impact and contact pressure significantly affected both FAD channel fluorescence and redox ratio. However, post-hoc analyses revealed no significant comparisons between paired condition levels.

4.5. Discussion

This study quantified the load-, location-, and time-dependent metabolic response to traumatic impact loading in articular cartilage. The observed patterns of metabolic flux indicate significant roles of each of these factors in cartilage mechanotransduction, as well as interplay between load and distance.

The location-dependent response to impact featured an immediate decrease in both channels closest to the impact site, while FAD increased steadily with distance and NAD(P)H had a variable response away from the impact site. Given the severity of the impacts delivered, it is reasonable to suppose that the observed decrease in accumulation of both metabolites and redox ratio closest to the impact site may be reflective of cell injury and dysfunction[42]. Conversely, the increase in redox ratio, a proxy for relative oxphos activity, observed beyond 2 mm away from the impact may reflect an effort to mount a regenerative response, as has been observed in cartilage undergoing biological distress[43].

Mechanical loading magnitude differentially affected individual metabolite channels. Dose-dependence of cartilage mechanotransduction has been established, although details of thresholds that are stimulatory versus inhibitory are case-specific[44–46]. Interestingly, low strain levels reduced fluorescence intensity compare to baseline in both channels, but high strain levels only reduced intensity in the FAD channel. This may suggest a threshold value between these two strain levels in the case of NAD(P)H. Like strain, the response of FAD to contact pressure was different than baseline in both contact pressure groups. Conversely, NAD(P)H was only affected by the largest contact pressures. While the contact pressures were on the low range of those predicted *in vivo* (e.g.,[47,48]), their ability to induce fracture suggests that they are relevant in the context of failure mechanobiology. Significant interaction effects, while difficult to interpret, suggest important interplay between regional and mechanical factors, which should be explored further.

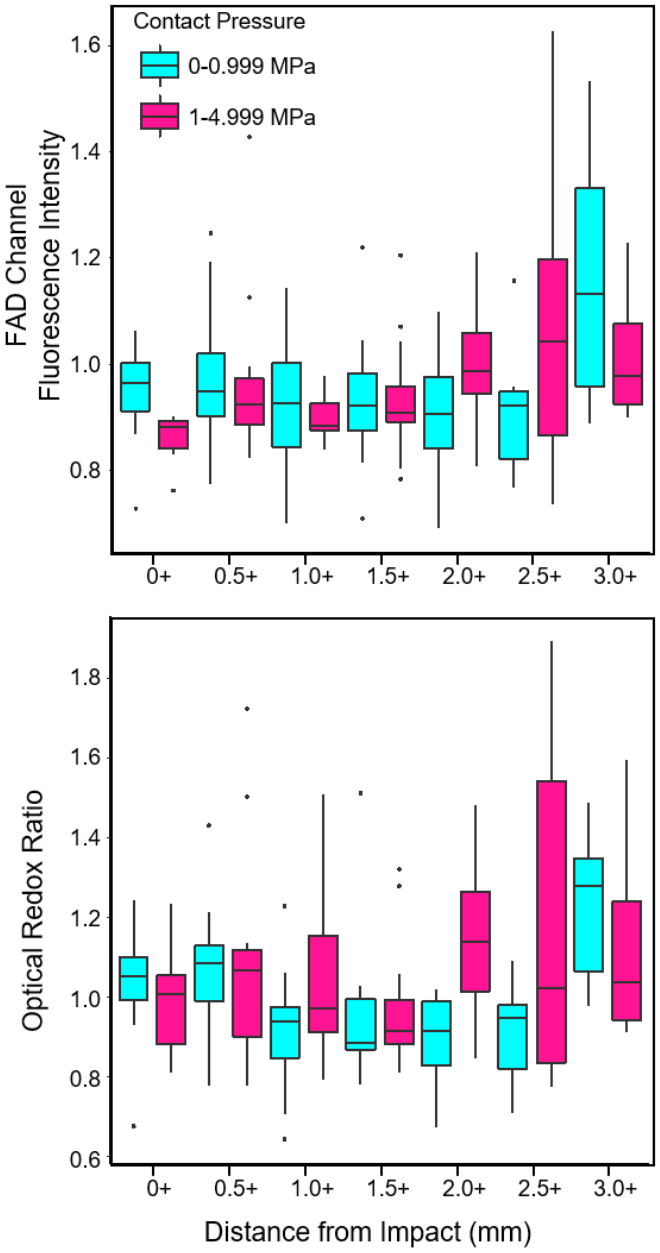

Figure 4-5. Metabolic response to impact loading with significant interaction effects. FAD channel intensity and redox ratio were affected by the interaction between contact pressure and distance from impact.

The results of this study can be compared to our previous study evaluating non-traumatic loading to provide insight into stimulatory and inhibitory effects of different loading magnitudes. For instance, the present study did not detect an increase in NAD(P)H channel intensity immediately post-loading as was observed in the previous study of non-injurious compression. Relatedly, while many of the loading effects observed in the case of non-traumatic loading subsided within 30 minutes of loading, the present study instead witnessed a reduction in NAD(P)H channel intensity 30 minutes after loading. This discrepancy makes sense in the context of our previous reasoning, wherein a mild compressive load induced short-term metabolic flux as a healthy homeostatic event. The current study, however, applied tissue damage more likely to incite a longer-term response, perhaps one of dysfunction rather than function, that would not be expected to dissipate within 30 minutes[49,50]. Additionally, impact loading resulted in a complex redox response with apparent contributions from both the NAD(P)H and FAD channels, whereas non-traumatic loading triggered a response primarily in the NAD(P)H channel. The slow, physiological loading response was postulated to be driven by glycolysis as a faster metabolic process than oxphos, and therefore potentially more sensitive to external perturbation[51,52]. It follows, then, that a traumatic event such as the high-impact load delivered in the present study would trigger a more robust response involving greater recruitment of metabolic faculties including mitochondrial oxphos, a slower but more energetically lucrative process[53]. Additionally, this response is consistent with previously demonstrated mitochondrial dysfunction following traumatic loading[37]. Previous studies have established functional links between mitochondrial activity and tissue biogenesis, as well as mitochondrial dysfunction and cartilage breakdown, respectively[37,43,54,55]. Perhaps the complexity of results observed in the present study is due, in part, to this dual involvement of mitochondrial function in cartilage repair and degradation.

The present study comes with several limitations. The applied impact loads were within a relatively narrow range, which limited our ability to determine load dose-dependent responses. However, this was intentional, as probing the full range of loads from physiological to injurious would be beyond the scope of a single study. While mechanical outputs were analyzed on a bulk scale, metabolic imaging was confined to the superficial zone to ensure adequate light penetration. Thus, bulk mechanics were used as a proxy for local mechanics at each imaging site. In addition, bulk mechanics were focused at the center of the impact, and it is possible that the responses measured far from impact resulted from the local mechanical stimuli rather than distance from impact alone. Although optical redox imaging has been demonstrated to detect metabolic flux with relatively high sensitivity, metabolic data must be interpreted conservatively as there are other autofluorescent molecules in addition to NAD(P)H and FAD, such as collagen, that are likely contributing to the fluorescence detected in each of the channels imaged. However, by using cartilage from animals of a consistent source and age, and without cartilage damage, the effects of other autofluorescence should be minimized in this study. Lastly, while the results of the present study are interpreted to have provided valuable mechanobiological information on a fundamental level, the simplicity of the experimental model must be accounted for when considering these findings from a physiological standpoint. Specifically, there are anatomic components lacking in the present model which likely affect cartilage behavior *in vivo* from mechanical and biological perspectives, namely subchondral bone and synovial fluid. Similarly, though porcine tissue is a common model for orthopedic research, translation of the present study to clinical relevance for human disease is ultimately limited by the health and age status of the samples tested and unavoidable interspecies variation.

Optical redox imaging has uncovered the differential response of articular cartilage to injurious and non-injurious loading with respect to relative oxphos and glycolysis activity. Future works will evaluate the downstream consequences of altered metabolic activity on gene expression and protein synthesis via mechanical loading as well as chemical metabolic inhibition. Additionally, upstream analysis will aim to elucidate the mechanobiological mechanisms responsible for translating mechanical stimuli into optical redox flux in chondrocytes.

Cartilage failure following traumatic loading and cartilage mechanobiology have been studied extensively, but largely independently of one another. However, as an avascular and aneural tissue, mechanical signals are critical to the activity of chondrocytes and, thus, the maintenance of tissue integrity. Given the significance of traumatic cartilage overload in this context, evaluating the failure mechanobiology response is of utmost importance. Technological advancements continue to enable observation of tissue mechanics and biology with greater precision, and it is crucial that such capabilities are employed in tandem as we work to advance our understanding of the intricate mechanosensitive signaling system driving articular cartilage function and dysfunction.

4.6. Acknowledgments

Funding from UW-Madison VCGRE is gratefully acknowledged. Tissue from the UW-Madison Meat Lab is gratefully acknowledged. Additional assistance on experiments from Alexey Minaev is gratefully acknowledged.

4.7. References

1. Murphy L, Helmick CG. 2012. The Impact of Osteoarthritis in the United States: A Population-Health Perspective. Am. J. Nurs. 112(3):13–19.
2. Zhang Y, Jordan JM. 2008. Epidemiology of osteoarthritis. Rheum Dis Clin North Am

34(3):515–529.

3. Sangha O. 2000. Epidemiology of rheumatic fever. Br. Soc. Rheumatol. 39:3–12.
4. Vina ER, Kwoh CK. 2017. Epidemiology of osteoarthritis: literature update. Curr. Opin. Rheumatol. .
5. Juhakoski R, Heliövaara M, Impivaara O, et al. 2009. Risk factors for the development of hip osteoarthritis: a population-based prospective study. Rheumatology (Oxford). 48(1):83–7.
6. Brown TD, Johnston RC, Saltzman CL, et al. 2006. Posttraumatic Osteoarthritis : A First Estimate of Incidence , Prevalence , and Burden of Disease. J. Orthop. Trauma 20(10):739–744.
7. Ferkel RD, Chams RN. 2007. Chronic lateral instability: arthroscopic findings and long-term results. Foot Ankle Int. 28(1):24–31.
8. Takao M, Uchio Y, Naito K, et al. 2005. Arthroscopic assessment for intra-articular disorders in residual ankle disability after sprain. Am. J. Sports Med. 33(5):686–92.
9. Randall D, Burggren W, French K. 2002. Eckert animal physiology: mechanisms and adaptations, 5th ed. W.H. Freeman and Company.
10. Martin JA, Martini A, Molinari A, et al. 2012. Mitochondrial electron transport and glycolysis are coupled in articular cartilage. Osteoarthr. Cartil. 20(4):323–9.
11. Blanco FJ, López-Armada MJ, Maneiro E. 2004. Mitochondrial dysfunction in osteoarthritis. Mitochondrion 4(5-6 SPEC. ISS.):715–728.
12. Coleman MC, Ramakrishnan PS, Brouillette MJ, Martin JA. 2016. Injurious loading of articular cartilage compromises chondrocyte respiratory function. Arthritis Rheumatol. 68(3):662–671.

13. Zignego DL, Hilmer JK, June RK. 2015. Mechanotransduction in primary human osteoarthritic chondrocytes is mediated by metabolism of energy, lipids, and amino acids. J. Biomech. 48(16):4253–4261.

14. Jutila AA, Zignego DL, Hwang BK, et al. 2014. Candidate mediators of chondrocyte mechanotransduction via targeted and untargeted metabolomic measurments. Arch. Biochem. Biophys. 545:116–123.

15. Jutila AA, Zignego DL, Schell WJ, June RK. 2014. Encapsulation of Chondrocytes in High-Stiffness Agarose Microenvironments for In Vitro Modeling of Osteoarthritis Mechanotransduction. Ann. Biomed. Eng. 43(5):1132–1144.

16. Adams SB, Setton LA, Kensicki E, et al. 2012. Global metabolic profiling of human osteoarthritic synovium. Osteoarthr. Cartil. 20(1):64–67.

17. Jurvelin J, Helminen H, Lauritsalo S, et al. 1985. Influences of Joint Immobilization and Running Exercise on Articular Cartilage Surfaces of Young Rabbits: A Semiquantitative Stereomicroscopic and Scanning Electron Microscopic Study. Acta Anat. (Basel). 122:62–68.

18. Videman T. 1982. The effect of running on the osteoarthritic joint: an experimental matched-pair study with rabbits`. Rheumatol. Rehabil. XXI(1):1–8.

19. Palmoski MJ, Brandt KD. 1981. Running Inhibits the Reversal of Atrophic Changes in Canine Knee Cartilage After Removal of a Leg Cast. Arthritis Rheum. 24(11):1329–1337.

20. Ni G-X, Zhou Y-Z, Chen W, et al. 2016. Different responses of articular cartilage to strenuous running and joint immobilization. Connect. Tissue Res. 57(2):143–151.

21. Walsh SK, Skala MC, Henak CR. 2019. Real-time optical redox imaging of cartilage metabolic response to mechanical loading. Osteoarthr. Cartil. 27(12):1841–1850.

22. Lee CM, Kisiday JD, McIlwraith CW, et al. 2013. Development of an in vitro model of injury-induced osteoarthritis in cartilage explants from compressive overload. Am. J. Vet. Res. 74(1).

23. Henak CR, Bartell LR, Cohen I, Bonassar LJ. 2017. Multiscale strain as a predictor of impact-induced fissuring in articular cartilage. J. Biomech. Eng. 139(3).

24. Argote PF, Kaplan JT, Poon A, et al. 2019. Chondrocyte viability is lost during high-rate impact loading by transfer of amplified strain, but not stress, to pericellular and cellular regions. Osteoarthr. Cartil. .

25. Rolauffs B, Kurz B, Felka T, et al. 2013. Stress-vs-time signals allow the prediction of structurally catastrophic events during fracturing of immature cartilage and predetermine the biomechanical, biochemical, and structural impairment. J. Struct. Biol. 183(3):501–11.

26. Leucht F, Dürselen L, Hogrefe C, et al. 2012. Development of a new biomechanically defined single impact rabbit cartilage trauma model for in vivo-studies. J. Invest. Surg. 25(4):235–41.

27. Borrelli J, Zaegel MA, Martinez MD, Silva MJ. 2010. Diminished cartilage creep properties and increased trabecular bone density following a single, sub-fracture impact of the rabbit femoral condyle. J. Orthop. Res. 28(10):1307–14.

28. Flachsmann R, Kistler M, Rentzios A, Broom ND. 2006. Influence of an initiating microsplit on the resistance to compression-induced rupture of the articular surface. Connect. Tissue Res. 47(2):77–84.

29. Oakley SP, Lassere MN, Portek I, et al. 2004. Biomechanical, histologic and macroscopic assessment of articular cartilage in a sheep model of osteoarthritis. Osteoarthr. Cartil. 12(8):667–679.

30. D'Lima DD, Hashimoto S, Chen PC, et al. 2001. Human chondrocyte apoptosis in response to mechanical injury. Osteoarthr. Cartil. 9(8):712–719.

31. Lewis JL, Deloria LB, Oyen-Tiesma M, et al. 2003. Cell death after cartilage impact occurs around matrix cracks. J. Orthop. Res. 21(5):881–887.

32. Waters NP, Stoker AM, Carson WL, et al. 2014. Biomarkers affected by impact velocity and maximum strain of cartilage during injury. J. Biomech. 47(12):3185–3195.

33. Stolberg-Stolberg JA, Furman BD, Garrigues NW, et al. 2013. Effects of cartilage impact with and without fracture on chondrocyte viability and the release of inflammatory markers. J. Orthop. Res. 31(8):1283–92.

34. Natoli RM, Scott CC, Athanasiou KA. 2008. Temporal effects of impact on articular cartilage cell death, gene expression, matrix biochemistry, and biomechanics. Ann. Biomed. Eng. 36(5):780–92.

35. Bartell LR, Xu MC, Bonassar LJ, Cohen I. 2018. Local and global measurements show that damage initiation in articular cartilage is inhibited by the surface layer and has significant rate dependence. J. Biomech. 72:63–70.

36. Huser CAM, Davies ME. 2007. Calcium signaling leads to mitochondrial depolarization in impact-induced chondrocyte death in equine articular cartilage explants. Arthritis Rheum. 56(7):2322–2334.

37. Delco ML, Bonnevie ED, Bonassar LJ, Fortier LA. 2017. Mitochondrial dysfunction is an acute response of articular chondrocytes to mechanical injury. J. Orthop. Res. 36(2):739–750.

38. Haudenschild DR, Carlson AK, Zignego DL, et al. 2018. Inhibition of early response genes prevents changes in global joint metabolomic pro fi les in mouse post-traumatic

osteoarthritis. Osteoarthr. Cartil. (December):1–9.

39. Skala M, Ramanujam N. 2010. Multiphoton redox ratio imaging for metabolic monitoring in vivo. Methods Mol. Biol. 594:155–62.

40. Briscoe BJ, Sebastian KS, Adams MJ. 1994. The effect of indenter geometry on the elastic response to indentation. J. Phys. D. Appl. Phys. 27(6):1156.

41. Schneider CA, Rasband WS, Eliceiri KW. 2012. NIH Image to ImageJ: 25 years of image analysis. Nat. Methods 9(7):671–675.

42. Aspden RM, Jeffrey JE, Burgin LV. 2002. Letter to the editor. Osteoarthr. Cartil. 10(7):588–589.

43. Tchetina E V., Markova GA. 2018. Regulation of energy metabolism in the growth plate and osteoarthritic chondrocytes. Rheumatol. Int. 38:1–12.

44. Zhang R-K, Li G-W, Zeng C, et al. 2018. Mechanical stress contributes to osteoarthritis development through the activation of transforming growth factor beta 1 (TGF-β1). Bone Joint Res. 7(11):587–594.

45. Gemmiti C V, Guldberg RE. 2009. Shear stress magnitude and duration modulates matrix composition and tensile mechanical properties in engineered cartilaginous tissue. Biotechnol. Bioeng. 104(4):809–20.

46. Bartell LR, Fortier LA, Bonassar LJ, Cohen I. 2015. Measuring microscale strain fields in articular cartilage during rapid impact reveals thresholds for chondrocyte death and a protective role for the superficial layer. J. Biomech. :3440–3446 [cited 2015 Dec 14] Available from: https://www.clinicalkey.com/#!/content/playContent/1-s2.0-S0021929015003255?returnurl=null&referrer=null.

47. Harris MD, Anderson AE, Henak CR, et al. 2012. Finite element prediction of cartilage

contact stresses in normal human hips. J. Orthop. Res. 30(7):1133–1139.

48. Wilson W, Van Rietbergen B, Van Donkelaar CC, Huiskes R. 2003. Pathways of load-induced cartilage damage causing cartilage degeneration in the knee after meniscectomy. J. Biomech. 36(6):845–851.

49. Vincent TL, McLean CJ, Full LE, et al. 2007. FGF-2 is bound to perlecan in the pericellular matrix of articular cartilage, where it acts as a chondrocyte mechanotransducer. Osteoarthr. Cartil. 15(7):752–763.

50. Millward-Sadler SJ, Wright MO, Davies LW, et al. 2000. Mechanotransduction via integrins and interleukin-4 results in altered aggrecan and matrix metalloproteinase 3 gene expression in normal, but not osteoarthritic, human articular chondrocytes. Arthritis Rheum. 43(9):2091–2099.

51. Pfeiffer T, Schuster S, Bonhoeffer S. 2001. Cooperation and Competition in the Evolution of ATP-Producing Pathways. Science (80-.). 292(5516):504–507.

52. Zheng J. 2012. Energy metabolism of cancer: Glycolysis versus oxidative phosphorylation (Review). Oncol. Lett. 4(6):1151–1157.

53. Agathocleous M, Harris WA. 2013. Metabolism in physiological cell proliferation and differentiation. Trends Cell Biol. 23(10):484–492.

54. Singh P, Marcu KB, Goldring MB, Otero M. 2018. Phenotypic instability of chondrocytes in osteoarthritis: on a path to hypertrophy. Ann. N. Y. Acad. Sci. .

55. Goetz JE, Coleman MC, Fredericks DC, et al. 2017. Time-dependent loss of mitochondrial function precedes progressive histologic cartilage degeneration in a rabbit meniscal destabilization model. J. Orthop. Res. 35(3):590–599.

Chapter 5: Fluctuation of Baseline Metabolism Throughout Articular Cartilage Maturation and Downstream Consequences on Tissue Health

Walsh, S.K. Arendt, L.M., Skala, M.C., Henak, C.R.

5.1. Abstract

OBJECTIVE: Eukaryotic cells derive energy through two main anaerobic metabolic pathways: glycolysis and oxidative phosphorylation (oxphos). In healthy cartilage, glycolysis has been associated with proliferation while oxphos has been linked to biogenesis. Recently, metabolic dysregulation has been implicated as a key feature of cartilage degradation and the progression of osteoarthritis (OA). When coupled with the strong correlation between aging and development of OA, these findings suggest that maturation predisposes cartilage to metabolic instability, with downstream consequences for tissue maintenance. The aims of this study were: (a) to evaluate maturation-dependent metabolic activity in cartilage, (b) to analyze consequences of metabolic inhibition on gene expression, and (c) to assess the correlation between metabolic activity and cartilage health. *METHODS:* Femoral cartilage samples were excised from pigs ranging from 3 days old to 6 years old. Age groups were chosen to span three porcine maturation stages: immature (0-4 months), adolescent (5-18 months), and mature (> 18 months). Maturation-dependent metabolism was analyzed via optical metabolic imaging (OMI), which leverages the autofluorescence of NAD(P)H, an electron donor, and FAD, an electron acceptor. Optical redox ratio, defined here as [FAD] / [NAD(P)H + FAD], provides a measure of the relative amounts of oxphos to glycolysis activity. After imaging, a subset of samples were sectioned and stained for

proteoglycan with Safranin O/Fast Green and scored for evidence of tissue degeneration via the OARSI scale. A separate set of samples was subjected to chemical inhibition of either glycolysis or oxphos, followed by gene expression analysis for the following cartilage maintenance genes: Col2, Col1, Col10, ACAN, SOX9, ADAMTS4, and ADAMTS5. *RESULTS:* NAD(P)H and FAD fluorescence channels both demonstrated increasing intensity with age, while redox ratio was lowest in adolescent samples compared to either immature or mature samples. Inhibition of glycolysis resulted in suppressed expression of Col2, Col1, ADAMTS4, and ADAMTS5 compared to control samples, while oxphos inhibition had no effect. Metabolic activity was moderately correlated with histological degeneration, with redox ratio demonstrating the strongest positive correlation with OARSI score. *CONCLUSIONS:* This study demonstrates maturation-dependent metabolic activity in cartilage and explores consequences of this differential activity with respect to tissue maintenance. This work provides valuable insight from multiple perspectives, aiding our basic understanding of cartilage biology and highlighting opportunity for potential diagnostic application.

5.2. Introduction

Articular cartilage, the hyaline cartilage cushioning long bone endings in synovial joints, loses all regenerative capacity once skeletal maturity has been reached[1–3]. This loss of function imminently predisposes cartilage to accumulation of damage over time, ultimately leading to a high prevalence of osteoarthritis (OA) amongst the aged population as well as those who have suffered from an orthopedic joint injury[4–6]. Although extensively studied, the biological underpinnings of loss of regenerative capacity with maturation are incompletely understood. This mechanistic knowledge gap poses a substantial barrier to development of effective therapies for

the prevention or reversal of cartilage degradation[3].

Metabolic dysregulation has recently been proposed to play a key role in OA progression[7–9]. Specifically, a growing body of evidence has demonstrated cartilage damage-associated mitochondrial dysfunction in the form of mitochondrial membrane depolarization, proton leakage, and reactive oxygen species (ROS) accumulation[10–13]. Furthermore, research across tissue types has revealed a correlation between the two major metabolic pathways in eukaryotic cells, oxidative phosphorylation (oxphos) and glycolysis, and tissue growth[14]. Specifically, the relative ratio of oxphos activity to glycolysis activity, sometimes referred to as redox ratio, has been correlated with differential proliferation and biosynthesis activity[15–18]. This phenomenon was perhaps first noted with the discovery of the Warburg Effect, in which cancer cells demonstrate increased glycolysis activity as they develop hyperproliferative functionality[19,20]. Interestingly, growth plate chondrocytes demonstrate metabolic zonal variation, with greater relative preference for glycolysis at the calcifying hypertrophic zone and greater relative preference for oxphos at the biosynthetic reserve front[15,21]. Given the dynamic nature of growth plate cartilage with respect to synthesis of new cartilage as well as bone formation, growth plate chondrocytes provide a useful model for determining the underpinnings of chondrocyte function that may have consequences for cartilage pathology. Indeed, OA cartilage has demonstrated altered metabolic activity akin to that of hypertrophic growth plate cartilage, such as expression of type X collagen and other differentiation-related genes as well as apoptosis, when compared with healthy articular cartilage[15,22–26]. However, the specific downstream consequences of altered metabolic activity observed in OA cartilage have not been characterized.

While relative rates of oxphos and glycolysis have been associated with differential tissue synthesis activity including the degenerative progression of OA, and post-adolescent loss of

regenerative capacity is well-established in cartilage, maturation-dependent oxphos and glycolysis activity have not been explicitly characterized in this tissue. Furthermore, the consequences of differential metabolic activity with respect to expression of genes pertinent to cartilage tissue homeostasis and regeneration have not been described. Therefore, the present study sought to determine maturation-dependent cartilage activity with respect to these two metabolic pathways, and to begin establishing connections between differential metabolic activity, extracellular matrix (ECM) maintenance, and tissue health. Specifically, this study sought to test the following three hypotheses: (a) Chondrocytes exhibit differential metabolic activity between immaturity (0-4 months), adolescence (5-18 months), and maturity (>18 months), (b) perturbation of metabolic activity has downstream consequences on expression of genes pertinent to cartilage tissue maintenance, and (c) severity of osteoarthritic tissue damage is positively correlated with glycolysis and oxphos activity as well as redox ratio in post-adolescent cartilage.

Optical metabolic imaging (OMI), a non-invasive metabolic imaging technique, was recently adapted for use in articular cartilage, and was employed in the present study to characterize maturation-dependent porcine femoral cartilage metabolic activity[27]. Downstream consequences of metabolic variation were interrogated by chemically inhibiting pathway-specific metabolic activity and analyzing resulting differential expression of a suite of cartilage maintenance genes. Finally, metabolic measurements were correlated with histological damage scores to establish a connection between metabolic activity and tissue health.

5.3. Methods

5.3.1. Sample Collection and Preparation

Articular cartilage samples were harvested from the stifle joints of pigs ranging from 3 days to 6 years old. Four-millimeter diameter femoral samples were harvested under sterile conditions

using a biopsy punch and scalpel blade. Samples were stored in chondrocyte media containing Ham's F-12 media (Mediatech, Inc., Manassas, VA), 10% fetal bovine serum (Hyclone, GE Healthcare Bio-Sciences, Pittsburgh, PA), 50 ug/ml ascorbic acid (Amresco, LLC., Solon, OH), 30 ug/ml alpha-ketoglutaric acid (Thermo Fisher Scientific Chemicals, Inc., Waltham, MA), 300 ug/ml L-glutamine, 100 IU/ml penicillin G, 100 ug/ml streptomycin, and 6 mg/ml HEPES buffer (Corning, Inc., Corning, NY) at room temperature for same-day use, or otherwise incubated at 37°C and 5% CO_2 for up to 3 days. Samples were bisected into hemicylinders prior to imaging.

5.3.2. Optical Metabolic Imaging

Optical metabolic imaging (OMI) was performed as previously described[27]. Briefly, imaging was performed on an inverted epifluorescent microscope with a metal halide fluorescent lamp and filter cubes to measure fluorescence intensity of channel 1 (DAPI filter, excitation 361-389 nm, emission 435-485 nm) in which glycolysis byproduct NADH fluoresces (50-250 ms exposure time), and channel 2 (green filter, excitation 470-490 nm, emission 500-550 nm) in which oxphos byproduct FAD fluoresces (1-9 s exposure time). Of note, while NADH is the glycolytic byproduct of interest, the phosphorylated metabolite NADPH shares the same fluorescence spectra. Thus, NADH fluorescence is referred to as NAD(P)H. Fluorescence intensities of channel 1 and channel 2 images were measured from images taken with a monochrome camera (DP80, Olympus, Tokyo, Japan) and normalized to corresponding fluorescence exposure times. ImageJ software was used to calculate the optical redox ratio, defined here as [channel 2]/[channel 1 + channel 2][16,28,29].

Samples were imaged on a coverslip at 40× magnification using a 1.6× extender. Samples were kept hydrated with room temperature and oxygen tension PBS throughout imaging. Three to six samples per animal were imaged, each at 4-8 locations spread approximately evenly across the articular surface of the tissue cross section to allow for sufficient light penetration. Following

imaging, samples were stored at -80°C until further use.

5.3.3. Histology and Scoring

A subset of samples previously subjected to metabolic imaging were thawed and fixed in 10% formalin in PBS for histological processing. After a minimum of 24 hours in fixative, samples were processed, embedded, and sectioned onto slides in 4 μm slices. Samples were stained with Safranin-O (Thermo Fisher Scientific, Waltham, MA) and Fast Green FCF (MP Biomedicals, LLC, Santa Ana, CA) for proteoglycan content analysis, and with Hematoxylin (Electron Microscopy Sciences, Hatfield, PA) and Eosin (VWR International, Radnor, PA) (H&E) for gross structural analysis. Stained samples were imaged via bright field microscopy (IX-71, Olympus Corporation, Tokyo, Japan) at 20× magnification. Tissue damage scores were assigned on a scale of 0-20 according to the OARSI microscopic grading system for cell necrosis, chondrone formation, fibrillation and fissuring, focal cell loss, and Safranin O stain uptake[30,31].

5.3.4. Metabolic Inhibition & Gene Expression Analysis

A separate set of samples was harvested from pigs approximately 5-6 months old and subjected to metabolic inhibition as previously described[27]. Briefly, following baseline metabolic imaging, samples were subjected to either glycolysis inhibition via incubation in 2-deoxy-D-glucose (10 mM, 24 hr, 37ºC), or oxphos inhibition via incubation in rotenone (20 μM, 0.5 hr, 37ºC). Following inhibitor incubation, samples were re-imaged to confirm metabolic suppression. Control samples were not subjected to metabolic imaging or inhibition. All samples were snap frozen in liquid nitrogen prior to being stored in -80°C until further use. RNA isolation, reverse transcription, and quantitative PCR were all conducted as previously described[32]. Expression of anabolic tissue synthesis genes Col2, Col1, Col10, ACAN, and SOX9, and catabolic enzyme genes ADAMTS4 and ADAMTS5 were analyzed via custom primers, designed as previously

described[32]. Gene expression data (C_T) were standardized to the expression of the housekeeping gene PPIA (ΔC_T) and calculated as fold change ($2^{-\Delta\Delta CT}$) from the average gene expression of the control group.

5.3.5. Statistical Analysis

Age-dependent metabolic data were not normally distributed and thus were subjected to nonparametric analysis. Channel 1 fluorescence intensity, Channel 2 fluorescence intensity, and optical redox ratio (ORR) were each compared across age groups via Aligned Rank Transform (ART) ANOVA with post-hoc Tukey-corrected pairwise comparisons. Data were binned as follows: the immature group consisted of animals age 0-4 months (n=17 animals), the adolescent group consisted of animals age 5-18 months (n=13 animals), and the mature group consisted of animals age 19-75 months (n=6 animals)[33].

Similarly, gene expression data were not normally distributed, and thus were subjected to nonparametric ART ANOVA comparisons across treatment groups with post-hoc Tukey-corrected pairwise tests. The expression of each of the 7 genes of interest was compared across three treatment groups: control (n=4 animals, 5 samples), 2DG (n=6 animals, 10 samples), and rotenone (n=4 animals, 6-7 samples).

Given the ordinal nature of OARSI scores, these data were correlated with metabolic data via Spearman's rank order analysis. Correlations tested averaged metabolic values within each sample against corresponding OARSI scores and were limited to samples harvested from animals ≥ 12 months of age (n=10 animals, 21 samples).

5.4. Results

Optical metabolic imaging revealed differential metabolic activity in porcine cartilage before, during, and following the period of adolescence, with redox ratio demonstrating nonlinearity

throughout maturation (Figure 1). Channel 1, which encompasses fluorescence of the glycolysis byproduct NAD(P)H, and Channel 2, which encompasses fluorescence of the oxphos byproduct FAD, both demonstrated increasing intensity across the three maturation groups. Optical redox ratio, calculated as [Ch.2] / [Ch.1 + Ch.2], was lowest in adolescent samples compared to immature and mature samples.

Gene expression analysis revealed suppression of select cartilage maintenance genes, both anabolic and catabolic in nature, following inhibition of glycolysis (Figure 2). The anabolic synthesis genes Col1 and Col2 as well as the catabolic enzyme genes ADAMTS4 and ADAMTS5 demonstrated suppressed expression in the glycolysis-inhibited (2DG) group compared to control samples. Oxphos-inhibited (rotenone) samples did not demonstrate altered expression of genes of interest compared to controls.

Cartilage metabolism demonstrated a moderate degree of correlation to cumulative OARSI score in animals 12-60 months of age (Figure 3). Spearman rank order testing revealed the strongest positive correlation between optical redox ratio and OARSI score (r_s=0.58, $p<0.01$), followed by Channel 2 fluorescence (r_s=0.39, $p=0.08$), with Channel 1 fluorescence demonstrating the weakest correlation with OARSI score (r_s=0.28, $p=0.21$).

5.5. Discussion

Metabolic imaging revealed maturity-dependent increases in both fluorescence channels, as well as differential optical redox ratio across groups. This uptick in metabolic activity within mature samples, especially in the FAD-encompassing Channel 2, may seem contradictory to previous studies demonstrating metabolic dysfunction as a key characteristic of cartilage damage. There are two opposing perspectives through which to interpret these findings. Given the fact that the mature samples, though adult, do not necessarily meet the criteria for truly being considered

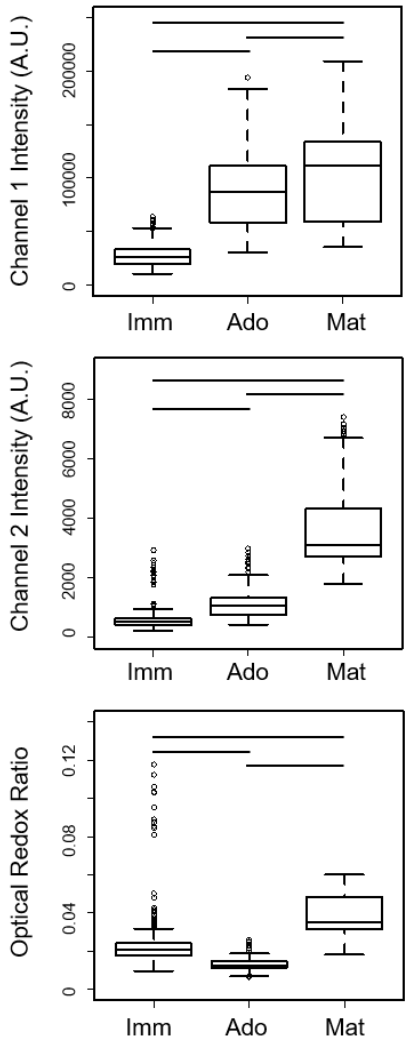

Figure 5-1. Metabolic activity as a function of age. NAD(P)H fluorescence intensity is captured by channel 1 (top), FAD intensity is captured by channel 2 (middle), and redox ratio (bottom) is calculated as [Ch2]/[Ch1 + Ch2]. Imm represents data from 17 immature animals (0-4 months), totaling 408 imaging locations from 54 samples. Ado represents data from 13 adolescent animals (5-18 months), totaling 312 imaging locations from 39 samples. Mat represents data from 6 mature animals (19-75 months), totaling 150 imaging locations from 24 samples. Bars indicate significance at $p \leq 0.01$.

aged, coupled with the lack of macroscopic evidence of degeneration in these samples, one could view these metabolic patterns as being simply a function of healthy tissue maintenance unaffiliated with any pathological processes[34]. Through this framework, the apparent increase in oxphos activity and corresponding increase in redox ratio in mature samples could represent sub-toxic oxidant-induced tissue maintenance, a phenomenon observed in other tissues such as the heart and intestine[35–37]. Specifically, increased ROS production has been associated with increased cell proliferation and tissue synthesis in cardiomyocytes, and exposure to hydrogen peroxide has promoted cardiac regeneration in zebrafish[36,37]. However, hypoxia-induced decrease in ROS accumulation has also been shown to promote heart growth through cardiomyocyte proliferation in infarcted mice[38,39]. Indeed, the existing body of literature paints a complex picture of oxidant-dependent cellular activity; interpretation of results across species and tissue types, particularly those of disparate regenerative capacity, must be exercised with caution.

Alternatively, one could suppose the mature sample group in the present study was instead demonstrating "pre-OA" metabolic activity, as cartilage irreversibly loses regenerative capacity following adolescence, rendering accumulation of tissue damage nearly inevitable. In this context, the increase in Channel 2 fluorescence along with the increase in redox ratio observed in mature tissue could be evidence of cellular phenotype shift toward chondrocyte hypertrophy[15]. Heightened metabolic reliance on oxphos is a hallmark of hypertrophic differentiation and has been described in OA tissue as well as mesenchymal stromal cells (MSCs) and chondrocytes within bone[40–44]. The Channel 1 fluorescence increase could also be explained through this framework, as excess accumulation of ROS produced by high oxphos activity has been shown to induce a compensatory increase in glycolysis activity[45]. Furthermore, OA chondrocytes have, by some metrics, demonstrated heightened glycolysis activity compared to healthy chondrocytes[46,47]. This notion of

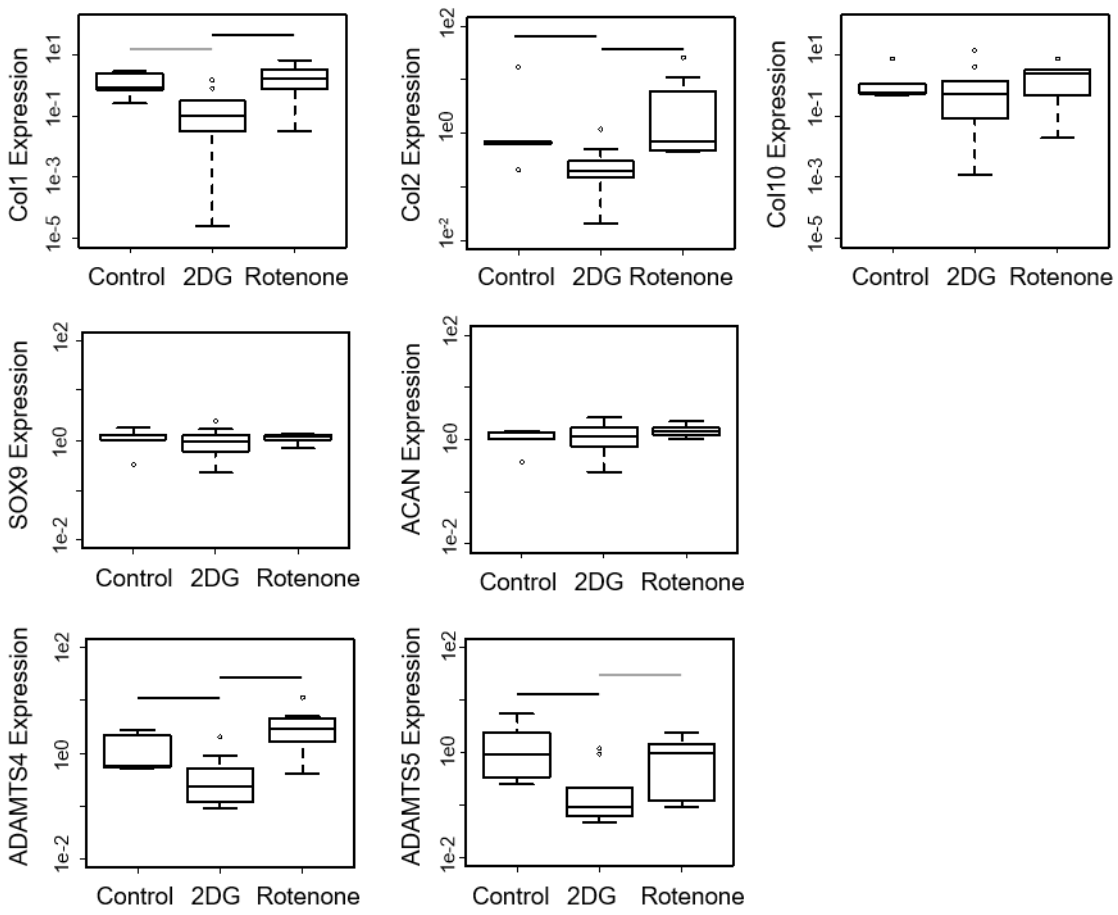

Figure 5-2. Effects of metabolic inhibition on gene expression. Treatment group data were normalized to average expression of control (uninhibited) samples. Control data represent 5 samples from 4 animals. 2DG data represent 10 samples from 6 animals. Rotenone data represent 6 (Col1) or 7 (all other genes) samples from 4 animals. Black lines indicate significance at $p<0.05$; grey lines indicate significance at $p<0.10$.

the mature cartilage group demonstrating signs of early pre-pathogenic metabolic activity is supported by the correlations observed between metabolic metrics and tissue damage scores. The relationship between optical redox ratio and OARSI score is particularly compelling as redox ratio deviated from the pre-adolescent trend and demonstrated nonlinearity across age groups,

suggesting the activity observed in mature samples may be somewhat pathologic in nature rather than merely a product of healthy maturation.

The accelerated metabolic activity observed in mature samples might seem counterintuitive given the well-established loss of regenerative activity post-adolescence in cartilage. However, there may be some precedence for this heightened energetic demand. Following hepatectomy involving up to 30% liver mass resection, metabolic activity in the remaining hepatocytes surges yet corresponding cell division is not observed[39,48]. Instead, the cells undergo hypertrophy as a mechanism of tissue repair; a phenotypic shift observed in OA chondrocytes as well[15,26,49]. ECM production requires a great deal of energy, as evidenced by the reduction in AMP kinase (AMPK) activity during osteogenesis[50]. AMPK limits ATP consumption, therefore reduction of this enzyme's activity allows the tissue to meet the energy demand of tissue synthesis. Interestingly, inhibition of AMPK activity in cartilage has resulted in promotion of degenerative catabolic activity, particularly in OA[42,51,52]. It is worth noting that the energy requirements and metabolic programs of chondrogenesis and osteogenesis differ, with chondrocytes demonstrating predominantly glycolytic metabolism and less reliance on oxidative metabolic activity than osteocytes[53]. Thus, the AMPK-reduction mechanism employed by osteocytes to meet the energetic demand of matrix production may not directly translate in the context of chondrogenesis.

Select tissue maintenance genes, both anabolic and catabolic in nature, demonstrated downregulated expression following inhibition of glycolysis in the present study, but inhibition of oxphos did not affect expression of the cartilage maintenance genes tested. This finding supports the established notion of glycolysis being of greater relative importance for chondrocytes than oxphos[15,54]. As previously discussed, glycolysis absorbs the cost of mitochondrial deficiency due to excess ROS accumulation, a condition which may have begun to materialize via increased

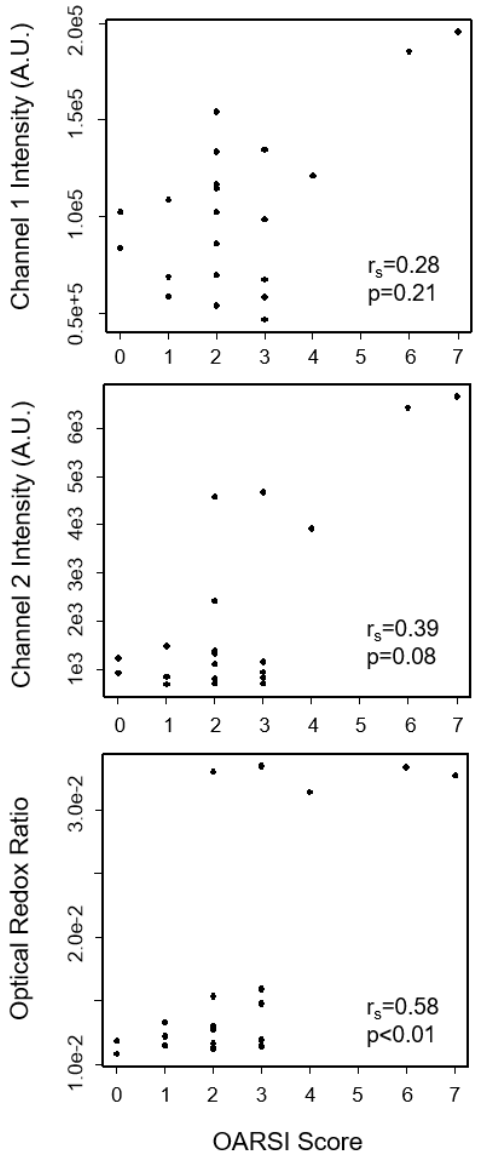

Figure 5-3. Metabolism vs. OARSI score. NAD(P)H fluorescence intensity is captured by channel 1 (top), FAD intensity is captured by channel 2 (middle), and redox ratio (bottom) is calculated as [Ch2]/[Ch1 + Ch2]. Each data point represents a sample (n=21 samples from 10 animals age 12-60 months) for which 8 metabolic imaging values have been averaged. Rho values and p-values correspond to Spearman's rank order correlation analyses.

oxphos in the mature tissue tested in the present study[45]. It then follows that glycolysis impairment would be expected to have a stronger detrimental effect on cartilage function than oxphos inhibition. The non-discriminant nature of gene expression downregulation, affecting both anabolic and catabolic cartilage maintenance genes, is intriguing, and may represent a generalized stress response aimed at conserving energy broadly[42,52,55].

The present study comes with a few limitations with respect to interpretation of results. First, in addition to NAD(P)H and FAD, collagen cross-links are autofluorescent, with excitation and emission spectra overlapping with those of NAD(P)H[56]. Collagen content and organization changes throughout cartilage maturation, particularly from birth to adolescence[57]. Therefore, age-dependent Channel 1 data must be interpreted conservatively, and further research is necessary to fully characterize the contributions of each fluorescent component in this channel. Additionally, the relationships observed between metabolism, age, and tissue health are merely associative. While the metabolic inhibition portion of this study began this work, additional studies are necessary to determine whether maturation-dependent metabolic activity is the driving force behind the clinically relevant factors observed, or simply a symptom. Lastly, tissue availability limited this study to inclusion of tissue up to 6 years old. As previously mentioned, this maturation state cannot necessarily be assumed to be aged, as pigs can naturally live to be twice this age[34]. Therefore, while this study sought to study cartilage maturation loosely in the context of age-related degeneration and predisposition to OA, the data presented here do not include aged samples comparable to the elderly human population.

Future works will seek to further characterize the up- and downstream cellular events of the differential metabolic activity demonstrated in the present study. Maturation-dependent sensitivity to pathway specific metabolic perturbation is of interest given the strong correlation between aging

and OA, the implication of metabolic dysregulation in OA, and the lack of effective therapies for prevention or reversal of age-related cartilage degeneration. Similarly, the present study and relevant works leave many questions regarding oxygen concentration and nutrient availability in cartilage and the effects of hypoxia vs. normoxia on metabolism which will be explored moving forward.

Articular cartilage metabolism is complicated by several confounding factors such as age, mechanical loading, genetics, and nutrition, which adds great complexity to determination of the fundamental mechanisms at play in this tissue. However, the central role of metabolic processes in cartilage homeostasis and pathogenesis is undeniable. The current study demonstrated maturation-dependent metabolic activity in cartilage pre- and post-adolescence and began to probe the downstream consequences of this differential activity on functional behavior of chondrocytes with respect to tissue homeostasis. Ultimately, determining the causes and consequences of differential metabolic activity in cartilage will substantially reduce the knowledge gap currently preventing development of effective therapies toward cartilage regeneration.

5.6. Acknowledgments

Funding from UW-Madison VCGRE and tissue from the UW-Madison Meat Science Lab and Swine Research and Teaching Unit is gratefully acknowledged.

5.7. References

1. Otsuki S, Grogan SP, Miyaki S, et al. 2010. Tissue neogenesis and STRO-1 expression in immature and mature articular cartilage. J. Orthop. Res. 28(1):96–102.
2. Mukoyama S, Sasho T, Akatsu Y, et al. 2015. Spontaneous repair of partial thickness linear

cartilage injuries in immature rats. Cell Tissue Res. 359(2):513–20.

3. Kloppenburg M, Berenbaum F. 2020. Osteoarthritis year in review 2019: epidemiology and therapy. Osteoarthr. Cartil. 28(3):242–248.
4. Jørgensen AEM, Kjær M, Heinemeier KM. 2017. The effect of aging and mechanical loading on the metabolism of articular cartilage. J. Rheumatol. :jrheum.160226.
5. Rahmati M, Nalesso G, Mobasheri A, Mozafari M. 2017. Aging and osteoarthritis: Central role of the extracellular matrix. Ageing Res. Rev. 40:20–30.
6. Li Y-S, Xiao W, Luo W. 2016. Cellular aging towards osteoarthritis. Mech. Ageing Dev. .
7. Drevet S, Gavazzi G, Grange L, et al. 2018. Reactive oxygen species and NADPH oxidase 4 involvement in osteoarthritis. Exp. Gerontol. 111:107–117.
8. Nishida T, Kubota S, Aoyama E, Takigawa Yz M. 2013. Impaired glycolytic metabolism causes chondrocyte hypertrophy-like changes via promotion of phospho-Smad1/5/8 translocation into nucleus. Osteoarthr. Cartil. .
9. Mobasheri A, Vannucci SJ, Bondy CA, et al. 2002. Glucose transport and metabolism in chondrocytes: a key to understanding chondrogenesis, skeletal development and cartilage degradation in osteoarthritis. Histol. Histopathol. 17(4):1239–67.
10. Coleman MC, Ramakrishnan PS, Brouillette MJ, Martin JA. 2016. Injurious loading of articular cartilage compromises chondrocyte respiratory function. Arthritis Rheumatol. 68(3):662–671.
11. Brouillette MJ, Ramakrishnan PS, Wagner VM, et al. 2014. Strain-dependent oxidant release in articular cartilage originates from mitochondria. Biomech. Model. Mechanobiol. 13(3):565–72.
12. Delco ML, Bonnevie ED, Bonassar LJ, Fortier LA. 2017. Mitochondrial dysfunction is an

acute response of articular chondrocytes to mechanical injury. J. Orthop. Res. 36(2):739–750.

13. Martin JA, McCabe D, Walter M, et al. 2009. N-Acetylcysteine inhibits post-impact chondrocyte death in osteochondral explants. J. Bone Jt. Surgery-American Vol. 91(8):1890–1897.
14. Agathocleous M, Harris WA. 2013. Metabolism in physiological cell proliferation and differentiation. Trends Cell Biol. 23(10):484–492.
15. Tchetina E V., Markova GA. 2018. Regulation of energy metabolism in the growth plate and osteoarthritic chondrocytes. Rheumatol. Int. 38:1–12.
16. Alhallak K, Rebello LG, Muldoon TJ, et al. 2016. Optical redox ratio identifies metastatic potential-dependent changes in breast cancer cell metabolism. Biomed. Opt. Express 7(11):4364–4374.
17. Shah AT, Heaster TM, Skala MC. 2017. Metabolic imaging of head and neck cancer organoids. PLoS One 12(1):1–17.
18. Hou J, Wright HJ, Chan N, et al. 2016. Correlating two-photon excited fluorescence imaging of breast cancer cellular redox state with seahorse flux analysis of normalized cellular oxygen consumption. J. Biomed. Opt. 21(6):60503.
19. Warburg O. 1956. On the origin of cancer cells. Science 123(3191):309–14.
20. Zheng J. 2012. Energy metabolism of cancer: Glycolysis versus oxidative phosphorylation (Review). Oncol. Lett. 4(6):1151–1157.
21. Ballock RT, O'Keefe RJ. 2003. Physiology and pathophysiology of the growth plate. Birth Defects Res. Part C Embryo Today Rev. 69(2):123–143.
22. Yagi R, McBurney D, Laverty D, et al. 2005. Intrajoint comparisons of gene expression

patterns in human osteoarthritis suggest a change in chondrocyte phenotype. J. Orthop. Res. 23(5):1128–1138.

23. Kirsch T, Swoboda B, Nah HD. 2000. Activation of annexin II and V expression, terminal differentiation, mineralization and apoptosis in human osteoarthritic cartilage. Osteoarthr. Cartil. 8(4):294–302.

24. Robertson CM, Pennock AT, Harwood FL, et al. 2006. Characterization of pro-apoptotic and matrix-degradative gene expression following induction of osteoarthritis in mature and aged rabbits. Osteoarthr. Cartil. 14(5):471–476.

25. Pullig O, Weseloh G, Ronneberger DL, et al. 2000. Chondrocyte differentiation in human osteoarthritis: Expression of osteocalcin in normal and osteoarthritic cartilage and bone. Calcif. Tissue Int. 67(3):230–240.

26. Singh P, Marcu KB, Goldring MB, Otero M. 2018. Phenotypic instability of chondrocytes in osteoarthritis: on a path to hypertrophy. Ann. N. Y. Acad. Sci. .

27. Walsh SK, Skala MC, Henak CR. 2019. Real-time optical redox imaging of cartilage metabolic response to mechanical loading. Osteoarthr. Cartil. 27(12):1841–1850.

28. Schneider CA, Rasband WS, Eliceiri KW. 2012. NIH Image to ImageJ: 25 years of image analysis. Nat. Methods 9(7):671–675.

29. Adavallan K, Gurushankar K, Nazeer SS, et al. 2017. Optical redox ratio using endogenous fluorescence to assess the metabolic changes associated with treatment response of bioconjugated gold nanoparticles in streptozotocin-induced diabetic rats. Laser Phys. Lett. 14(6):065901.

30. Schmitz N, Laverty S, Kraus VB, Aigner T. 2010. Basic methods in histopathology of joint tissues. Osteoarthritis Cartilage 18 Suppl 3:S113-6.

31. McIlwraith CW, Frisbie DD, Kawcak CE, et al. 2010. The OARSI histopathology initiative – recommendations for histological assessments of osteoarthritis in the horse. Osteoarthr. Cartil. 18:S93–S105.

32. Walsh SK, Schneider SE, Amundson LA, et al. 2020. Maturity-dependent cartilage cell plasticity and sensitivity to external perturbation. J. Mech. Behav. Biomed. Mater. 106:103732.

33. Reiland S. 1978. Growth and skeletal development of the pig. Acta Radiol. Suppl. 358:15–22.

34. Helcel J. 2017. An Evaluation of Contraceptive Viability in Wild Pig Management | Texas A&M NRI. [cited 2020 Apr 12] Available from: https://nri.tamu.edu/blog/2017/september/an-evaluation-of-contraceptive-viability-in-wild-pig-management/.

35. Aw TY. 1999. Molecular and cellular responses to oxidative stress and changes in oxidation-reduction imbalance in the intestine. Am. J. Clin. Nutr. 70(4):557–65.

36. Murray TVA, Smyrnias I, Schnelle M, et al. 2015. Redox regulation of cardiomyocyte cell cycling via an ERK1/2 and c-Myc-dependent activation of cyclin D2 transcription. J. Mol. Cell. Cardiol. 79:54–68.

37. Han P, Zhou XH, Chang N, et al. 2014. Hydrogen peroxide primes heart regeneration with a derepression mechanism. Cell Res. 24(9):1091–1107.

38. Nakada Y, Canseco DC, Thet S, et al. 2017. Hypoxia induces heart regeneration in adult mice. Nature 541(7636):222–227.

39. Iismaa SE, Kaidonis X, Nicks AM, et al. 2018. Comparative regenerative mechanisms across different mammalian tissues. npj Regen. Med. 3(1):1–20.

40. Salim A, Nacamuli RP, Morgan EF, et al. 2004. Transient changes in oxygen tension inhibit osteogenic differentiation and Runx2 expression in osteoblasts. J. Biol. Chem. 279(38):40007–40016.

41. Loeffler J, Duda GN, Sass FA, Dienelt A. 2018. The metabolic microenvironment steers bone tissue regeneration. Trends Endocrinol. Metab. 29(2).

42. Zhou S, Lu W, Chen L, et al. 2017. AMPK deficiency in chondrocytes accelerated the progression of instability-induced and ageing-associated osteoarthritis in adult mice. Sci. Rep. 7(1):1–14.

43. Moussavi-Harami F, Duwayri Y, Martin JA, et al. 2004. Oxygen effects on senescence in chondrocytes and mesenchymal stem cells: consequences for tissue engineering. Iowa Orthop. J. 24:15–20.

44. Chen C-T, Shih Y-R V., Kuo TK, et al. 2008. Coordinated changes of mitochondrial biogenesis and antioxidant enzymes during osteogenic differentiation of human mesenchymal stem cells. Stem Cells 26(4):960–968.

45. Liemburg-Apers DC, Willems PHGM, Koopman WJH, Grefte S. 2015. Interactions between mitochondrial reactive oxygen species and cellular glucose metabolism. Arch. Toxicol. 89(8):1209–1226.

46. Yang X, Chen W, Zhao X, et al. 2018. Pyruvate kinase M2 modulates the glycolysis of chondrocyte and extracellular matrix in osteoarthritis. DNA Cell Biol. 37(3):271–277.

47. Liu-Bryan R, Terkeltaub R. 2015. Emerging regulators of the inflammatory process in osteoarthritis. Nat. Rev. Rheumatol. 11(1):35–44.

48. Miyaoka Y, Ebato K, Kato H, et al. 2012. Hypertrophy and unconventional cell division of hepatocytes underlie liver regeneration. Curr. Biol. 22(13):1166–1175.

49. Ripmeester EGJ, Timur UT, Caron MMJ, Welting TJM. 2018. Recent insights into the contribution of the changing hypertrophic chondrocyte phenotype in the development and progression of osteoarthritis. Front. Bioeng. Biotechnol. 6:18.

50. Kasai T, Bandow K, Suzuki H, et al. 2009. Osteoblast differentiation is functionally associated with decreased AMP kinase activity. J. Cell. Physiol. 221(3):740–749.

51. Terkeltaub R, Yang B, Lotz M, Liu-Bryan R. 2011. Chondrocyte AMP-activated protein kinase activity suppresses matrix degradation responses to proinflammatory cytokines interleukin-1β and tumor necrosis factor α. Arthritis Rheum. 63(7):1928–1937.

52. Wang L, Shan H, Wang B, et al. 2018. Puerarin attenuates osteoarthritis via upregulating AMP-activated protein kinase/proliferator-activated receptor-γ coactivator-1 signaling pathway in osteoarthritis rats. Pharmacology 102(3–4):117–125.

53. Pattappa G, Heywood HK, de Bruijn JD, Lee DA. 2011. The metabolism of human mesenchymal stem cells during proliferation and differentiation. J. Cell. Physiol. 226(10):2562–2570.

54. Lane RS, Fu Y, Matsuzaki S, et al. 2015. Mitochondrial respiration and redox coupling in articular chondrocytes. Arthritis Res. Ther. 17(1).

55. Liu-Bryan R. 2015. Inflammation and intracellular metabolism: New targets in OA. Osteoarthr. Cartil. 23(11):1835–1842.

56. Croce AC, Bottiroli G. 2014. Autofluorescence spectroscopy and imaging: a tool for biomedical research and diagnosis. Eur. J. Histochem. 58(4):2461.

57. Julkunen P, Harjula T, Iivarinen J, et al. 2009. Biomechanical, biochemical and structural correlations in immature and mature rabbit articular cartilage. Osteoarthr. Cartil. 17:1628–1638.

Chapter 6: Conclusions

Aging and mechanical overloading play an irrefutable role in articular cartilage pathogenesis, yet many of the mechanisms underlying these relationships remain incompletely understood. Consequentially, OA remains globally burdensome as clinical solutions are limited to symptom mitigation rather than tissue restoration. The overarching aim of this body of work was to reduce the knowledge gap associated with cartilage degeneration, specifically with respect to the complex relationships between maturation, mechanical loading, and tissue metabolism.

The effects of tissue maturation and mechanical loading were analyzed with respect to progenitor cell population and anabolic cartilage gene expression in *Chapter 2*. This work identified age-dependent expression of chondroprogenitor cell markers and matrix synthesis genes—factors which are proposed to play an important role in the post-adolescent loss of regenerative capacity demonstrated by cartilage. While expression of some markers and genes demonstrated linear trends with age, others unexpectedly showed greater similarity between immature and mature samples compared to the intermediate adolescent samples. Interestingly, this analysis also revealed differential sensitivity to mechanical loading and artificial tissue culture such that expression of progenitor markers and genes of interest were less affected by these environmental perturbations in skeletally mature tissue than in juvenile and adolescent tissue. This finding has important implications for development of regenerative therapies; effective interventions will need to circumnavigate the resiliency to perturbation demonstrated by mature tissue.

A metabolic imaging technique, optical metabolic imaging (OMI), was adapted for use in articular cartilage in *Chapter 3*. This technique enables cost-effective longitudinal analysis of cell metabolism with some degree of pathway-specificity without the use of dyes or labels—

information which has been historically challenging to capture, if not entirely unobtainable, in articular cartilage explants. The data yielded by OMI complements the existing literature on cartilage metabolism by leveraging the current understanding of fundamental metabolic mechanisms in cartilage and allowing that knowledge to be paired with environmental perturbations of various natures (e.g., chemical, mechanical) in real-time. Validation of OMI was conducted via chemical metabolic inhibition of glycolysis and oxphos, respectively, to ensure sufficient sensitivity of the imaging and data processing protocol for cartilage.

OMI was first employed to analyze the effects of a single compressive load, of physiological rate and magnitude, on cartilage metabolism in *Chapter 3*. This work established the feasibility of monitoring metabolic activity on the order of seconds to minutes post-loading, and demonstrated transient metabolic flux following compression primarily affecting the glycolytic fluorescence channel with few changes observed in the oxphos fluorescence channel. The observed time-dependent response subsided within 30 minutes of loading, as was expected given the mild nature of the applied load. This work was then juxtaposed to a complementary study in which a superphysiological impact was delivered to cartilage explants prior to OMI in *Chapter 4*. Unlike the previous study, this study aimed to induce tissue failure, both in the biological and mechanical sense, and to analyze the corresponding mechanobiological response. Cartilage demonstrated post-impact metabolic activity different from that of physiological compression, affecting fluorescence in both glycolysis and oxphos-relevant channels in a manner dependent upon proximity to impact, both in time and physical distance. Furthermore, metabolic effects of high-impact loading did not subside within 30 minutes as they had appeared to following physiological compression, suggesting longer-term metabolic monitoring as an attractive next step.

Lastly, the metabolic consequences of maturation were studied by mapping baseline metabolic activity as a function of age in a wide range of samples spanning pre- and post-adolescence in *Chapter 5*. This work revealed maturation-dependent metabolic activity in both the glycolytic and oxphos fluorescence channels and revealed an interesting pattern of nonlinearity in optical redox ratio across age groups. The consequences of this differential activity were probed via pathway-specific chemical inhibition, which highlighted the particular importance of glycolysis for cartilage function as glycolytic inhibition suppressed expression of both anabolic and catabolic genes pertinent to tissue maintenance while oxphos inhibition did not. Finally, OMI metrics were analyzed as a function of histological OARSI score to detect correlations between the metabolic activity observed in mature samples and degree of tissue damage. This analysis revealed a striking association between optical redox ratio and OARSI score in mature cartilage—another finding which poses important questions and highlights an obvious starting point for further research.

The potential impact of this work can be viewed from both short- and long-term perspectives. This research provides evidence that post-adolescent cartilage may be attempting to mount a regenerative response to combat the adverse effects of aging. Therefore, although these observed changes in redox activity and gene expression do not directly translate into functional tissue synthesis in mature cartilage, these findings can serve to inform research in the immediate future by identifying specific aspects of tissue regeneration that demonstrate some promise in mature cartilage. In a broader, longer-term view, OMI opens many doors as this method can accommodate longitudinal, pathway-specific metabolic monitoring during and after environmental perturbations. The studies presented in this dissertation have demonstrated a few possible applications of this technique with respect to tissue maturation and mechanical loading. Moving forward, OMI

provides the opportunity to gain novel insights into articular cartilage physiology and to test potential therapeutics from a metabolic perspective.

This body of work sought to answer fundamental questions of cartilage biology with an eye toward translational application. There are several lines of research which naturally follow the studies described here. The differential metabolic activity detected with respect to tissue age and mechanical loading coupled with the age-dependence of chondroprogenitors residing in cartilage opens questions as to the cell-specific metabolic activity throughout tissue maturation. Heterogeneity in the cells residing within cartilage tissue, such as the demonstrated zonal variations in cell populations, is likely mirrored by cell-specific metabolic activity[162,197,254]. Specifically, performance of cell functionalities pertinent to tissue regeneration such as proliferation, gene expression, or vulnerability to inflammatory cytokine insult, as a function of metabolic status as determined by OMI would be of great interest. Considering the autofluorescence of NAD(P)H and FAD, cell sorting based on metabolic activity is a logical and feasible approach to answering these questions.

Additional cutting-edge technologies can be employed to better characterize the consequences of the metabolic findings outlined here with respect to tissue regeneration. Enhanced physiological relevance of mechanical loading and/or time series studies can be achieved through use of a bioreactor setup, wherein relevant environmental conditions such as temperature, nutrient availability, and oxygen tension can be precisely controlled. Effects of varying oxygen concentration are especially compelling; oxidative stress and oxygen availability are core tenets of the mechanistic theories underlying current interpretation of cartilage metabolism data. Similarly, a more detailed account of total ATP production as well as individual contributions of aerobic and anaerobic pathways would substantially aid the interpretation of the metabolic findings described

throughout this body of work. Commercially available products such as the Seahorse XF assays from Agilent have recently enabled such analyses and could be of great benefit to the field of cartilage research. It is worth noting, however, that the high density of the ECM and low cellularity of adult cartilage may preclude the use of such techniques in their current form and may require isolation of chondrocytes via tissue digestion prior to analysis.

As with any biomedical research, identifying opportunities for therapeutic intervention greatly motivated the present studies and should continue to guide future works. Given the existing paradigm of glycolysis and oxphos as intertwined yet distinct sources of tissue energy with differential responses to environmental stressors, artificial manipulation of these pathways may hold promise as a therapeutic avenue by which to maintain or restore optimal cell functionality, particularly in the early stages of cartilage degeneration prior to macroscopic breakdown. One can conceive of two types of metabolic programs by which this strategy could be approached: a "pulling" mechanism, wherein a metabolic pathway is directly stimulated through use of a molecular agonist, or a "pushing" mechanism, wherein one pathway is inhibited in order to induce compensatory upregulation of an alternative pathway. While these candidate treatments could be applied directly to ailing tissue, they could also hold potential for enhancement of existing treatments. For example, metabolic priming of auto- or allograft cells or tissues prior to implantation could conceivably improve the integration and regeneration activity of the products following implantation. Of course, this application would require preliminary work to determine the optimal metabolic status of implanted cells, for which the solutions could vary across anatomical location, patient age, or other clinical variants.

Lastly, the ability of OMI to provide metabolic information about cartilage without requiring the use of exogenous dyes or destructive techniques begs the question whether this technique could

be leveraged clinically as a diagnostic imaging technique. Intraarticular arthroscopic imaging is a common practice and is considered relatively non-invasive. Adaptation of OMI for clinical use similar to arthroscopic imaging could potentially improve clinical evaluation of cartilage health in the early stages of pathogenesis, as metabolic dysregulation likely precedes macroscopic tissue degradation characteristic of OA in many cases. Furthermore, information gathered through clinical use of OMI on a range of orthopedic patients could serve to improve our understanding of the differing OA phenotypes—a source of variation which is purported to inhibit efficacy of current OA treatments.

In conclusion, this thesis took an integrative approach to studying cartilage function through the perspectives of aging, mechanics, metabolism, and the interplay between these cofactors. This work synthesized aspects of cell biology, tissue mechanics, orthopedics, and cancer imaging to yield meaningful insights into cartilage function and dysfunction. The current lack of effective therapies for the regeneration of damaged cartilage and the prevention of OA progression can be attributed to the knowledge gap relevant to these complex yet fundamental drivers of cartilage biology. Therefore, future works should continue along this interdisciplinary vein, drawing upon the expertise, methodologies, and lessons learned from neighboring fields of research with the ultimate goal of improving patient outcomes.

APPENDIX A

Chapter 2 Supplementary Data

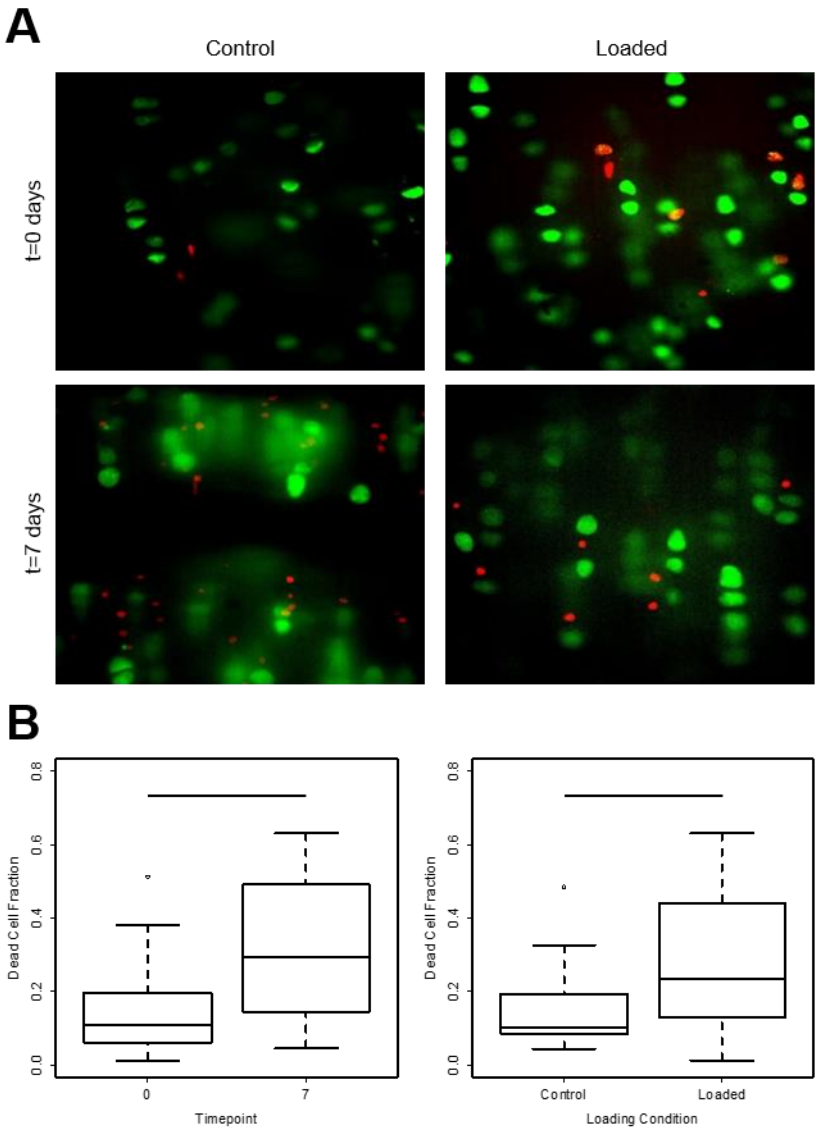

Supplementary Figure 1. Cell viability analysis. (A) Representative set of viability images from a mature animal. (B) Effect of culture time and loading on cell viability averaged across all other factors. Significance bars indicate $P < 0.05$.

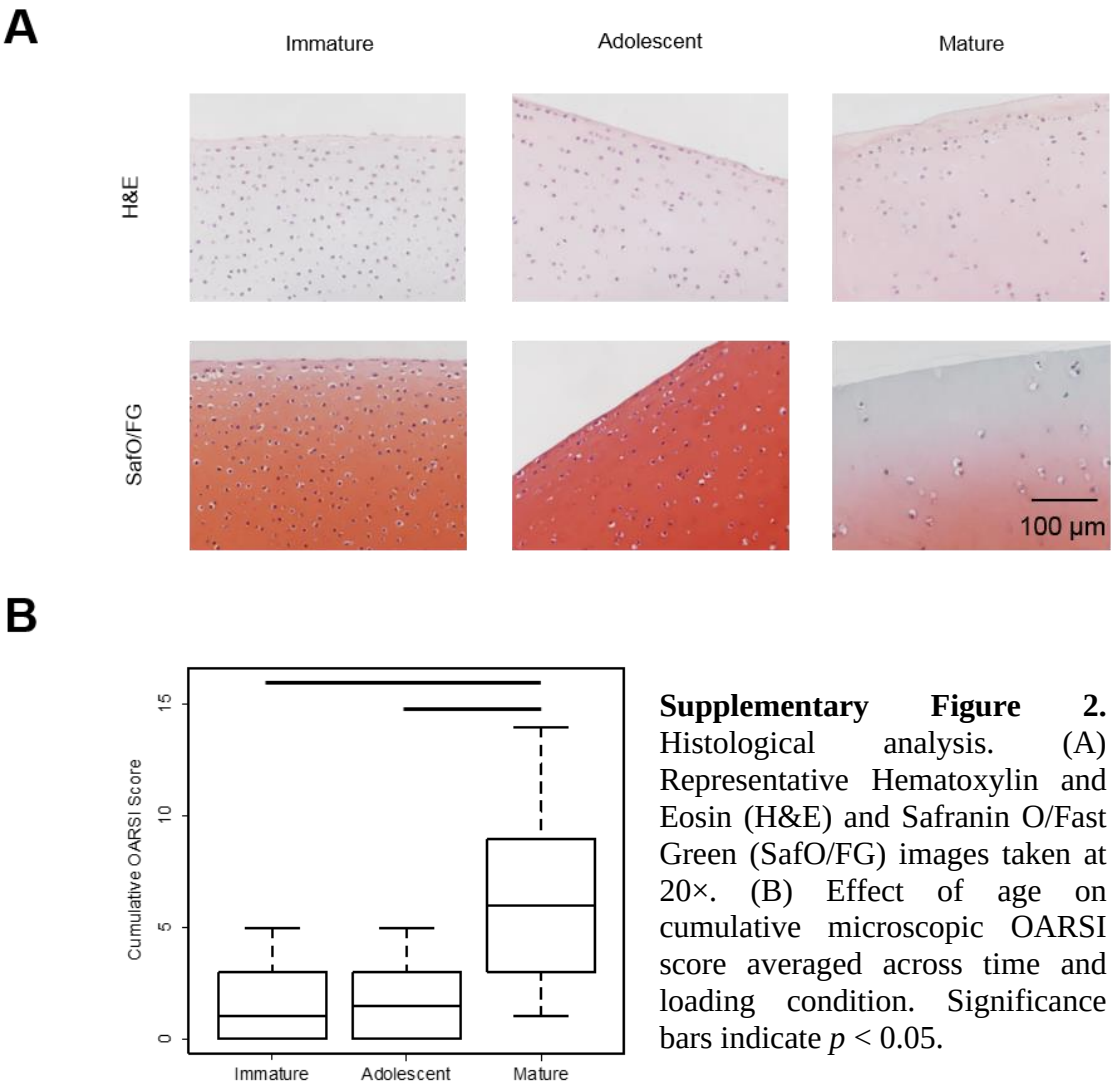

Supplementary Figure 2. Histological analysis. (A) Representative Hematoxylin and Eosin (H&E) and Safranin O/Fast Green (SafO/FG) images taken at 20×. (B) Effect of age on cumulative microscopic OARSI score averaged across time and loading condition. Significance bars indicate $p < 0.05$.

APPENDIX B

Chapter 3 Supplementary Data

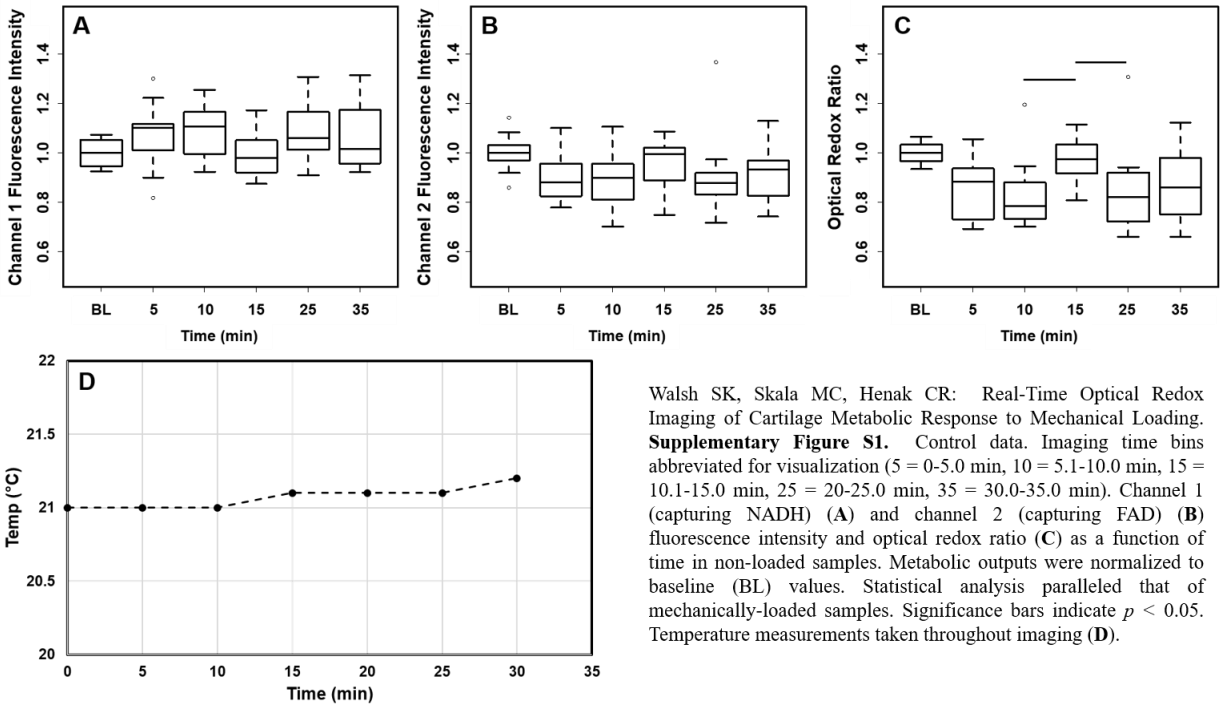

Walsh SK, Skala MC, Henak CR: Real-Time Optical Redox Imaging of Cartilage Metabolic Response to Mechanical Loading. **Supplementary Figure S1.** Control data. Imaging time bins abbreviated for visualization (5 = 0-5.0 min, 10 = 5.1-10.0 min, 15 = 10.1-15.0 min, 25 = 20-25.0 min, 35 = 30.0-35.0 min). Channel 1 (capturing NADH) (**A**) and channel 2 (capturing FAD) (**B**) fluorescence intensity and optical redox ratio (**C**) as a function of time in non-loaded samples. Metabolic outputs were normalized to baseline (BL) values. Statistical analysis paralleled that of mechanically-loaded samples. Significance bars indicate $p < 0.05$. Temperature measurements taken throughout imaging (**D**).

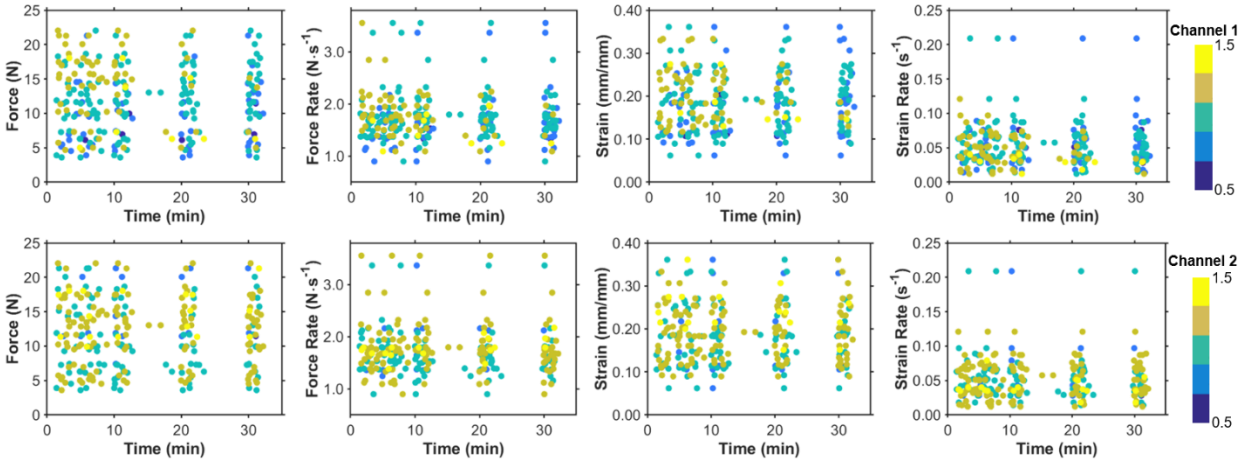

Walsh SK, Skala MC, Henak CR: Real-Time Optical Redox Imaging of Cartilage Metabolic Response to Mechanical Loading. **Supplementary Figure S2.** Channel 1 (capturing NADH) and channel 2 (capturing FAD) fluorescence intensity as a function of time and mechanical load. Qualitative trends, wherein both time and loading affect the intensity in both channels, are visible.